2012-01-01

Characterization of Thrust Faults on the Moon Using Fault Dynamics and 3D Visualizations

Jaclyn Danielle Clark
University of Texas at El Paso, jdclark@miners.utep.edu

CHARACTERIZATION OF THRUST FAULTS ON THE MOON USING FAULT DYNAMICS AND 3D VISUALIZATIONS

Jaclyn D. Clark

Department of Geological Sciences

APPROVED:

_____

José M. Hurtado, Jr., Ph.D., Chair

_____

Bridget Konter, Ph.D.

_____

Eric Hagedorn, Ph.D.

_____

Benjamin C. Flores, Ph.D.

Interim Dean of the Graduate School

CHARACTERIZATION OF THRUST FAULTS ON THE MOON USING FAULT DYNAMICS AND 3D VISUALIZATIONS

by

Jaclyn D. Clark, B.S.

THESIS

Presented to the Faculty of the Graduate School of

The University of Texas at El Paso

in Partial Fulfillment

of the Requirements

for the Degree of

MASTER OF SCIENCE

Department of Geological Sciences

THE UNIVERSITY OF TEXAS AT EL PASO

May 2012

ACKNOWLEDGMENTS

First I want to thank Dr. José Hurtado for giving me this great opportunity to conduct planetary geology research. It's been a real joy to work with Dr. Hurtado, always pushing me to do my best. Thru Dr. Hurtado, I was also given the exciting opportunity to participate in NASA Desert RATS 2011. The UTEP Geological Sciences department has been a great place to grow with great opportunities and hanging around such great people. My parents have also been a big support throughout my life but a big thank you goes out to my Mother. She always had been there for me, supporting me whenever I need it the most. Thank you Alexandra Massad for being the greatest friend a person can have. Lastly, I want to dedicate this research to my Grandma Walker who passed away right before I started my first semester at UTEP. She was so excited I was continuing my education and was a great person for conversations.

ABSTRACT

Many small, lobate scarps, interpreted to be the surface traces of thrust faults, have been found all over Earth's moon by previous researchers. Fault dynamical calculations, assuming an initially completely molten Moon, have shown that these scarps can form due to compressional stresses that accumulate over time as the result of large-scale contraction of the Moon as it cooled. With high-resolution images from the Lunar Reconnaissance Orbiter Camera (LROC), previously undetected lobate scarps can be found globally and viewed at high resolution. By investigating these fault scarps, we can determine better constraints on the amount of crustal shortening and improve our understanding of the stress state of the Moon. In addition, the lobate scarps allow us to further test between competing models for the initial thermal state of the Moon, i.e. whether it was initially completely molten or if the molten portion was limited to a global magma ocean. To address these issues, I conducted basic structural analyses of lobate scarps at two locations on the Moon. One location lies in the highly cratered highlands between the craters Apollo and Korolev near the South Pole Aitken Basin. The other location lies between Mare Imbrium and Mare Serentatis near the Apollo 15 landing site. Simple calculations using Mohr-Coulomb failure laws are used to constrain quantities such as fault dip, maximum depth of faulting, and the magnitude of compressive stresses. Input parameters for these calculations – including the radius of curvature of the scarps, fault trace length, and orientation – were directly measured from high-resolution LROC imagery. Using crater counting methods, the ages of the fault scarps at the study sites were also determined. The amount of shortening and the rate of slip on faults were then calculated from the modeled ages and geologic cross-sections. We find 41.2 m to 1.3 km of total horizontal throw across the lobate scarps we studied, and horizontal throw rates that range from 1.1 m/Ma to 93.3 m/Ma. The total vertical throw was found to be 15 m to 115 m, with total vertical throw rates of 0.6 m/Ma to 8.2 m/Ma. Total net

slip was also calculated and ranges from 51.5 m to 1.3 km, with net slip rates of 1.3 m/Ma to 93.6 m/Ma. Because the lobate scarps we studied have crisp morphologies, young modeled ages, and high stress values, we favor the ITM thermal model for the Moon.

TABLE OF CONTENTS

Page

LIST OF TABLES

Page

LIST OF FIGURES

Page

1. INTRODUCTION

It is widely accepted that the Moon was formed from a large impact on the proto-Earth (Hartman and Davis, 1975; Cameron and Ward, 1976). As a result of this large impact, the initial thermal state of the Moon was most likely molten, either completely (Binder and Lange, 1980) or, alternatively, to depths of up to 1000 km, forming a magma ocean (Solomon and Chaiken, 1976; Solomon and Head, 1979; Elkins-Tanton, 2011). In either case, the Moon's mantle and crust have cooled from an initially molten state, and, due to this cooling, the Moon's crust has contracted, creating thrust faults that manifest themselves as surface ruptures and lobate scarps (Binder, 1982; Watters et al., 2010). According to Binder and Lange (1980), the lunar radius has decreased by 5 km as a result of this faulting. More recently, estimates of the strain released by the formation of the scarps have suggested a much smaller decrease in lunar radius of approximately 100 m (Watters et al., 2010).

Early studies by Binder and Gunga (1985) were conducted using images from the Apollo Panoramic Camera, leaving research confined to the equatorial region. With new, high resolution images from the Lunar Reconnaissance Orbiter (LRO), the global spatial distribution of lobate scarps can be mapped and the morphology and topography of the lunar surface can be viewed in greater detail than possible before, allowing quantitative structural measurements to be made of the scarps and the faults that produced them. Furthermore, by applying the crater counting method on surfaces cut by the faults, we can determine the age of the scarps and determine how recently active faulting has been on the Moon.

Basic lunar geologic knowledge is crucial for an effective regional/global survey of lobate scarps and how they correlate with the theory of a contracting Moon. A structural understanding of the Moon is imperative since there are no plate tectonics. If tectonic activity is

recent, such vital information about the recency of fault movement is needed in the prospect of building safe infrastructure in seismically safe locations. By investigating previously undetected fault scarps, this research will further test between the initially totally molten (ITM) and the lunar magma ocean (LMO) thermal models, determine better constraints on the resulting amount and timing of crustal shortening, and improve our understanding of the stress state of the Moon. To do this, I have investigated two geologically diverse and unexplored areas, both of which contain lobate scarps: (1) Apollo and Korolev craters near South Pole Aitken Basin (Figure 1); and (2) the area between Mare Imbrium and Mare Serentatis, near the Apollo 15 landing site (Figure 2).

2. BACKGROUND

Knowledge of lunar geology, particularly the nature of the lunar crust and structural features such as lobate scarps, is essential for this research. This work is theoretically based on fault mechanics applied to the structural analysis of thrust fault scarps, and that material is also presented here in detail.

2.1 Lunar Geology and Thermal History

The Moon's crust comprises two terrane types: maria and highlands. The maria form smooth basaltic plains within large impact basins and are easily seen from Earth as the distinctive dark areas on the near side of the Moon. The maria range in age from ~2 to 4 Ga (Lee, 1997; Hiesinger, 2000). Maria only cover 1% of the surface on the far side while covering 31.2% of the near side of the Moon (Gillis and Spudis, 1996). The lunar highlands are composed of anorthositic rocks that are older than 4 Ga, and they are highly saturated with impact craters (Lee, 1997). The highlands characteristically include the areas of both the highest topography and albedo, and, unlike the maria, which are concentrated on the nearside, the highlands are distributed all over the Moon. Lobate scarps have been found in both the mare and highlands (Binder, 1982; Watters et al., 2010).

Unlike Earth, the Moon has no plate tectonics, making tidal forces and meteoroid impacts the most common sources of global-scale stresses, with observed maximum stress values reaching 100 kPa, regardless of thermal history (Binder and Gunga, 1985). According to the ITM model, the lunar surface should have young (<1 Ga) thrust faults created from modern compressional stresses of up to 350 MPa (Binder, 1982). Alternatively, if the Moon had a relatively shallow LMO with depths between 300-1000 km and a cool interior at 1700-1800 K

(Solomon and Chaiken, 1976; Solomon and Head, 1979; Spohn, 2001), the global stresses in the crust should now be less than 100 MPa, insufficient to allow thrust faults to initiate. As a result, the LMO model predicts that the lunar surface should be free of young, compressional tectonic features, with thrust faulting limited to the Moon's early geologic history (>3 Ga) (Solomon and Chaiken, 1976). In addition, since more stress is required to break faults in the highlands versus the mare, the LMO model predicts that the highlands should not have lobate scarps or other compressional features of any age (Solomon and Chaiken, 1976; Solomon and Head, 1979).

The fact that lobate scarps are indeed observed in the highlands as well as the mare would seem to discount the LMO model. Studies of scarps observed in Apollo imagery and thermoelastic stress models (Binder and Lange, 1980; Binder, 1982; Binder and Gunga, 1985) have shown that compressional stresses related from cooling a completely molten Moon would currently be up to 350 MPa, much higher than those predicted by the LMO model, and sufficient to allow thrust faults to occur in both the highlands and the mare. Recently, demonstrably young thrust faults have been discovered throughout the lunar surface in LROC images, which further suggests that large compressional stresses have persisted to recent time (Banks et al., 2012).

However, a recent study by Banks et al. (2012) suggests that faults can still occur in the highlands under the LMO model. Investigation of observed lobate scarps in the lunar highlands by Banks et al. (2012) demonstrated compressional stress values of ~16 MPa, too low for the ITM model but consistent with the LMO model. Further uncertainty has been produced by the discovery of young, shallow (depths ranging from ~1 m to ~17 m) graben on the Moon (Watters et al., 2012). The existence of these features is problematic since the high compressional stresses (< 350 MPa) predicted by the ITM model for recent time should suppress the majority of normal faulting (Watters et al., 2012).

A key uncertainty in all of these arguments is also how ancient or recent these tectonic features are, since the timing of compression (and extension) is poorly constrained. Given these uncertainties and the conflicting conclusions of previous studies, it is not clear which model best explains the current stress state and the initial thermal state of the Moon.

2.2 Lobate Scarps

Scattered throughout the lunar surface are morphologic features called lobate scarps. Based on their general crisp appearance and the lack of superimposed large-diameter impact craters, lobate scarps are among the youngest (≤500 Ma to 1 Ga) landforms on the Moon (Binder, 1986; Watters et al, 2010). These scarps are interpreted to be compressional tectonic features created by reverse slip on faults (Binder, 1982). Cross-cutting relationships of partially concealed, small impact craters shows that these scarps are the result of thrust faults (Watters et al., 2010). Characteristically, lobate scarps have steeply dipping scarp faces and a linear or curvilinear asymmetric shape, leading to interpretation that the faults have an arcuate (conical) geometry (Binder and Gunga, 1985; Watters et al., 2010). Typically, the lobate scarps occur in complexes that consist of a set of smaller, connected segments. (Binder, 1982). The traces of the lobate scarps can be as long as 10 km, occurring in a series of 10 or more subscarps. Previous research (Binder and Gunga, 1985; Watters et al., 2010) has shown that lunar thrust faults have a low dip angle, averaging 21˚ ± 0.5˚, and they have a maximum depth of 6 km.

For dip slip faults, the height of the scarp is an estimate of the vertical displacement of the fault. Previous work has shown that the maximum relief – and, therefore, the net vertical slip – across the lobate scarps is generally <100 m (Watters et al., 2010). Recent studies have shown

scarps exhibiting a maximum relief of 150 m (Banks et al., 2012), and they generally have no preferred orientation, suggesting there is no favored direction of compressional stresses (Binder and Gunga, 1985). Lobate scarps have been recently found using high-resolution images from LROC at all latitudes between the equator and ± 60˚, and the distribution of scarps at middle to low latitudes on both the nearside and the far side of the Moon suggests that thrust faults are globally distributed and consistent with a large-scale contractional strain (Watters et al., 2010).

2.3 Fault Mechanics

In this study, Mohr-Coulomb failure was used to understand the compressional stress state of the Moon following the methodology of Binder and Gunga (1985) and Binder (1982). The compressional tangential stress (σ) needed to produce a thrust fault can be calculated using the formula (Binder and Gunga, 1985):

$$\sigma \geq K\rho g z + S \qquad (1),$$

where ρ is the density of the material (mare basalts, ρ = 3200 kg/m^3; highlands, ρ = 2500 kg/m^3), g is the gravitational acceleration (1.623 m/s^2 for the Moon; Binder, 1982), z is the depth of faulting, and S is the crushing strength of rock (400 ± 300 MPa Binder, 1986). The first term in Equation (1) accounts for the frictional strength of a fault, while the second term accounts for the intrinsic material strength needed to be overcome to break a new fault. Laboratory experiments by Binder (1982) using a circular box with moist sand, showed that the faults only form after brecciated material has compacted, in which case there is an effective S that accounts for the crushing strength of the material. Binder and Gunga (1985) estimated S for the lunar regolith and megaregolith to be 150 to 700 MPa (400 ± 300 MPa).

The parameter K in Equation (1) is a function of the coefficient of friction (F) (Binder and Gunga, 1985):

$$K = \frac{\sqrt{1+F^2}+F}{\sqrt{1+F^2}-F} \qquad (2),$$

where

$$F = \frac{1}{\tan\left(\frac{4}{\pi}\psi\right)} \qquad (3),$$

and ψ is the half angle of the scarp (discussed in further detail in Section 3.1). Equations (1)-(3) yield constraints on the amount of compressional stress needed to produce faulting. Other quantities, such as the maximum depth of faulting (Z) and the dip angle (θ), are given by (Binder and Gunga, 1985):

$$Z = R \tan(0.63\ \psi) \qquad (4)$$

and

$$\theta = \frac{2}{\pi}\psi \qquad (5),$$

where R is the radius of the scarp and ψ is the half angle of the scarp (Figure 3). Measurement of R and ψ from LROC images of lobate scarps will be discussed in further detail in Section 3.2.

2.4 Crater Counting

The relatively crisp appearance of lobate scarps is an indication that they are young morphologic features. It is important to determine the age of the faults that create the lobate

scarps because the two competing lunar thermal models have different predictions about the timing of crustal shortening. The LMO model predicts that compressional faulting occurred early in lunar geologic history (~3 Ga) while the ITM model predicts that compressional faulting occurred more recently (<1Ga).

Determining the regency of these lobate scarps can be accomplished with crater counting. Crater counting is a method for obtaining model ages for planetary surfaces. Given a measured crater size-frequency distribution (CSFD) and an assumed impact flux over time, an age (since the last resurfacing event) can be calculated (Öpik, 1960; Baldwin, 1964; Shoemaker et al, 1970a, 1970b; Neukum, 1971). Finding absolute ages is accomplished by fitting a cumulative CSFD of a selected area to a known production function (PF) and a known a chronology function (CF) for a user-specified range of crater sizes. The PF defines the relationship between the number of craters of a given size and the number of craters of any other size, while the CF describes the number of impact events as a function of time (i.e. cratering rate). For this research, crater count results are illustrated with cumulative crater frequency (N_{cum}) isochron plots (Kneissl et al, 2011). This plot shows the cumulative crater frequency as function of crater diameter in log-log space. On such a plot, one can define contours of constant age, which are termed isochrons. When the CSFD is plotted on such a diagram the data will define linear arrays parallel to the isochrons, and an age can be determined by interpolating between isochrons. We used the CF and PF of Neukem et al. (2001) to model surface ages.

Resurfacing and erosional events commonly decrease the number of craters, ultimately changing the CSFD, by preferentially eliminating the smaller impact craters due to their low topography and relatively small size. Therefore, the oldest surfaces, in an absolute sense, may have experienced multiple resurfacing events over time, and, in some cases, it is possible to

interpret this from the N_{cum} plot (Michael and Neukum, 2010). Characteristically, resurfacing events will result in a 'kink' between linear arrays of data points in the N_{cum} plot. Previous modeling work has shown that the hanging wall surface proximal to a lobate scarp will display a younger crater count age than the footwall (van der Bogert et al., 2012). This difference in age is interpreted to be caused by seismic activity during scarp formation. Such seismic activity could destroy small craters and therefore cause partial resurfacing, yielding a younger apparent surface age.

3. METHODS

Remote sensing, geologic mapping, structural analyses, and 3D visualizations were used to characterize and investigate lunar lobate scarps. These methods are described in detail below.

3.1 Remote Sensing Data

For almost three years, LRO has been continuously mapping the lunar surface, returning a vast amount of imagery and topographic data, and exceeding its original one-year mission around the Moon. Of the seven instruments on the LRO spacecraft, this study utilizes two: LROC (Lunar Reconnaissance Orbiter Camera) and LOLA (Lunar Orbiter Laser Altimeter).

LROC (http://www.lroc.asu.edu/) comprises three high-resolution cameras: two Narrow Angle Cameras (NACs) and one Wide Angle Camera (WAC). The main purpose of NAC is to investigate meter-sized surface features in relation to future landing sites, along with characterizing conditions of polar illumination and identification of possible resources. WAC imagery is intended to characterize polar illumination and identify potential resources. NAC images are panchromatic (400-760 nm) with a resolution of 0.5 to 2 m/pixel over a 5-km wide and 25-km long swath (Robinson et al., 2010). WAC images include seven color bands (320-690 nm), each of which has a spatial resolution of 100 m/pixel over a 105-km long and 60-km wide swath (Chin et al., 2007; Robinson et al., 2010). To date, there is complete global coverage of the Moon with WAC images whereas NAC global imagery coverage is still being obtained by LROC. In this study, WAC images were primarily utilized to search for previously unidentified scarps because they offer a wider, synoptic view of the lunar surface than the NAC images. We used NAC images for detailed photointerpretative mapping, for making the measurements required by the Mohr-Coloumb calculations, for extracting topography using photoclinometry, and for preparing visualizations.

LOLA is a laser altimeter designed to precisely map the topography of the Moon. It determines the global topography at high resolution using a pulse detection laser altimeter (Chin et al., 2007). The LOLA digital elevation models (DEMs) have an along-track horizontal spatial resolution of 20 m/pixel while providing a characteristic height resolution of 30 m. LOLA DEMs were used in the creation of 3D visualizations.

3.2 Remote Sensing Methods

For the initial search for previously unidentified scarps in the LROC WAC and NAC database, the LROC Quick Map tool (http://target.lroc.asu.edu/da/qmap.html) was used. This tool is a fast and easy interface to globally mosaicked LROC imagery in the Planetary Data System (PDS; http://pds.nasa.gov/) database. It includes a zoomable map with resolutions down to 50 cm/pixel, feature overlays (including known craters and Apollo landing sites), a search tool to identify available LROC images in the search area, and a 3D ground view. The zoomable map can be viewed in three map projections: south and north pole orthographic maps for latitudes greater than ± 60° latitude; and a equidistant cylindrical global map that covers up to ±75° latitude. Overlay features help to search for and identify known locations. To assist in locating lobate scarps with the Quick Map tool, previously found scarps were used as a morphology reference (Binder and Gunga, 1985; Watters et al., 2010). The 3D ground views allow one to select an area of interest and view a WAC monochrome mosaic draped onto the global WAC DEM. Once a scarp was identified using the Quick Map tool, the search tool was used to find and extract NAC or WAC images for the desired area. These images were used in further analyses (see Section 3.3).

ENVI 4.6 was used for NAC image orientation correction, georeferencing, and image preparation for structural analysis. Not all NAC images were in the correct orientation (e.g. some images are transposed and rotated 90° counterclockwise). These images had to be reoriented (e.g. top of image is the northern edge) in order to accurately georeference them and in order to use them for photointerpretation. To georeference the NAC imagery, geographic corner coordinates and pixel sizes obtained from the image metadata provided by the PDS were applied to the image. All images were projected into an equirectangular projection (see Table 1 for projection parameters). Because of their extremely-high resolution, NAC image files are quite large, causing problems even on workstations with a lot of memory. To produce image basemaps of reasonable size for use in software such as ArcMap, NAC images were resized in ENVI using nearest neighbor resampling. Image resolutions were reduced from 0.61-1.46 m/pixel to 1.73-4.17 m/pixel, reducing the image size from ~500 MB to ~60 MB. To create even smaller image files for use in ArcMap, the resampled NAC scenes were then subsetted to inclue only the immediate area around the slobate scarps.

Once the NAC images were preprocessed, photogeologic maps were created in ArcMap, at scales between 1:100,000 and 1:200,000. The purpose of the photogeologic mapping is to display and identify geologic features such as rock types, impact craters, and faults. Mapping these geologic features reveals superposition relationships between surface units and geologic structures (eg. craters, lobate scarps), which yields important relative timing information. Map units were dominantly variations in anorthositic highlands rocks, as well as various impact ejecta units. The distinctions made among the anorthositic materials were differences in surface texture (e.g. smooth versus more cratered), albedo, and density of impact craters.

Structural measurements were then made from the photogeologic maps and these were used for fault dynamic calculations (Equations (1)-(5)). Using ArcMap, measurements of the radii (R) and half angles (ψ) of fault scarps (Figure 3) were made from the NAC-derived photogeologic maps. This process can prove difficult due to the scarp's morphology. A characteristic of lobate scarps is that they consist of a series of arcuate segments, with the smaller segments having the smallest radii of curvature (Figure 4). However, the smaller segments typically define the trace of a larger compound scarp. As shown in Figure 4, the trace of the compound scarp lies tangent to the centers of the smaller subscarp segments. The compound scarp is the ideal one to measure as it correctly represents the geometry of the fault plane (Binder, 1982). All measurements were recorded in Excel spreadsheets (Table 2) and the data were processed with a MATLAB code (Appendix A) that was created to implement Equations (1)-(5). The dip results of the Mohr-Coloumb calculations were draped onto maps created in ArcMap (Figures 5-9) to show spatial variations of the measured and calculated parameters as a function of distance along the scarp.

We were interested in obtaining quantitative measurements of scarp height from which estimates of vertical and horizontal slip could be made. Unfortunately, the available LOLA DEMs lack sufficient resolution to extract the required scarp profiles. Specifically, LOLA DEMs provide a characteristic height resolution of 30 m. This is at the limit of the observed average vertical relief (35 m) reported by Banks et al. (2012), making it difficult to measure scarp relief in the LOLA DEMs. In order to obtain topographic data of suitable resolution to extract topographic profiles we employed photoclinometry. This process calculates a DEM from a single 2D, high resolution NAC image by modeling the geometric relationships between solar illumination, topography, and shadows in the image (Lena, 2009). A MATLAB code (Appendix

B) created by Cordova and Hurtado (2011) was used to extract terrain models using the algorithm described by Lena (2009). First a section (~16 to 25 km^2 area) of a full-resolution NAC image that includes the scarp was cropped using ENVI. Since our experience shows that unenhanced images produce DEMs with a large quantity of noise, making them useless for profile extraction, a contrast stretch was then applied using ENVI. Contrast stretching is a simple image enhancement technique that improves the contrast in the image (and the quality of the extracted DEM) by histogram adjustment using a variety of functions (e.g., Gaussian and Equalization). The preprocessed NAC subset was then used as input to the MATLAB photoclinometry code. In addition, the code requires a variety of other input parameters that are included in the NAC image metadata: incidence angle, phase angle, emission angle, pixel size, and the solar azimuth. The output of the code is a gridded surface model at the same spatial resolution as the input image with heights relative to an arbitrary datum. Despite the contrast stretch applied during preprocessing, the output DEMs usually exhibit pervasive striping, an artifact of the algorithm that imparts high-frequency noise to the DEM (Figure 10). To mitigate this problem, scarp profiles extracted from the resulting DEMs using the ENVI profiling tool were manually low-pass filtered.

Scarp height measurements were made from the filtered profiles, and these scarp heights were used as estimates of net vertical displacement. The photoclinometrically-derived topographic models and the photogeologic maps were then used in the creation of simple geologic cross-sections. The cross-sections were produced with Adobe Illustrator and used the dips obtained from the Mohr-Coulomb calculations to project the faults into the subsurface. The cross-sections were then used to compute the net amount of horizontal fault displacement using simple trigonometry.

3.3 Visualization and Structural Data Analysis

To explore the geometries of the lobate scarps, LOLA DEMs were obtained from the PDS and used to create 3D visualizations of the scarps by draping NAC images onto the topography using the Fledermaus visualization software. The resulting 3D visualizations allow us to view the scarps and the surrounding terrain in perspective for geologic interpretations.

In order for the LOLA DEM data to be brought into the Fledermaus software, it was converted from its native integer format to a floating-point format using a code created in MATLAB (Appendix B). The resulting visualizations allowed structural measurements like strike and dip to be made using three-point solutions. Calculation of planar attitudes from three points is solely based on the fundamental theorem of geometry where three points define a representative plane. Calculations were done using the spreadsheet tool developed by Allison (2009). Elevations required for the calculations were measured directly from the LOLA DEMS in Fledermaus while bearings and distances were measured using ENVI.

NAC images and visualizations were viewed at the Cyber-ShARE Visualization Center (C2VIS) at UTEP (http://cybershare.utep.edu/projects/c2vis). C2VIS houses a visualization system comprising a 45 monitor display matrix that is driven by 45 workstations and is interconnected by a high speed network. In collaboration with C2VIS, ENVI 4.6 was installed on their Linux operating system to view NAC imagery. C2VIS had earlier installed both MATLAB and Fledermaus. However, the main purpose of the visualization center in this research is to view the fault scarps at high resolution on a larger scale compared to normal computer monitor to interpret the geologic morphology.

3.4 Crater Counting

For this study, crater counts were performed on surfaces cut by faults using the *CraterTools* extension in ArcMap (Kneissl et al., 2011). *CraterTools* allows the user to define a selected area of an image in which to manually digitize crater diameters. Once an area has been defined, all craters are digitized by using a standard circle tool (included with the extension), allowing users to define the diameter by selecting two points along the rim. The size-frequency statistics for the populations of digitized craters are used to define the CSFD for the area in question. For this study, crater statistics were gathered from both the hanging wall and the footwall surfaces of the scarps we studied. Although there is no minimum requirement, for this study area sizes depended on the extent of the geologic surface and ranged from ~25 to 60 km^2.

After crater digitization is completed, the *CraterTools* extension performs statistical analyses of the resulting CSFD over the digitized area to generate an apparent model age for that surface (Kneissl et al., 2010). The output is a text-file which contains the CSFD and digitized surface area. The file can then be read by a companion program, *CraterStats*, for doing statistics, plotting CSFDs, and determining model ages. Model ages were determined by performing linear fits to linear arrays of data on the N_{cum} plots produced by *CraterStats*. Fits were made by adjusting the range of crater sizes such that secondary craters were excluded. Multiple regressions were performed to converge on a best fit age that included the most craters and with the smallest uncertainty. In addition to the N_{cum} plot, *CraterStats* outputs other vital statistical data (e.g. the number of craters measured and the size of the digitized area). *CraterTools* and *CraterStats* are both freely available for download at http://hrscview.fu-berlin.de/software.html.

Ages were then interpreted with the help of the geologic mapping. Surfaces with model ages that overlap within uncertainly are interpreted to be the same age, e.g. indistinguishable in age. In situations where the model ages for the hanging wall and footwall surfaces do not overlap within uncertainty, we infer a scenario in which resurfacing has occurred. For example, seismic activity could preferentially eliminate small craters proximal to the fault on the footwall side (van der Bogert, 2012). Another possibility is for resurfacing to be caused by ejecta emplacement after a nearby impacts. In this case, the mapping is crucial as it can be used to identify impact ejecta cross-cut by faults (or vice versa), observations that provide the context needed to interpret an age as a maximum or minimum. Finally, the age constraints for the lobate scarps, along with the vertical and horizontal offset measurements obtained from the cross-sections, were used to compute estimated, average rates of net displacement.

4. STUDY AREAS

The two study areas chosen for this research are: (1) Apollo and Korolev craters near South Pole Aitken (SPA) Basin (Figure 1); and (2) the area between Mare Imbrium and Mare Serentatis, near the Apollo 15 landing site (Figure 2). These sites are located in areas with significant geologic differences between them and on opposite sides of the Moon. The goal in researching these areas is to determine if the lobate scarps at these sites were created under similar or different compressional stress regimes, establish whether their timing was similar or not, and obtain evidence to support either the LMO or ITM thermal models for the Moon.

4.1 Far Side of the Moon (Study Area 1)

Study Area 1 (Figure 1) is located in the rugged, densely cratered anorthositic highlands on the far side of the Moon. It has been chosen for its geologic setting, dominated by the highlands and as an unexplored research area for lobate scarps. Located at the southern portion of the study area, the SPA is 2,500 km in diameter and 13 km deep, making it the largest and deepest impact crater on the Moon (Petro and Pieters, 2004). Situated within the SPA, Apollo crater (36.1˚S, 151.8˚W) is a double ringed impact crater with an outer ring diameter of 480 km (Spudis, 1993; Wilhems, 1987) that marks the southernmost section of Study Area 1. Korolev crater (4.0˚S, 157.4˚W) is another double ringed impact crater, situated just outside the SPA. With a diameter of 440 km (Spudis, 1993; Wilhems, 1987), it marks as the northernmost section of Study Area 1.

Three northwest-trending scarp complexes were investigated in Study Area 1: Plummer, Barringer, and Wilsing. Each was named after a prominent crater adjacent to the scarp complex. While these lobate scarp complexes all lie in the same cratered highlands area, they transect a

range of terrain types. Based on differences in the density of craters on the surfaces they cut, the faults associated with these scarp complexes may span a range of ages.

4.2 Near Side of the Moon (Study Area 2)

Two large impact basins enclose Study Area 2 (Figure 2): Mare Imbrium and Mare Serenitatis. Imbrium (32.8˚N, 15.6˚W) is 1,145 km in diameter with a total depth of 12 km (Spudis, 1993). It was formed after a large object struck the Moon no more than 4.25 Ga ago (Compston et al., 1971). A few hundred million years following the impact (~3 to 2.5 Ga), lava began to fill the Imbrium basin forming the mare (Schaber, 1973). Serentatis was formed by an impact over 4 Ga years ago with the earliest mare lava infill event occurring at ~3.8 Ga (Sharpton and Head, 1982). The Serentatis basin has a diameter of 674 km and a depth of 2.4 km. Located between these mare basins, sits the Apollo 15 landing site (2˚67'55.99˚N, 3˚38'1.90˚E) next to anorthositic highlands.

Two scarp complexes were investigated from this area: Joy-1 and Joy-2. They were named for their proximity to Joy crater. Compared to Study Area 1, Study Area 2 has more recent impact craters with associated high albedo ejecta. Both scarp complexes are locating in a hummocky terrain within the highlands, yet they exhibit differences in fault trends. The Joy-1 scarp complex trends northeast while the Joy-2 scarp complex trends north-south.

5. RESULTS

5.1 Study Area 1

5.1.1 Plummer Scarp Complex

Plummer scarp complex (23˚30’25”S, 153˚5’33”W) lies in a topographically low area in which the elevation gradually increases to the north (Figure 11). Anorthositic highlands dominate the area and there are several craters without high albedo ejecta (Figure 12). Plummer is a northwest-southeast trending fault complex, with the entire fault trace spanning ~14 km in length. Five lobate scarps in the Plumber complex were mapped and measured at this location (Figure 12).

The Mohr-Coulomb calculations yield a depth of faulting between ~0.5 km and 1.6 km for these scarps. The faults responsible for the lobate scarps exhibit steeper dip angles (~28˚) in the southeast portion of the area as compared to the northwest section (~10°) (Figure 5). Three-point solutions indicate that the fault has an average strike of 296˚. Calculated stresses range from 411.5 MPa to 481.6 MPa, with an average value of 445 MPa (Table 2).

Figure 13 shows the topographic profiles and interpretive geologic cross sections across the five scarps studied. The lobate scarp in cross-section E-E’ (Figure 13), exhibits a smooth and steeply dipping scarp face, with a vertical offset of 38 m. Profile D-D’ (Figure 13) was taken just east and slightly south of profile E-E’. Along this profile, the scarp appears to be more rugged, with a slight step in the middle of the scarp face, possibly an indication of multiple displacement events or artifacts from the DEM. The total vertical throw represented here is 61 m. Profile B-B’ (Figure 13) displays the typical asymmetrical shape of lobate scarps found by Banks et al. (2012). The other two profiles (A-A’ and C-C’ in Figure 13) have a more symmetrical shape. The average total vertical throw across all the lobate scarps in the Plummer complex is 52.8 m, with a range of 21 m to 100 m and a standard deviation of 30 m. The amount

of total horizontal throw ranges from 71 m to 290 m, with an average of 170 m (standard deviation of 96.6 m). We also calculated an average total net slip of 180 m (standard deviation: 98 m), with a range of 51 m to 1.3 km.

Crater counts reveal that the footwall surface age is 20.8 ± 1.8 Ma and the hanging wall surface age is 22.3 ± 1.7 Ma (Figures 14 and 15). Because the model ages lie within uncertainty of one another, we take ~21 Ma to be the age of the surface cut by the fault scarp. Given the crater count-derived age, we determine average horizontal throw rates for the Plummer scarp complex that range from 3.4 m/Ma to 13.8 m/Ma, with an average of 8.2 m/Ma. The average vertical throw rate ranges between 1 m/Ma to 4.8 m/Ma, with an average of 8.1 m/Ma. For the average net slip rate, Plummer scarp has a range of 3.9 m/Ma to 14.6 m/Ma, with an average of 8.6 m/Ma.

5.1.2 Barringer Scarp Complex

Barringer scarp complex (28˚16'13.19"s, 154˚15'14.23"W) lies in a heavily impact-bombarded area in the highlands of Study Area 1 (Figure 16). The Barringer fault scarps trace ~12 km up topography and have a northwest-southeast trend. The fault cross-cuts a large hill, possibly an old eroded crater wall (Figure 17). The footwall and the upper northeast corner of the hanging wall are both heavily cratered (Figure 16). The bulk of the smooth highlands unit is on the hanging wall, with only a small section on the footwall (Figure 16). Craters in the surrounding area have no fresh impact ejecta, implying that they were not recently created.

The Barringer scarps have an average dip of ~19˚, exhibiting steeper dips (~24˚) in the southeast portion (Figure 6). Calculated depths of faulting range from 1 km to 1.5 km. The

stress calculated for this scarp complex is an average of 446 MPa, with values ranging from 428.8 to 474.1 MPa. (Table 2).

Three cross-sections were extracted for Barringer scarp complex (Figure 18). The lobate scarp in cross-section A-A' (Figure 18) exhibits a smooth and steeply dipping scarp face with a vertical offset of 15 m. Profile B-B' (Figure 18) was taken adjacent to profile A-A'. Here the scarp also appears smooth and with a similar steepness slope to scarp profile A-A'. The measured vertical offset along B-B' is 15 m. Cross-section C-C' (Figure 18) displays the same scarp morphology as scarp profiles A-A' and B-B'. The average total vertical throw across all the lobate scarps studied at Barringer is 20.6 m, with a range of 15 m to 22 m (standard deviation of 5.1 m). The amount of total horizontal throw ranges from 48 m to 81 m, with an average of 61 m (standard deviation of 18 m). The average total net slip is 64 m, with a range of 53 m to 85 m (standard deviation of 18 m).

At first, we had assumed that the highlands cratered units (Figure 16) in both the footwall and the hanging wall were age equivalent because their similar heavily cratered appearances. Crater counts, however, have shown that these two surfaces, in fact, have different ages and are therefore representative of multiple resurfacing events (Figures 19 and 20). Highlands cratered unit 1 (in the footwall) is the oldest at 126 ± 8 Ma, with the highlands cratered unit 2 (in the hanging wall) at 20.7 ± 2.5 Ma. The highlands smooth unit (Figure 16) has the youngest age, 10.6 ± 1.5 Ma. Because the fault cuts the highlands smooth unit (Figure 16), the scarp likely is post-10 Ma in age. Based on this timing, the average horizontal throw rates for the Barringer scarp complex range from 4.8 m/Ma to 8.1 m/Ma, with an average rate of ~6.1 m/Ma. The average vertical throw rate is 2 m/Ma, with a range of 1.5 m/Ma to 2.5 m/Ma. The average net slip rate is 6.4 m/Ma with a range of 5.3 m/Ma to 8.5 m/Ma.

5.1.3 Wilsing Scarp Complex

Wilsing scarp (20˚21'40.34"S, 156˚8'41.10"W) sits within a large, ancient crater in a densely cratered area in Study Area 1 (Figures 21 and 22). Located in the highlands, the scarps in this complex trace over 19 km in a northwest to southeast direction, except for one scarp that trends north-south. Compared to the all the other scarps measured in this study, the scarps in the Wilsing complex have the shallowest dip angles (~4˚) and contain some of the highest stress values (~760.3 MPa). The average dip of lobate scarps in the Wilsing complex is ~17.6˚, with shallower dips (~5˚) in the northwest portion (Figure 7). Three-point solutions indicate that the fault has an average strike of 306.3˚, although one scarp has a calculated strike of 006˚. Faulting can reach depths of up to ~1.7 km and can be as shallow as 500 m (Table 2).

Five cross-sections were extracted to show the geometry of the faults (Figure 23). The lobate scarp in cross-sections A-A' – E-E' (Figure 23), all exhibits a smooth scarp face. Profile B-B' shows the smallest amount of vertical displacement (25 m). Profile E'-E' (Figure 23) was taken in the southeast section of the complex. This scarp here has the same smooth shape as scarps A-A'-D-D', though it has a more prominent asymmetrical morphology. The average total net slip across all the lobate scarps in the Wilsing complex is 77 m, with a range of 91 m to 1.3 km (standard deviation of 521 m). The amount of total horizontal throw ranges from 88 m to 1.3 km, with an average of 578 m (standard deviation of 528 m). The total vertical throw is an average of 76.4 m, with a range of 25 m to 115 m (standard deviation of 33.3 m).

Crater counts in the area proximal to the scarp reveal complicated differences in surface age. The hanging wall contains more and larger craters while the footwall had more recent impacts displaying high albedo ejecta (Figure 22). Crater counts reveal two resurfacing events

that affected the hanging wall (Figures 24 and 25). The first event occurred at 30.9 ± 8.2 Ma and the second at 13.5 ± 0.85 Ma. The footwall was found to have a surface age of 6.39 ± 0.94 Ma.

We interpret the young footwall age (~6 Ma) to be the result of recent impacts into the higher topography area adjacent to the fault, an area that has been blanketed by higher albedo ejecta material (Figure 25). The area in the footwall of the scarp complex that has not been affected by the higher albedo impact craters is similar to the hanging wall surface and best represents the age of the surface cut by the fault (~14 Ma), which we take to be the maximum age of faulting. The older age (~31 Ma) obtained for the hanging wall probably represents an older resurfacing event, likely predating the fault, that occurred in association with the large impact crater at the westernmost edge of Figure 25.

Average horizontal throw rates for the Wilsing scarp complex range from 6.3 m/Ma to 93.3 m/Ma, with an average rate of ~ 41.3 m/Ma. The average vertical throw rate ranges from 1.8 m/Ma to 8.2 m/Ma, with an average of 5.4 m/Ma. The calculated average net slip rate is 36.3 m/Ma and has a range of 6.6 m/Ma to 93.6 m/Ma.

5.2 Study Area 2

5.2.1 Joy-1 Scarp Complex

Joy-1 scarp (25˚21'56.29"N, 6˚52'54.61E) is a northeast-southwest trending lobate scarp complex that lies in hummocky highland terrain (Figures 26 and 27). Most of the faults seem to dip towards the east while a few dip towards the west (Figure 8). Calculated dips ranged from 5.5° to 36°, with an average of 19.7°. The average strike of the Joy-1 scarps is 042°, with two scarps trending 305.5°. The main trace of the fault is 18 km in length. Calculated depths of faulting range from 500 m to 1.7 km, with an average of just under 1 km. Compressional

stresses needed to initiate faulting are calculated to be approximately 470 MPa and range from 407.8 to 610.4 MPa (Table 2).

Eleven cross-sections were extracted to show the geometry of the faults (Figure 28). The lobate scarp in cross-section C-C' (Figure 28) exhibits an asymmetric shape similar to scarps investigated by Banks et. al. (2012) and has a vertical offset of 17 m. The scarp in profile C-C' best presents the steeply dipping scarp face seen in other profiles for the Joy-1 complex. The scarp in profile B-B' (Figure 28) displays a shallower scarp face with a vertical displacement of 33 m. In profile I-I' (Figure 28), the hanging wall of the lobate scarp slopes steeply to the west at an angle (28°) that is simlar to the dip of the fault.

Based on the topographic profiles, the total vertical throw across all the lobate scarps in the Joy-1 complex is 42 m, with a range of 17 m to 55 m (standard deviation of 13.2 m). The amount of total horizontal throw ranges from 45.4 m to 186.5 m, with an average of 97 m (standard deviation of 95 m). Total net slip along the fault averages 147 m, with a range of 52 m to 341 m (standard deviation of 93 m).

In the southeast section of the Joy-1 scarp complex, crater counts yield an age for the footwall surface 24.6 ± 6.5 Ma and 38.2 ± 7.9 Ma for the hanging wall (Figures 29 and 30). These ages lie within statistical uncertainty of each other, although the uncertainties are large. However, we believe the younger footwall age demonstrates that resurfacing may have occurred as a result of a fresh impact crater next to the fault (Figure 27). A close inspection of this impact reveals that the Joy-1 scarps cross-cuts the bright ejecta rays produced by the impact (Figure 31) implying the fault is younger than the crater.

In the northeast portion of the Joy-1 scarp complex, crater counts reveal younger ages than those determined for the southwest section. In the northeast area, the footwall is 12.1 ± 1.9

Ma and the hanging wall is 16.7 ± 5 Ma (Figures 29 and 32). Since these ages overlap within their uncertainties, we cannot distinguish those surfaces as being different in age (ca. 14 Ma), so we interpret the fault to have a maximum age of 14 Ma. Young ages in the northeastern section are likely due to resurfacing due to ejecta from a large fresh impact crater south of the scarp. The large fresh impact crater lies southwest of the Joy-1 scarp complex and likely emplaced ejecta past the northernmost Joy-1 scarp. The age that was used to calculate the rates was 14 Ma.

Average vertical throw rates for the Joy-1 scarp complex range from 2.4 m/Ma to 13.3 m/Ma, with an average rate of 6.45 m/Ma. The average horizontal throw rate is 9.4 m/Ma, with a range of 1.2 m/Ma to 3.9 m/Ma. The calculated average net slip rate for the Joy-1 scarp complex is 9.8 m/Ma, with a range of 3.6 m/Ma to 24.4 m/Ma.

5.2.2 Joy-2 Scarp Complex

Joy-2 scarp complex (25˚8'33.93"N, 7˚48'53.35"E) is the only north-south trending fault complex in this study (Figures 33 and 34). Joy-2 lies in hummocky terrain on the outer eastern edge of the highlands, adjacent to Mare Serenitatis (Figures 2 and 34). The area is free of >1km diameter impact craters and contains several recent, small impact craters. The fault trace is ~16 km in length. The Joy-2 scarps exhibit the steepest dips (18° to 37˚) and the greatest depths of faulting (3.4 km to 4.1 km) of any of the scarps investigated in this study. Using three-point solutions, we calculated an average strike of 327˚. The compressional stress for the Joy-2 scarp complex ranges between 440.7 MPa and 523.6 MPa, with an average of ~481 MPa (Table 2).

Two cross-sections were extracted to show the geometry of the Joy-2 faults (Figure 35). The lobate scarp in cross-section A-A' (Figure 35) exhibits a smooth scarp face, with a vertical offset of 29 m. Profile B-B' (Figure 35) was taken south of profile A-A'. This scarp has the

same smooth shape as scarp profile A-A' (Figure 35), though its vertical offset is significantly less (24 m). The total vertical throw across all the lobate scarps in the Joy-2 complex is 27 m, with a range of 24 m to 29 m (standard deviation of 3.5 m). The amount of total horizontal throw ranges from 45 m to 72 m, with an average of ~58.7 m (standard deviation of 1 m). The total net slip is an average of 65 m, with a range of 54 m to 76 m (standard deviation of 16 m).

Crater counts yield a footwall surface age of 40.3 ± 4.3 Ma and a hanging wall surface age of 41.6 ± 2.6 Ma (Figures 36 and 37). Because they are indistinguishable within uncertainty, we interpret the last resurfacing event to have occurred at ~41 Ma, with faulting post-dating this. Given this timing, the average vertical throw rates for the Joy-2 scarp complex range from 1.1 m/Ma to 1.8 m/Ma, with an average of ~1.4 m/Ma. The average horizontal throw rate is 1.4 m/Ma, with range of 1.1 m/Ma to 1.7 m/Ma. The average net slip rate across the Joy-2 scarp complex is 1.5 m/Ma, with a range of 1.3 m/Ma to 1.9 m/Ma.

6. DISCUSSION

6.1 Structural Geology of the Lobate Scarps

There is very little variation in the fault dynamic results between the study areas, suggesting that a uniform compressional process dominates the formation of lobate scarps in both areas. Structural analyses of the lobate scarps show that the thrust faults producing them have average depth of 1.2 km, with a maximum depth of 4.1 km into the megaregolith. Most of the scarps have low dip angles (<36˚), which are comparable to thrust faults found by Banks et al. (2012). However, Study Area 2 does contain scarps with greater fault depths and steeper dips. Even though the scarps measured are all located in the highlands, the surrounding mare basalt could have an effect on how the lobate scarps are formed. Since mare basalt has a higher density than the anorthositic highlands, faults will break at greater depths in a consolidated material. While all the scarps have fairly uniform compressional stress values (ca. 400 MPa) in both study areas, there are some stress values that are greater than 500 MPa, mainly associated with scarps with shallow dip angles (Figure 38). For faults with shallow dips (<10˚), larger stresses are needed to push over a nearly horizontal plane. Dip angles greater than 10˚ are associated with compressional stress values between 400 MPa and 490 MPa. There is a positive correlation between the dip and depth, with larger dips with increasing depth (Figure 39).

Crater counts yield model ages of 10 Ma to 123 Ma for the lobate scarps analyzed in both study areas. Some locations exhibited multiple resurfacing events, with the footwall typically having the younger surface age, which is the opposite of the pattern reported by van der Bogert (2012).

The amount of total vertical throw for all the lobate scarps studied in both study areas ranges from 46 m to 578 m, with an average of 193 m. Average vertical throw rates range from 1.43 m/Ma to 41.33 m/Ma, with an average of 12.7 m/Ma. Horizontal throw estimates based on

our analyses show an average of 193 m of displacement on the faults we studied at an average rate of 12.7 m/Ma.

The topographic profiles created from the photoclinometrically-derived DEMs show that that many of the scarps have an asymmetric shape. The relief on the scarp faces ranges from 10 m to 105 m, with a mean relief of 43 m. These values are similar to those measured by Banks et al. (2012) on other faults using digital terrain models (DTMs) derived from LROC NAC stereo image pairs. This shows that photoclinometry is a useful tool for estimating terrain shape when other sources of topographic data are lacking.

6.2 Thermal History of the Moon

Figure 40 is a plot of stress vs. depth that illustrates the predictions of the LMO and ITM models. The curves numbered curves show the predicted stresses as a function of depth for different times in lunar history (3 Ga, 2 Ga, 1 Ga, and the present) assuming the ITM thermal history (Binder and Lange, 1980). The green box shows the range of maximum surface stress values predicted by the LMO hypothesis (Solomon and Head, 1979). The blue lines in Figure 40 represent the maximum (dashed), minimum (dashed), and average (solid) stresses needed to initiate thrust faulting according to Equation (1) and for an S of 400 ± 300 MPa. The results of the Mohr-Coulomb failure calculations presented here show compressional stresses that range from 407 MPa to 765 MPa, with an average value of 473 MPa, for an average depth of faulting of 1.2 km (red circle). Note that our calculated average stress plots near the intersection between the 0 Ga curve for the ITM model and the Mohr-Coulomb failure line (Figure 40). This implies that the scarps in this study should be young (<1Ga), assuming the ITM model is correct (Binder and Gunga, 1985). In fact, crater counts on the surfaces cut by the lobate scarps we studied indicate that the thrust faulting is young (<130 Ma).

The fact that our calculated stresses are far larger than the maximum stresses allowed by the LMO model (green box in Figure 40) suggests that the LMO model may be incompatible with what we know about the lobate scarps. It is important to note that this is the direct result of the choice of *S* in Equation (1). In this study and previous work by Binder and Gunga (1985), *S* dominates the calculated results since it is assumed that breaking faults in the lunar crust will be dominated by the material strength, e.g. the crushing and compacting of void space in the brecciated regolith, rather than only the frictional strength on existing faults. In the latter case, *S* would be small, close to 0 MPa, and, if we eliminate *S* from Equation (1), our stress values would lie in the 10's MPa to 100's MPa range. These are very similar to the values calculated by Banks et al. (2012) who assumed that production of lobate scarps on the Moon would be dominated only by the frictional strength of pre-existing faults. If Figure 40 is replotted for Equation (1) with an *S* of 0 MPa (e.g. Banks et al. 2012) and with our results adjusted for the new choice of *S* (Figure 41), our results become compatible with the small modern stresses predicted by the LMO model. Alternatively, our results would be compatible with the ITM model, but only if the scarps are close to 2-3 Ga in age, which our crater counts show to not be the case.

To resolve this uncertainty, we point out that the crisp morphologies, young crater count ages, and geologic cross-cutting relationships observed relative to the lobate scarps at Study Areas 1 and 2 shows that these features have been recently active. We also note that the relatively small scarp heights also may suggest that the faults have not been active for very long. We argue, then, that the lobate scarps are the result of relatively new thrust faults breaking through the upper lunar crust rather than progressive slip on pre-existing faults over the bulk of

lunar history. This suggests a non-zero choice of *S*, likely within the range estimated by Soloman and Head (1979) and Binder and Gunga (1985). We therefore prefer the ITM model.

7. SUMMARY AND CONCLUSIONS

The Moon has been subject to compressional stresses caused by changes in volume as it has cooled (Binder, 1982). Our results demonstrate the ability to make structural geologic measurements of thrust faults at various scales using LROC imagery. These measurements and the calculations based on the measurements yield constraints on the thermal history of the Moon. Previous work has shown that if the initial thermal state of the Moon included a shallow magma ocean, the Moon would have old scarps (>3 Ga) with small compressional stresses (10's MPa to 100's MPa) (Solomon and Chaiken, 1976; Solomon and Head, 1979; Watters et al., 2010). In contrast, the ITM model predicts young (<1 Ga) scarps with high stress values (Binder and Lange, 1980; Binder and Gunga, 1985). Our study has shown that the stresses associated with lobate scarp complexes in two geologically distinct regions of the Moon are associated with compressional stresses in excess of 400 MPa and that the formation of the faults that produced the scarps was likely dominated by the material strength of the upper lunar crust. Model ages from crater counting show that the faults that produced these lobate scarps range from 10 Ma to 123 Ma, implying recent faulting. Together these results suggest that the ITM model is more correct.

REFERENCES

Allison, D. T., 2009, Stuctural Geology Laboratory Manual, 3rd edition, http://www.usouthal.edu/geography/allison/GY403/StructureSpreadsheets.html.

Baldwin, R. B., 1964, Lunar crater counts: *Astronomical Journal*, v. 69, n. 377.

Banks, M. E., Watters, T. R., Robinson, M. S., Tornabene, L. L., Tran, T., Ojha, L, and Williams, N. R., 2012, Morphometric analysis of small-scale lobate scarps on the Moon using data from the Lunar Reconnaissance Orbiter: *Journal of Geophysical Research*, v. 117, doi: 10.1029/2011JE003907.

Binder, A. B., 1982, Post-Imbrium global tectonism: Evidence for an initially totally molten Moon: *Moon and Planets*, v. 26, p. 117-133.

Binder, A. B., 1986, The initial thermal state of the Moon: *Papers Presented to the Conference on the Origin of the Moon*, p. 425-433.

Binder, A. B. and Gunga, H., 1985, Young thrust-fault scarps in the highlands: Evidence for an initially totally molten Moon: *Icarus*, v. 63, p. 421-441.

Binder, A. B. and Lange, M. A., 1980, On the thermal history, thermal state, an related tectonism of a Moon of fission origin: *Journal of Geophysical Research*, v. 85, p. 3194-3208.

Cameron, A. G. W. and Ward, W. A., 1976, The origin of the Moon: *Lunar Science VII*, p. 120-122.

Chin, G., Brylow, S., Foote, M., Garvin, J., Kasper, J., Keller, J., Litvak, M., Mitrofanov, I., Paige, D., Raney, K., Robinson, M., Sanin, A., Smith, D., Spence, H., Spudis, P., Stern,

S. A., and Zuber, M., 2007, Lunar Reconnaissance Orbiter overview: The instrument suite and mission: *Space Science Reviews*, v. 129, n. 4, p. 391-419.

Clark, S.P. (Jr.), 1966, *Handbook of Physical Constants* (*Geological Society of America Memoir*, v. 97), 586 p.

Compston, W., Vernon, M. J., Berry, H., and Rudowski, R., 1971, The age of the Fra Mauro Formations: A radiometric older limit: *Earth and Planetary Sciences Letters*, v. 12, n.1, p. 55-58.

Cordova, J. A. and Hurtado, J. M. (Jr.), 2011, Extraction of elevation models using photoclinometric methods: *Proceedings of the 42nd Lunar and Planetary Science Conference*

Elkins-Tanton, L. T., Burgess, S., and Yin, Q., 2011, The lunar magma ocean: Reconciling the solidification process with lunar petrology and geochronology: *Earth and Planetary Science Letters*, v. 304, p. 326-336.

Gillis, J. J., and Spudis, P. D., 1996, The Composition and Geologic Setting of Lunar Far Side Maria: *Lunar and Planetary Science*, v. 27, p. 404-413.

Hartman, W. K. and Davis, D., 1975, Satellite-sized planetesimals and lunar origin: *Icarus*, v. 24, p. 504-515.

Hiesinger, H., Jaumann, R., Neukum, G., and Head, III, J. W., 2000, Ages of mare basalts on the lunar nearside: *Journal of Geophysical Research*, v. 105, n. E12, p. 29,239-29,275.

Kneissl, T., van Gasselt, S., and Neukum, G., 2010, New software tool for map-projection-independent crater size-frequency determination in ArcGIS: *Proceedings of the 42nd Lunar and Planetary Science Conference*, abstract #1638.

Kneissl, T., van Gasselt, S., and Neukem, G., 2011, Map projection-independent crater size frequency determination in GIS environments-New software tool for ArcGIS: *Planetary and Space Science*, v. 59, p. 1243-1254.

Neukum, G., 1971, *Untersuchungen über Einschlagskrater auf dem Mond.* (Ph.D Thesis): Universität Heidelberg, Germany,

Neukum, G., Ivanov, B. A., and Hartmann, W. K., 2001, Cratering records in the inner solar system in relation to the lunar reference system: *Space Science Reviews*, v. 96, p. 55-86.

Lee, D.-C., Halliday, A. H., Snyder, G. A., and Taylor, L. A., 1997, Age and Origin of the Moon: *Science*, v. 278, n. 5340, p. 1098-1103, doi: 10.1126/science.278.5340.1098.

Lena, R., 2009, A Shape from Shading Refined method for Lunar Domes Heights derived from Carlotto Algorithm: *Selenology Today*, v.16, p. 6-29.

Öpik, E. J., 1960, The lunar surface as an impact counter: *Monthly notices of the Royal Astronomical Society*, v. 120, n. 404, p. xxx-xxx.

Petro, N. E. and Pieters, C. M., 2004, Surving the heavy bombardment: Ancient material at the surface of the South Pole-Aitken Basin: *Journal of Geophysical Research*, v. 109, doi: 10.1029/2003JE0021182.

Schaber, G. G., 1973, Lava flows in Mare Imbrium: Geologic evaluation from Apollo orbital photography: *Proceedings of the Fourth Lunar Science Conference*, v. 1, p. 73-92.

Sharpton, V. L. and Head, J. W., 1982, Stratigraphy and Structural Evolution of Southern Mare Serenitatis: A Reinterpretation Based on Apollo Lunar Sounder Experiment Data: *Journal of Geophysical Research*, v.87, n. B13, p. 10,983-10,998.

Shoemaker, E. M., Batson, R. M., Bean, A. L., Conrad, J. C., Dahlem, D. H., Goddard, E. N., Hart, M. H., Larson, K. B., Schaber, G. G., Schleicher, D. L. S. R. L., Swann, G. A., and Waters, A. C., 1970a., Preliminary geologie investigation of the Apollo 12 landing site, part A. Geology of the Apollo 12 landing site: *Apollo 12 Preliminary Science Report NASA*, n. 235

Shoemaker, E. M., Hait, M. H., Swann, G. A. Schleicher, D. L., Dahlem, D. H., Schaber, G. G., and Sutton. R. L., 1970b, Lunar regolith at tranquility base: *Science*, v. 167, p. 452-455.

Solomon, S. C. and Chaiken, J., 1976, Thermal expansion and thermal stress in the Moon and terrestrial planets: Clues to early thermal history: *Proceedings of the 7th Lunar Science Conference*, p. 3,229-3,243.

Solomon, S. C. and Head, J. W., 1979, Vertical movement in mare basins: Relation to mare implacement basin tectonics and lunar thermal history: *Journal of Geophysical Research*, v. 84, p. 1667-1682.

Spohn, T., Konrad, W., Breuer, D., and Ziethe, R., 2001, The Longevity of Lunar Volcanism: Implications of Thermal Evolution Calcaulations with 2D and 3D Mantle Convection Models: *Icarus*, v.149, p. 54-65.

Spudis, P. D., 2003, *The Geology of Multi-Ring Impact Basins*: Cambridge University Press (New York), 263 p.

Terazono, J., 2007, Implementation of the moonquake database: *Proceedings of the Seventh International Conference on Computer and Information Technology* (October 2007, Fukushima, Japan), p. 139-144, doi: 10.1109/CIT.2007.91.

Turcotte, D. L. and Schubert, G., 2002, *Geodynamics* (2nd edition): Cambridge University Press, 466 p.

van der Bogert, C. H., Hiesinger, H., Banks, M. E., Watters, T. R., and Robinson, M. S., 2012, Derivation of Absolute Model Ages for Lunar Lobate Scarps: *Proceedings of the 43rd Lunar and Planetary Science Conference*, abstract #1847.

Watters, T. R. and Johnson, C. L., 2010, Lunar Tectonics, in *Planetary Tectonics* (edited by Watters, T. R. and Schultz, R. A.), p 121-182. Cmabridge University, Press, New York.

Watters, T. R., Robinson, M. S., Banks, M. E., Tran, T. and Denevi, B. W., 2012, Recent extensional tectonics on the Moon revealed by the Lunar Reconnaissance Orbiter Camera: *Nature Geoscience* , doi:10.1038/NGEO01387.

Watters, T. R., Robinson, M.S., Beyer, R.A., Banks, M. E., Bell, J. F. (III), Pritchard, M. E., Hiesinger, H., van der Bogert, C. H., Thomas, P. C., Turtle, E. P., and Williams, N. R., 2010, Evidence of recent thrust faulting on the Moon revealed by the Lunar Reconnaissance Orbiter Camera: *Science*, v. 329, p. 936-940.

Wilhelms, D., 1987, *The Geologic History of the Moon* (*U.S. Geological Survey Professional Paper*, n. 1348), 302 pp.

Table 1: LROC and LOLA Data.

LROC NAC
M145624586LC
M145631465RC
M1031744532RC
M104476195RC
M104469044LC

LOLA
LDEM_1024_30S_15S_180_210
LDEM_1024_15N_30N_000_030

Map Projection
Lunar Radius: 1,737.4km
Datum: WGS-84 (in meters)
Projection: Geographic Latitude/Longitude

Table 2: Results from Mohr-Coulomb Calculations.

Complex	Scarp	Latitude	Longitude	Radius (R) (km)	Half-Angle (Ψ) (deg)	Dip (deg)	Depth (km)	Coefficient of Friction (F)	Stress (MPa)	Horizontal Displacement (m)	Vertical Displacement (m)	Net Displacement (m)	Horizontal Rate (m/Ma)	Vertical Rate (m/Ma)	Net Rate (m/Ma)
Plummer	1.1	-23.53898	-156.01613	1.5229	43.9	28.0	0.8	0.69	411.7	72	38	81	3.4	1.8	3.9
	1.2	-23.53446	-156.01325	3.0029	43.7	27.8	1.6	0.69	422.9	116	61	131	5.5	2.9	6.2
	1.3	-23.49714	-155.98126	3.5978	15.8	10.0	0.6	2.76	482.7	119	21	121	5.7	1.0	5.7
	1.4	-23.48874	-155.96924	3.0253	15.3	9.7	0.5	2.85	471.7	257	44	260	12.2	2.1	12.4
	1.5	-23.47398	-155.94825	3.3269	29.8	19.0	1.1	1.29	439.3	291	100	307	13.8	4.8	14.6
Barringer	1.1	-28.28545	-154.0945	5.3190	25.2	16.1	1.5	0.34	475.1	52	15	54	5.2	1.5	5.4
	1.2	-28.27444	-154.15008	3.1864	26.9	17.1	1.0	1.64	442.1	81	25	85	8.1	2.5	8.5
	1.3	-28.30277	-154.1789	3.2660	38.4	24.4	1.5	6.96	429.2	48	22	53	4.8	2.2	5.3
Wilsing	1.1	-20.42461	-156.06427	2.3825	56.2	35.8	1.7	5.05	413.4	160	115	197	11.4	8.2	14.1
	1.2	-20.424	-156.09888	2.3935	24.8	15.8	0.7	0.92	441.6	88	25	92	6.3	1.8	6.6
	1.3	-20.40191	-156.11293	6.4605	6.5	4.1	0.5	0.62	764.9	1307	94	1310	93.3	6.7	93.6
	1.4	-20.39356	-156.12783	5.8147	8.9	5.6	0.6	3.27	639.4	760	75	764	54.3	5.4	54.6
	1.5	-20.36912	-156.13959	3.3097	37.5	23.8	1.4	1.61	430.4	165	73	181	11.8	5.2	12.9
Joy-1	1.1	25.2527	6.818064	1.7870	58.1	37.0	1.3	0.30	409.6	41	31	52	2.9	2.2	3.7
	1.2	25.27121	6.83961	4.8043	8.7	5.5	0.5	5.13	601.1	340	33	342	24.3	2.4	24.4
	1.3	25.29525	6.855911	6.3233	12.8	8.2	0.9	3.44	579.3	119	17	120	8.5	1.2	8.6
	1.4	25.31086	6.865739	2.5283	16.1	10.2	0.5	2.70	457.0	139	25	141	9.9	1.8	10.1
	1.5	25.32771	6.86872	6.6110	11.3	7.2	0.8	3.93	613.1	286	36	288	20.4	2.6	20.6
	1.6	25.35037	6.871461	3.3302	36.2	23.0	1.4	0.97	413.8	85	36	92	6.1	2.6	6.6
	1.7	25.32868	6.902706	1.0314	40.2	25.6	0.5	0.81	408.7	75	36	83	5.4	2.6	5.9
	1.8	25.31127	6.906225	1.0386	44.0	28.0	0.5	0.68	407.9	103	55	117	7.4	3.9	8.4
	1.9	25.38034	6.972383	3.2915	43.7	27.8	1.7	0.69	425.3	45	24	51	3.2	1.7	3.7
	2.1	25.45411	6.981186	2.5507	30.2	19.2	0.9	1.27	429.7	129	45	137	9.2	3.2	9.8
	2.2	25.42883	6.963731	3.3168	40.4	25.7	1.6	0.81	428.0	87	42	97	6.2	3.0	6.9
Joy-2	1.1	25.20577	7.819133	6.5644	51.6	32.8	4.2	0.46	441.4	45	29	54	1.1	0.7	1.3
	1.2	25.11185	7.817372	10.2244	28.8	18.3	3.4	1.35	426.0	72	24	76	1.8	0.6	1.9

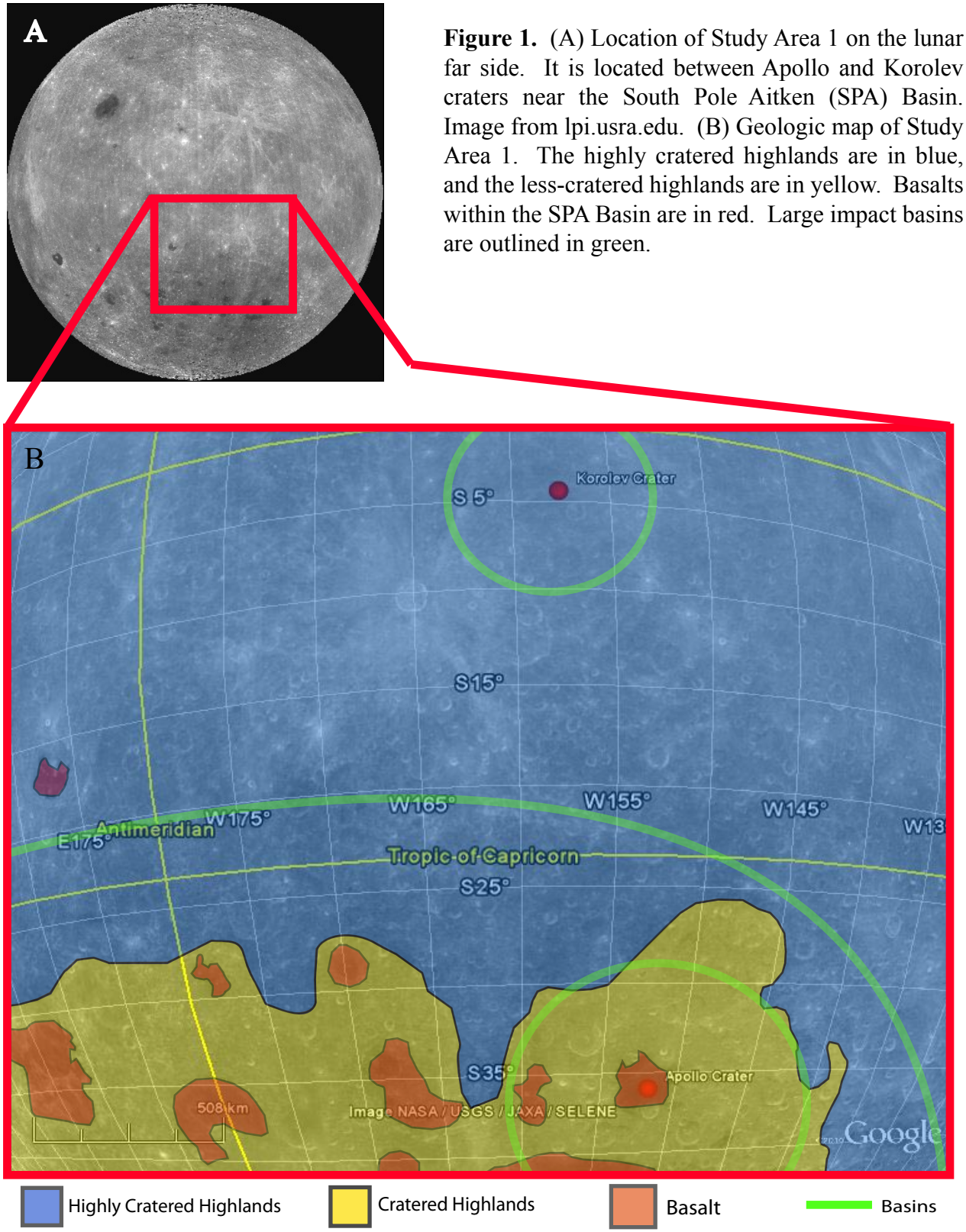

Figure 1. (A) Location of Study Area 1 on the lunar far side. It is located between Apollo and Korolev craters near the South Pole Aitken (SPA) Basin. Image from lpi.usra.edu. (B) Geologic map of Study Area 1. The highly cratered highlands are in blue, and the less-cratered highlands are in yellow. Basalts within the SPA Basin are in red. Large impact basins are outlined in green.

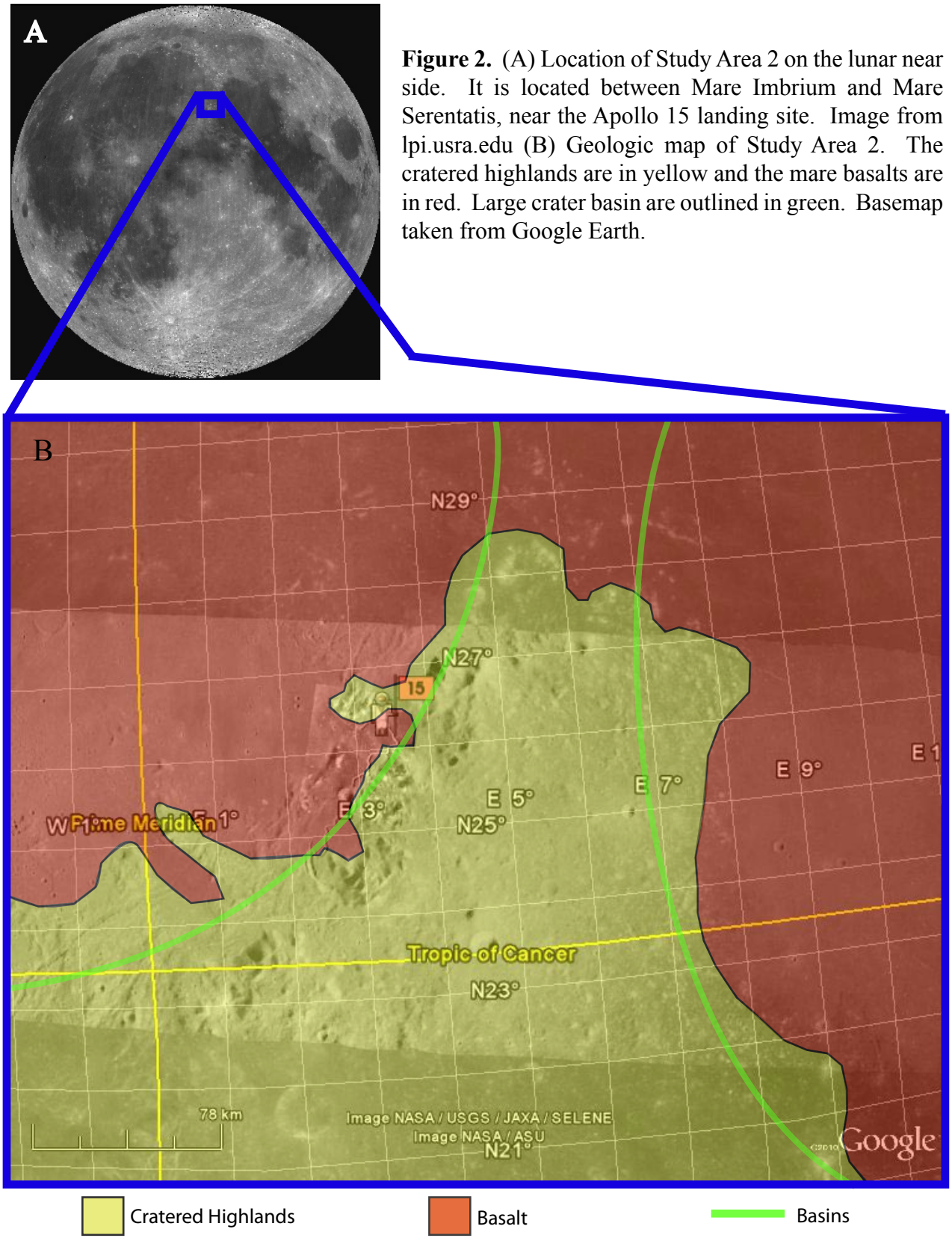

Figure 2. (A) Location of Study Area 2 on the lunar near side. It is located between Mare Imbrium and Mare Serentatis, near the Apollo 15 landing site. Image from lpi.usra.edu (B) Geologic map of Study Area 2. The cratered highlands are in yellow and the mare basalts are in red. Large crater basin are outlined in green. Basemap taken from Google Earth.

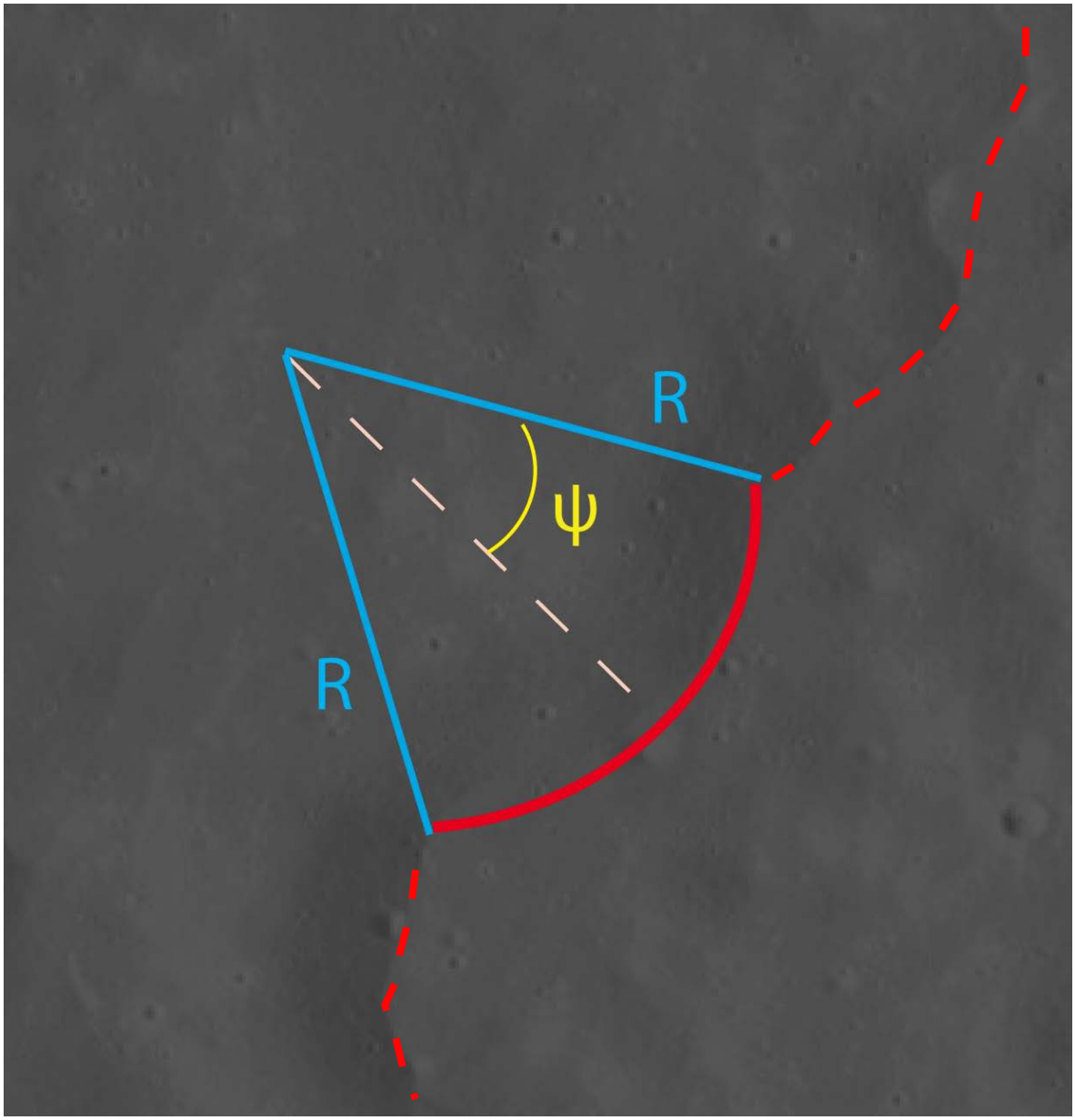

Figure 3. Example of how measurements from individual scarps were made. Red lines show three scarps within this scarp complex. Solid red line shows the trace of the scarp being measured. Radii of curvature, R (blue lines), and the half angle, ψ can be measured directly from photogeologic maps made from LROC imagery.

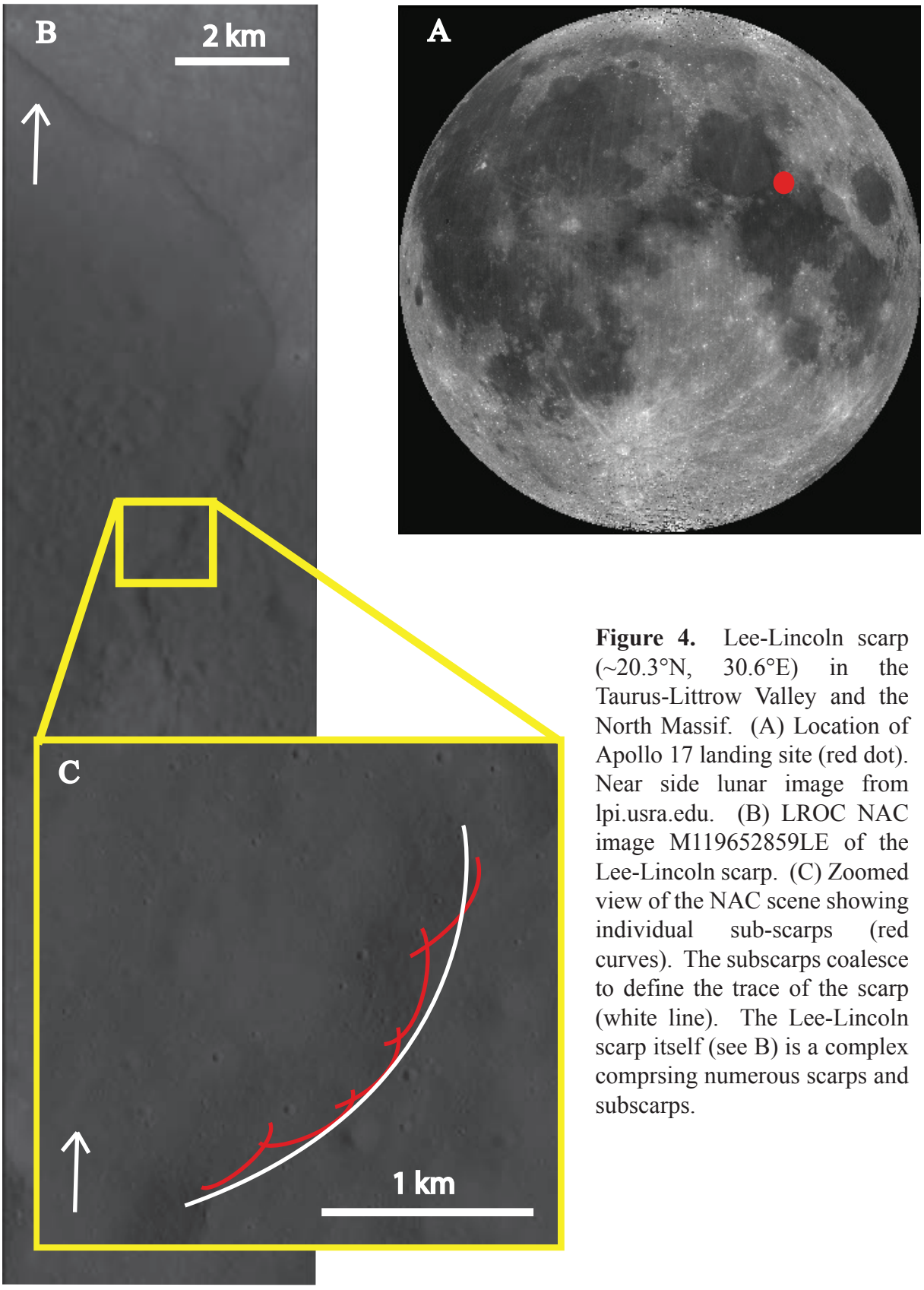

Figure 4. Lee-Lincoln scarp (~20.3°N, 30.6°E) in the Taurus-Littrow Valley and the North Massif. (A) Location of Apollo 17 landing site (red dot). Near side lunar image from lpi.usra.edu. (B) LROC NAC image M119652859LE of the Lee-Lincoln scarp. (C) Zoomed view of the NAC scene showing individual sub-scarps (red curves). The subscarps coalesce to define the trace of the scarp (white line). The Lee-Lincoln scarp itself (see B) is a complex comprsing numerous scarps and subscarps.

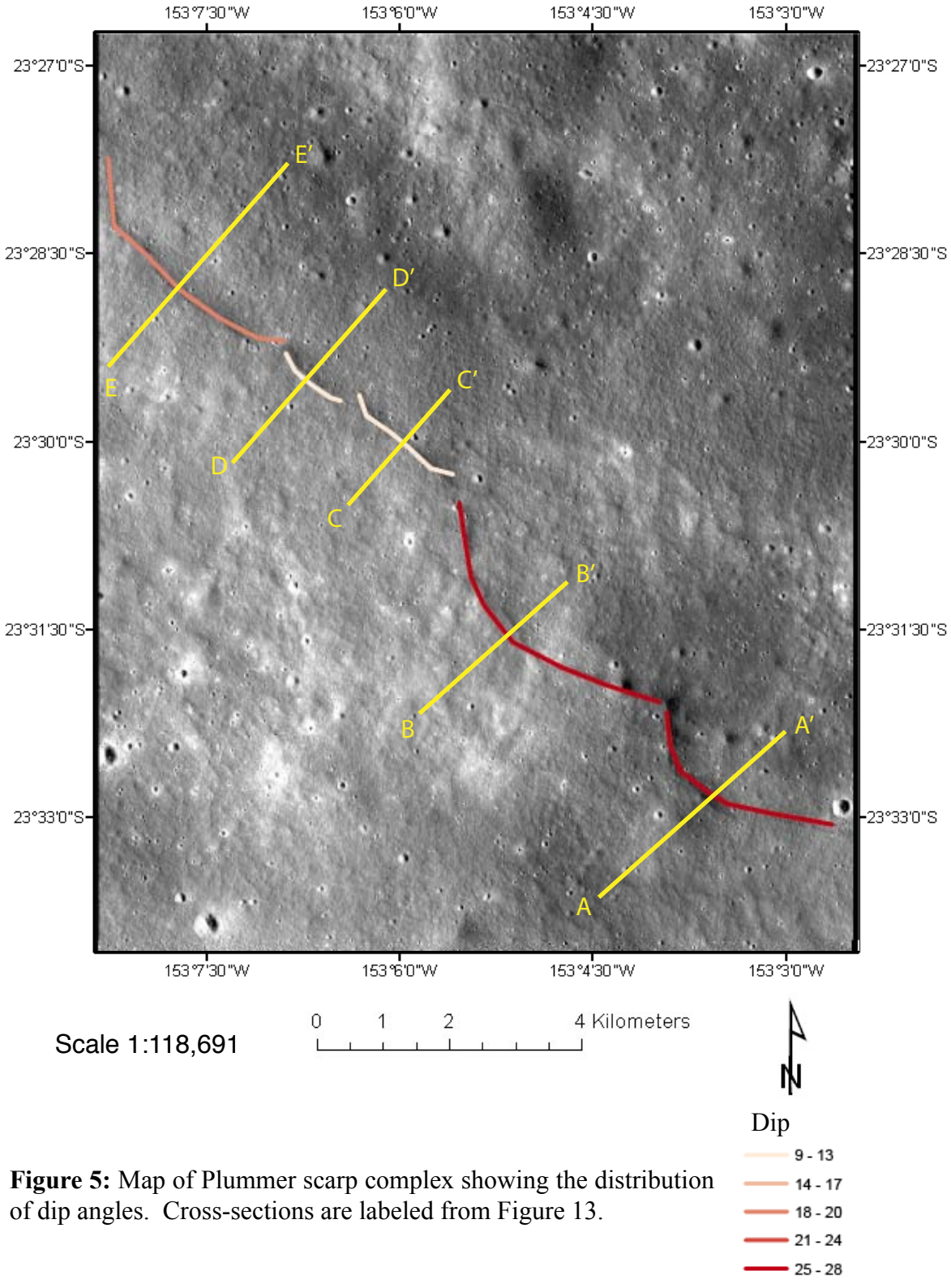

Figure 5: Map of Plummer scarp complex showing the distribution of dip angles. Cross-sections are labeled from Figure 13.

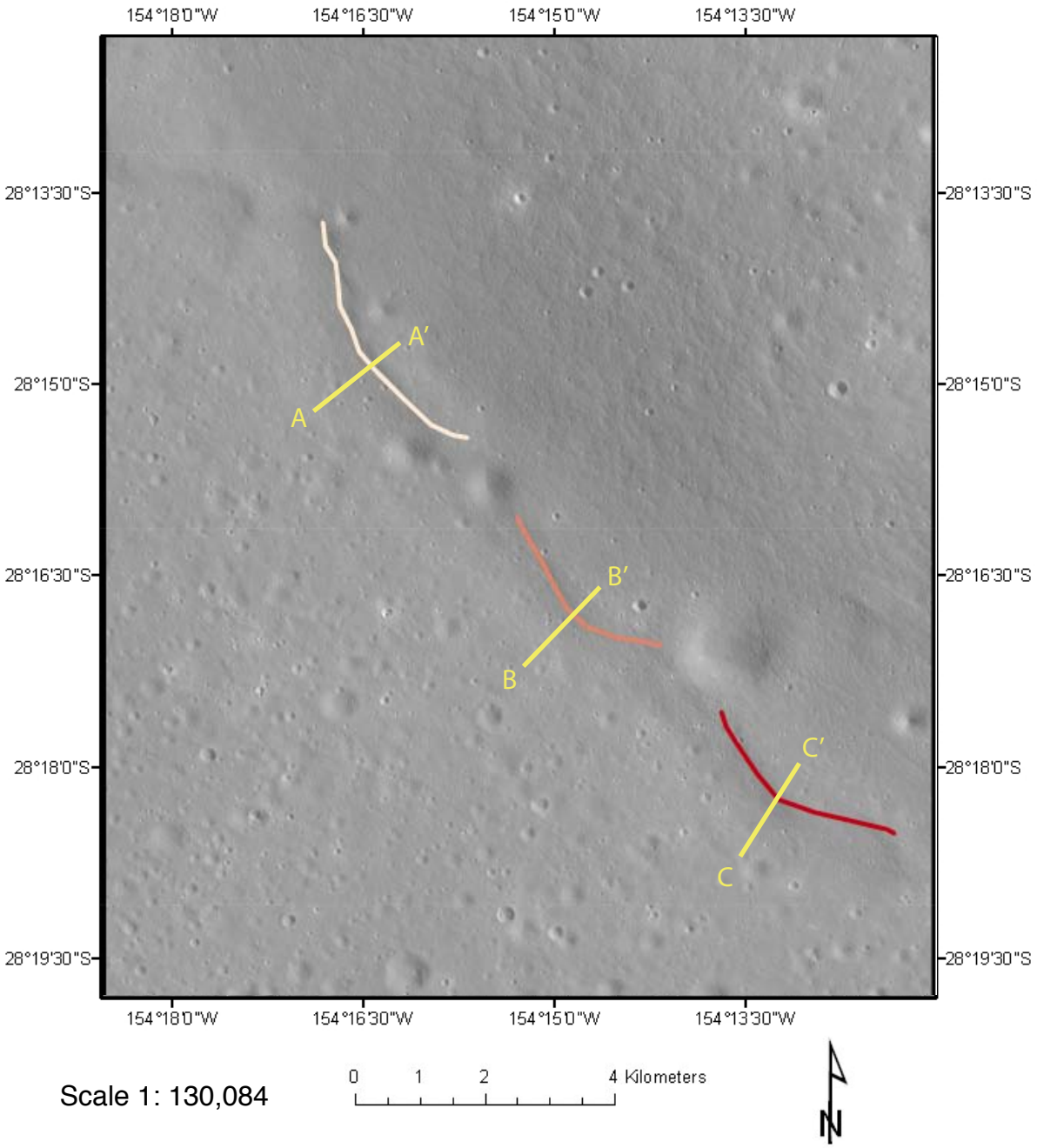

Figure 6: Map of Barringer scarp complex showing the distribution of dip angles. Cross-sectionS are labeled from Figure 18.

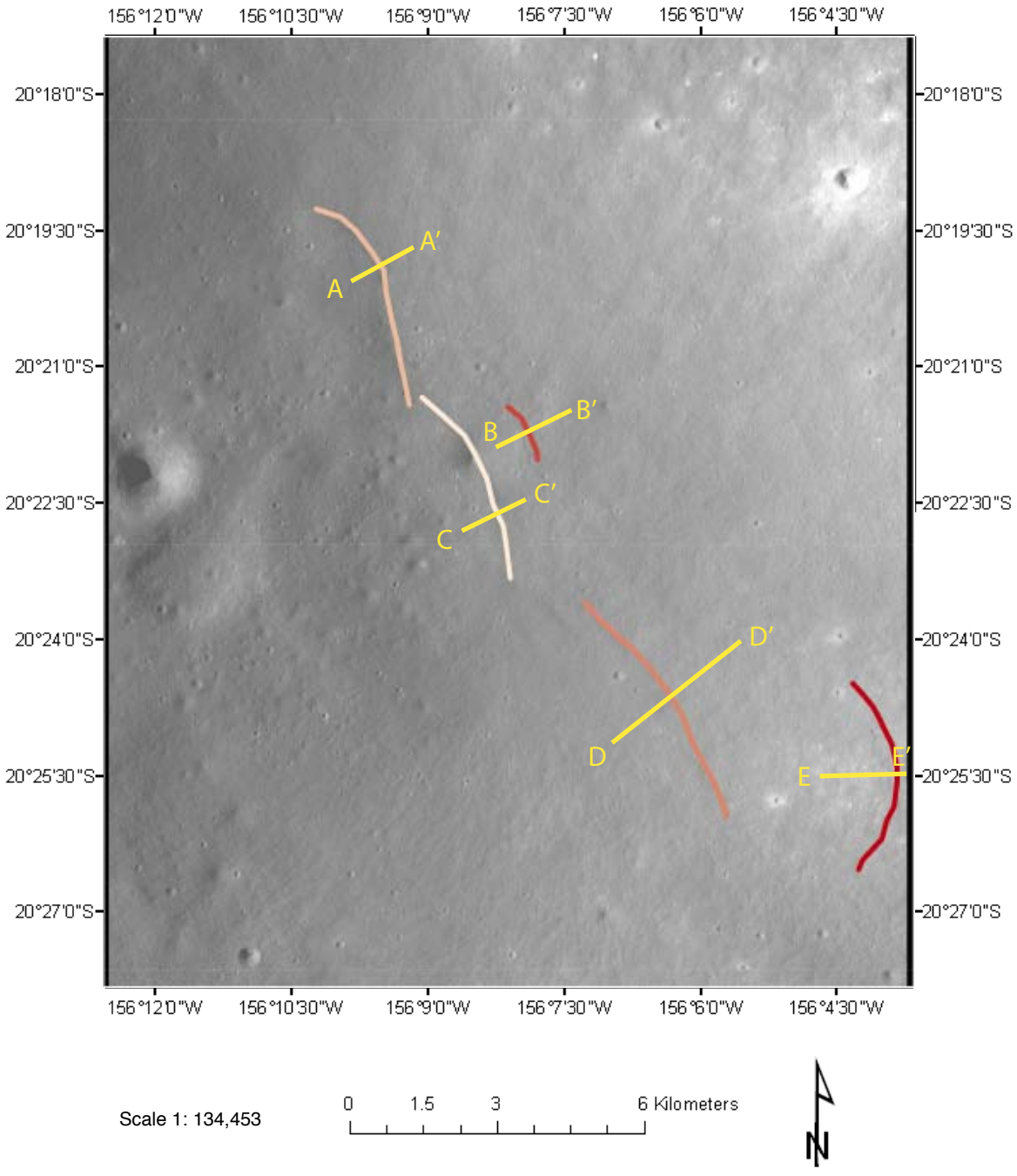

Figure 7: Map of Wilsing scarp complex showing the distribution of dip angles. Cross-sections are labeled from Figure 23.

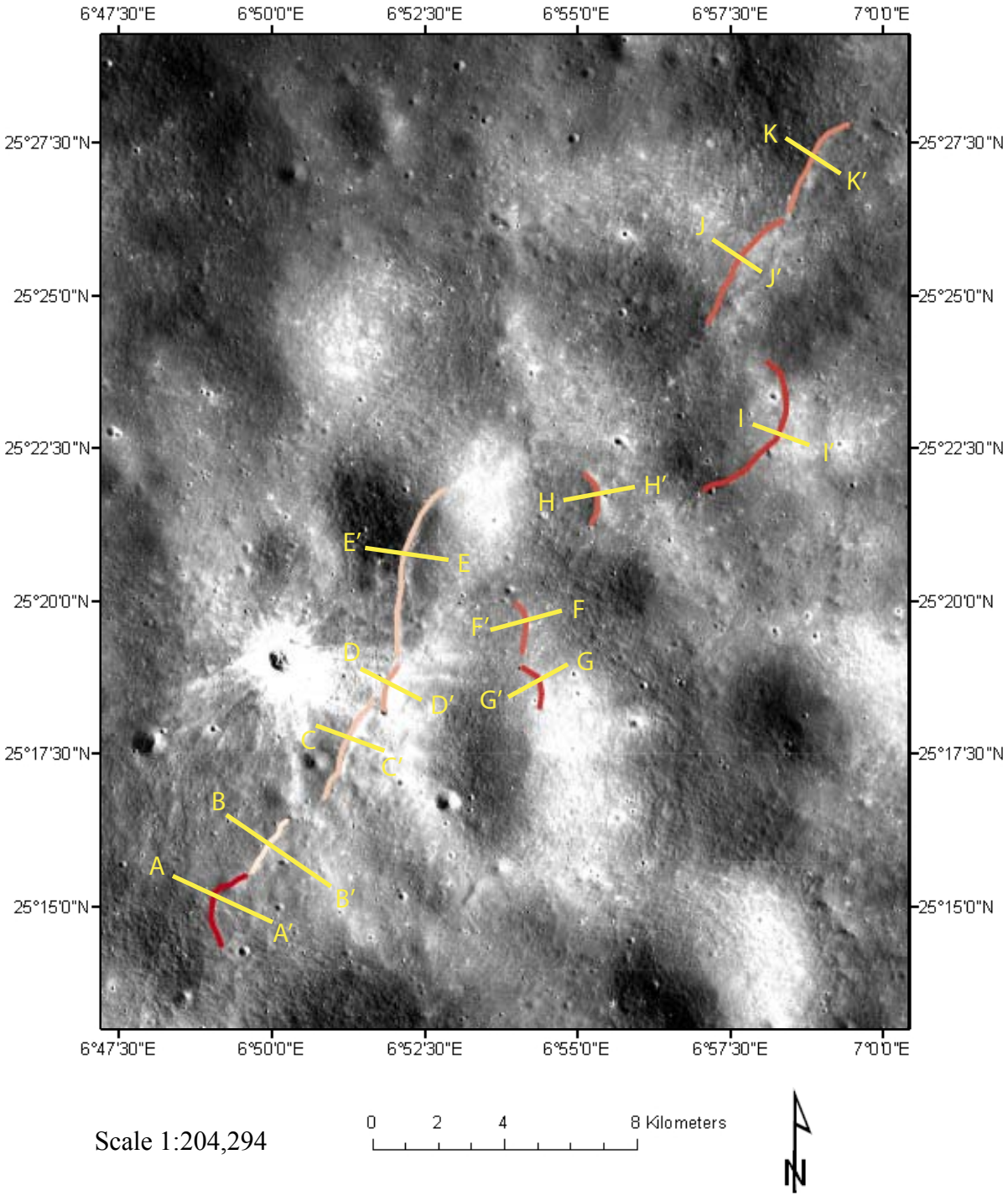

Figure 8: Map of Joy-1 scarp complex showing the distribution of dip angles. Cross-sections are labeled from Figure 28.

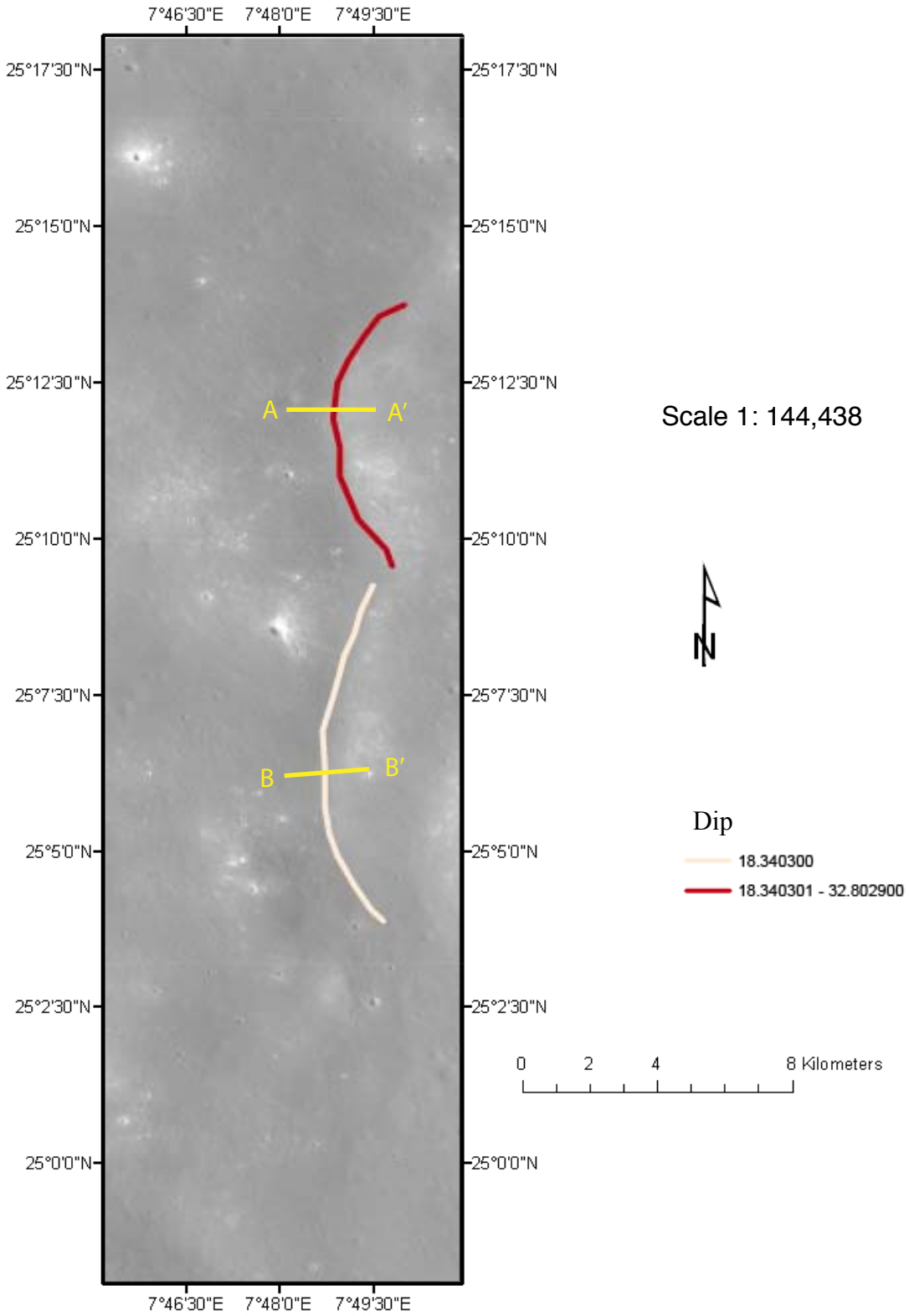

Figure 9: Map of Joy-2 scarp complex showing the distribution of dip angles. Cross-sections are labeled from Figure 35.

Figure 10: DEM created using the photoclinometry method exhibiting pervasive striping. Red arrows indicate the trace of the lobate scarp.

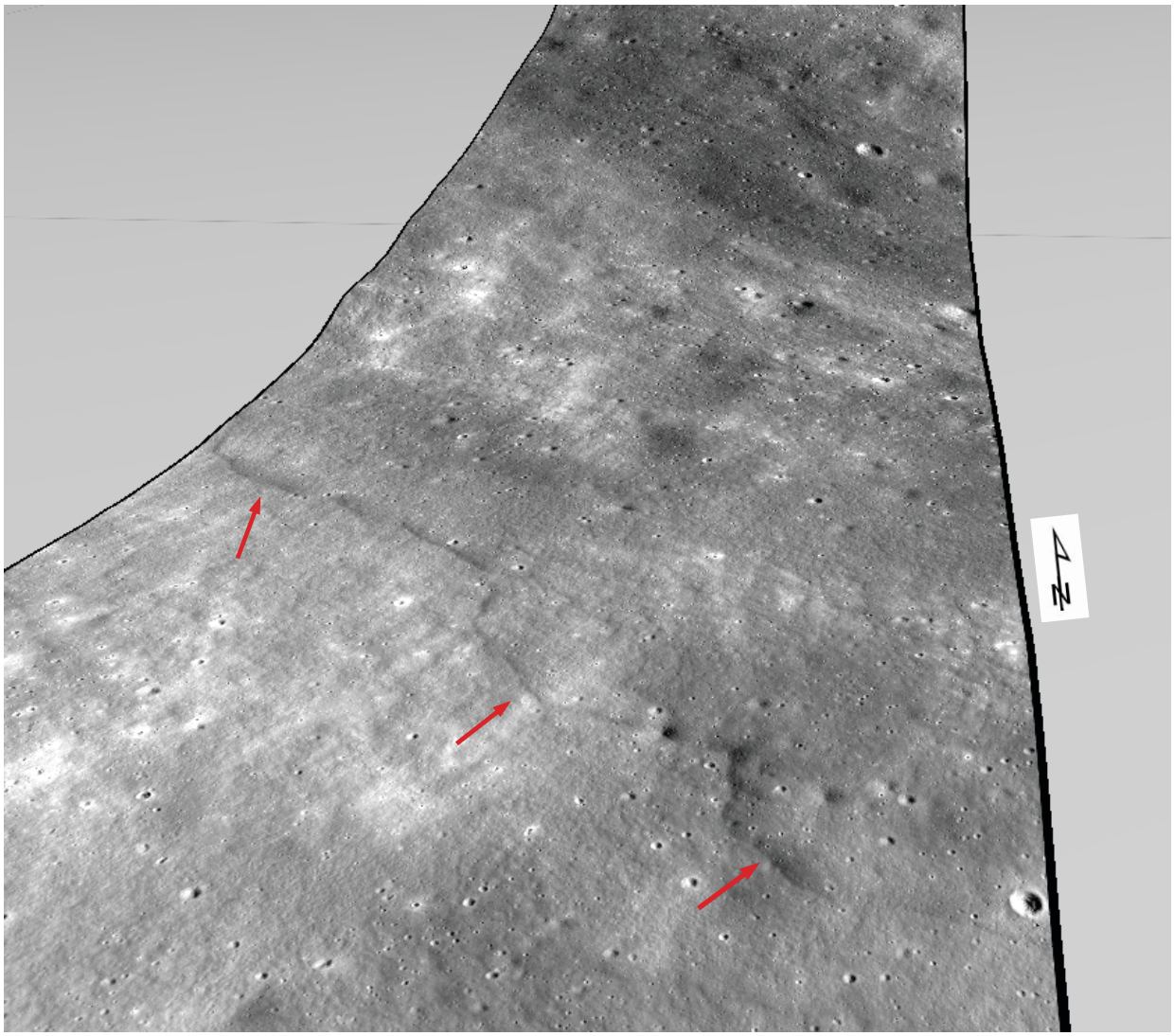

Figure 11: 3D visualization of Plummer scarp complex created in Fledermaus. Red arrows point out lobate scarps. LROC NAC image M145624586LC draped onto LOLA DEM.

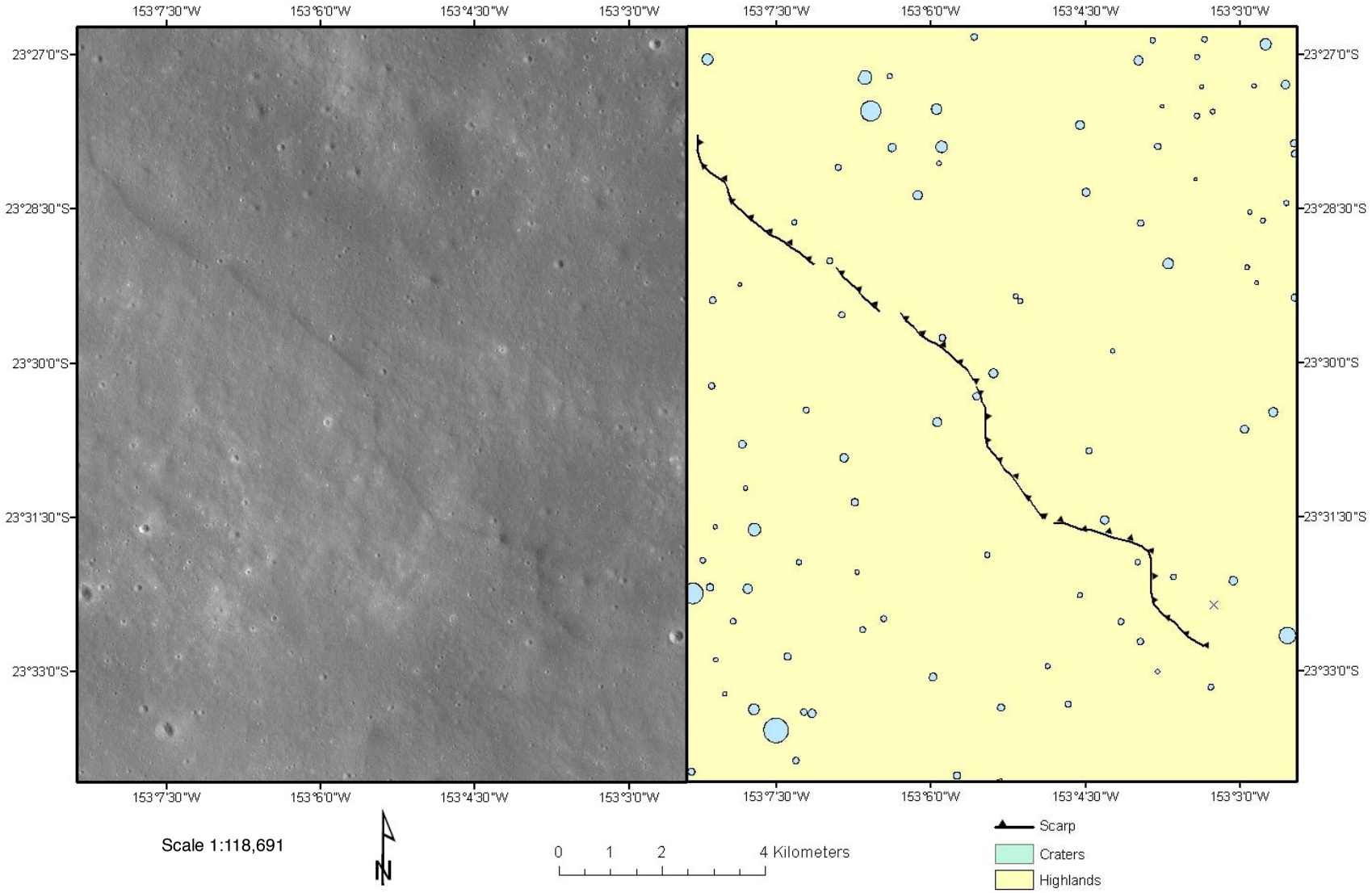

Figure 12. Plummer scarp complex. On the left is LROC NAC image M145624586LC and on the right is the photogeologic map.

Figure 13: Cross-sections A-A' - E-E' for Plummer scarp complex.

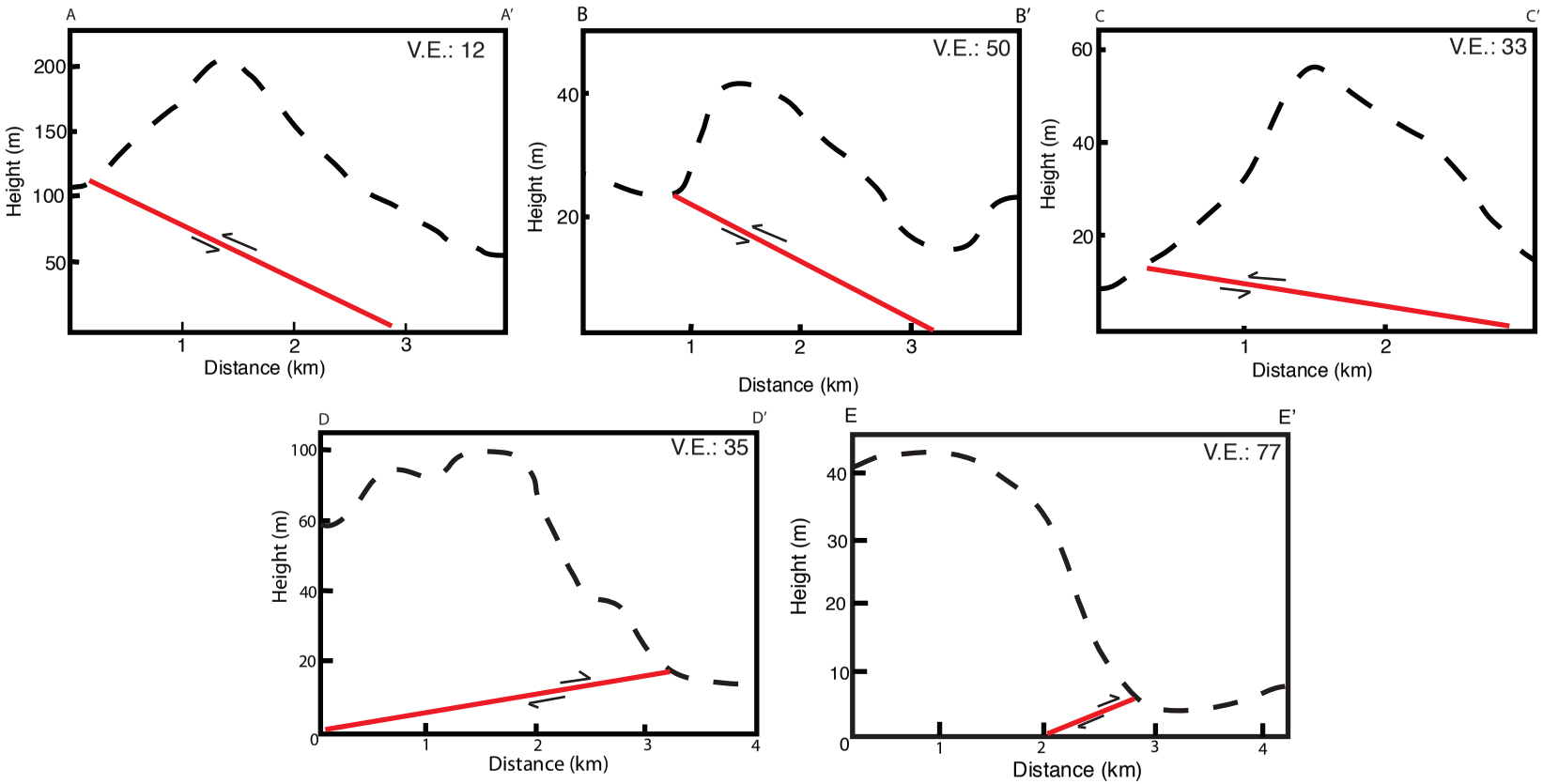

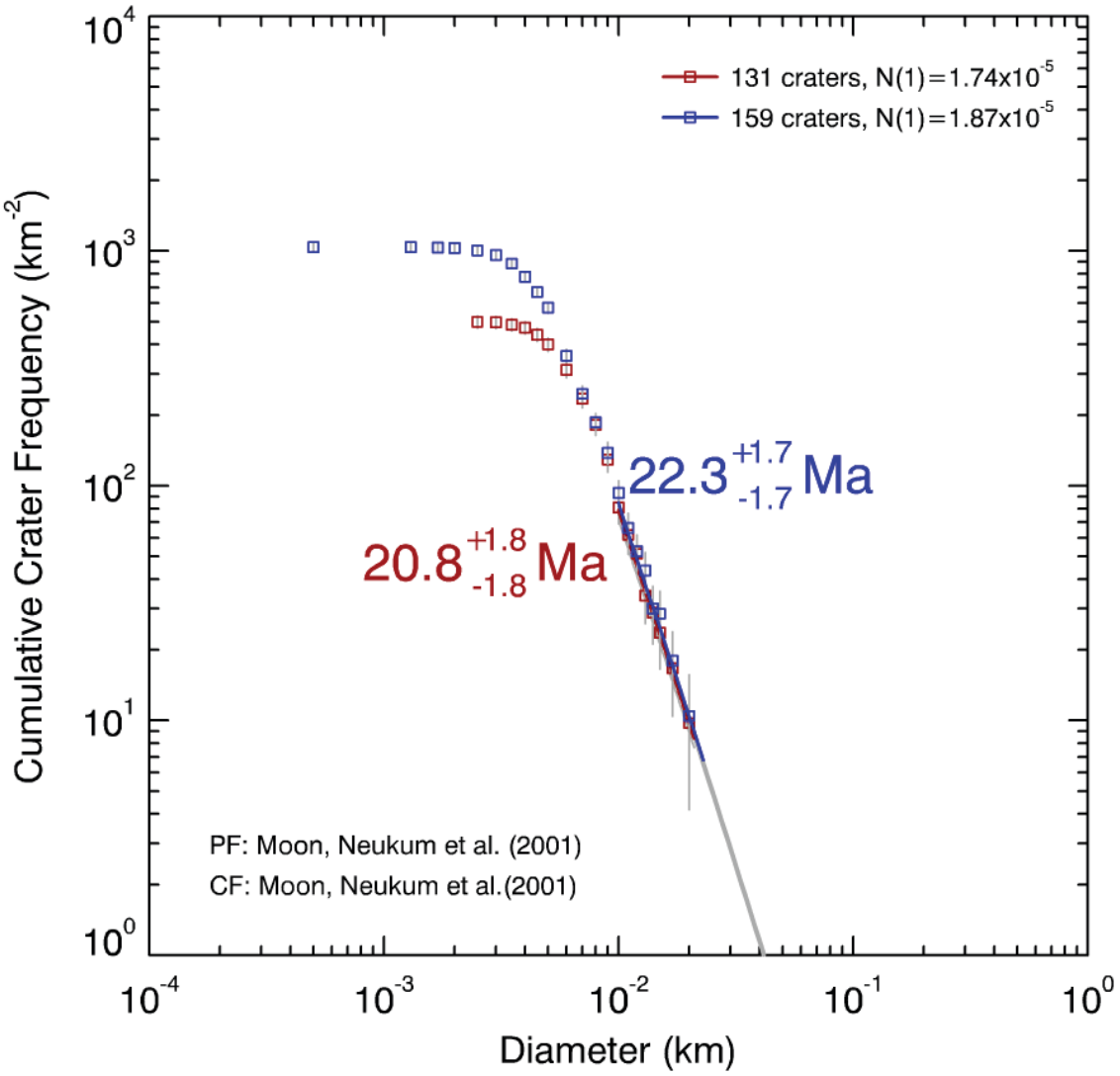

Figure 14: N_{cum} plot for Plummer scarp complex. The highlands footwall is 20.8 ± 1.8 Ma and the highlands hanging wall is 22.3 ± 1.7 Ma.

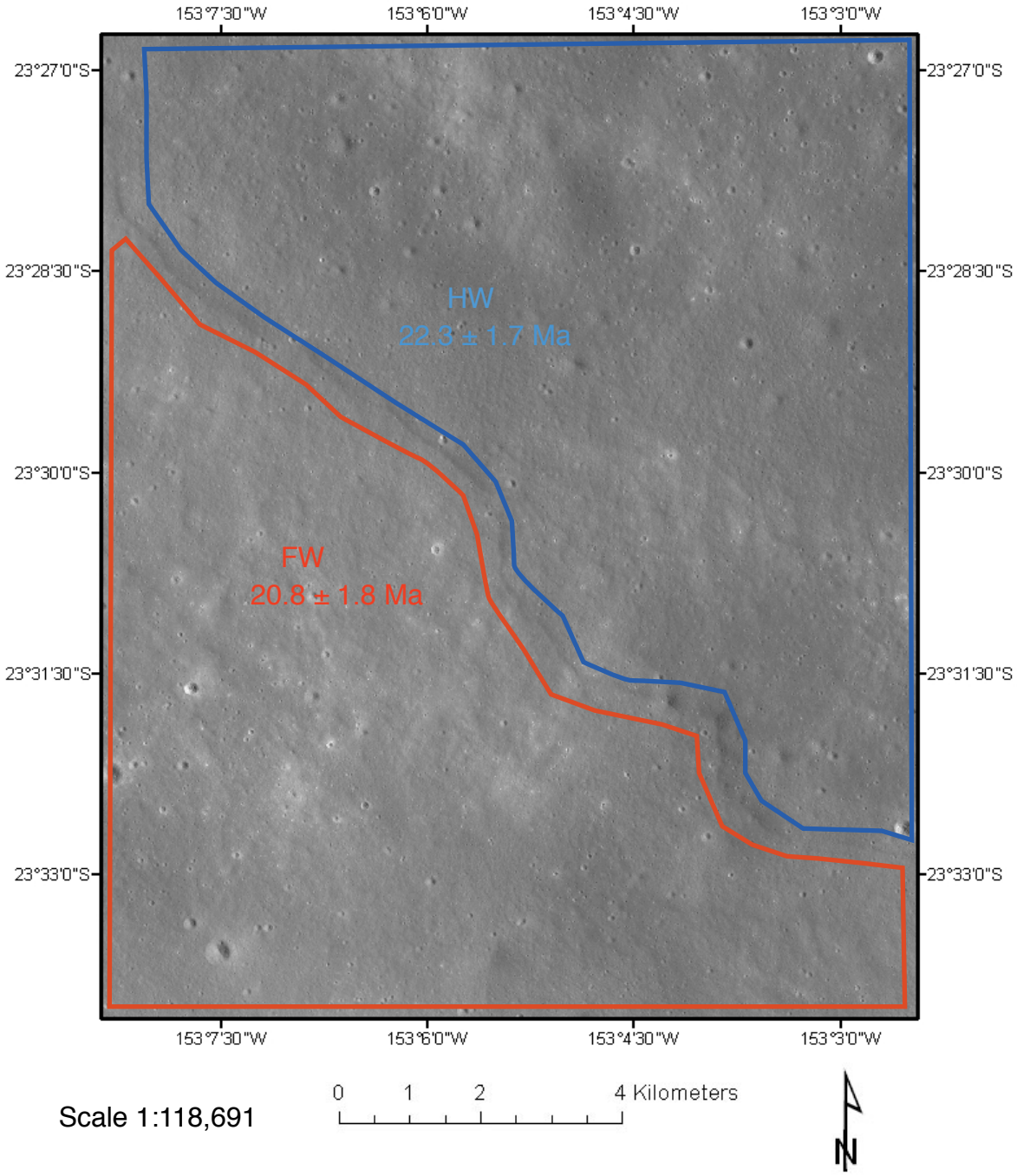

Figure 15: Map of Plummer scarp complex showing areas that were used for crater counting. Figure 14 has the N_{cum} plot.

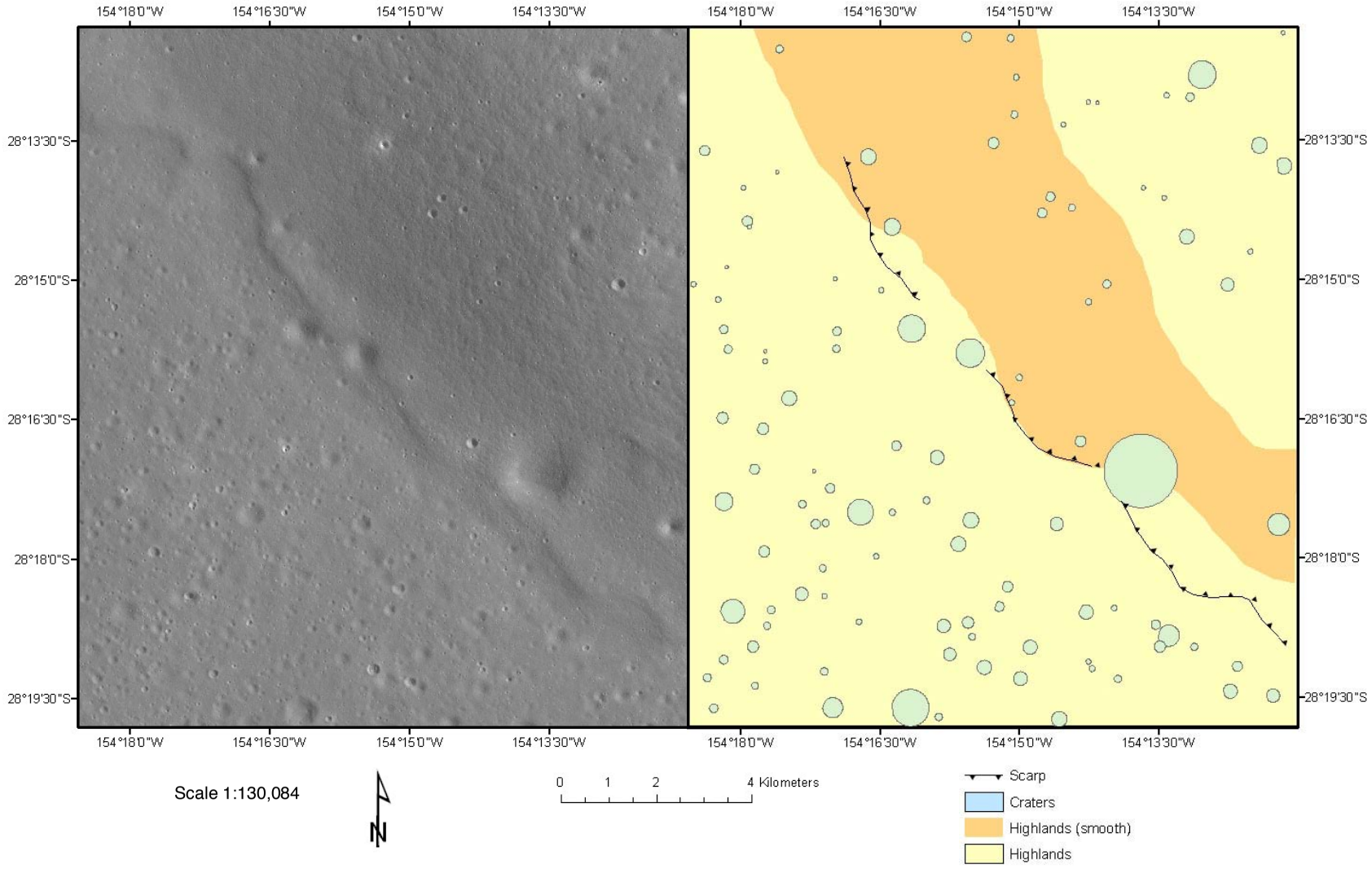

Figure 16. Barringer scarp complex. On the left is LROC NAC image M145631465RC and on the right is the photogeologic map.

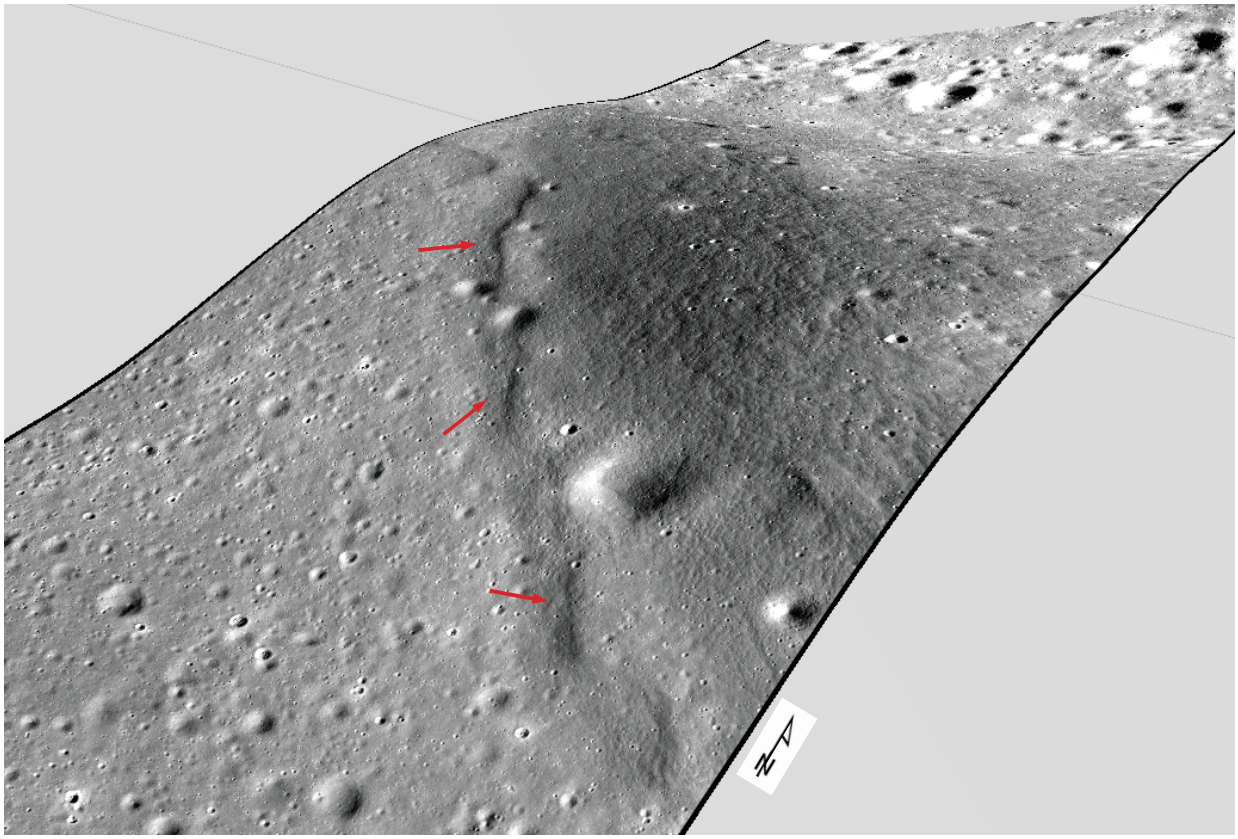

Figure 17: 3D visualization of Barringer scaro complex created in Fledermaus. Red arrows point out lobate scarps. LROC NAC image M145631465RC draped onto LOLA DEM.

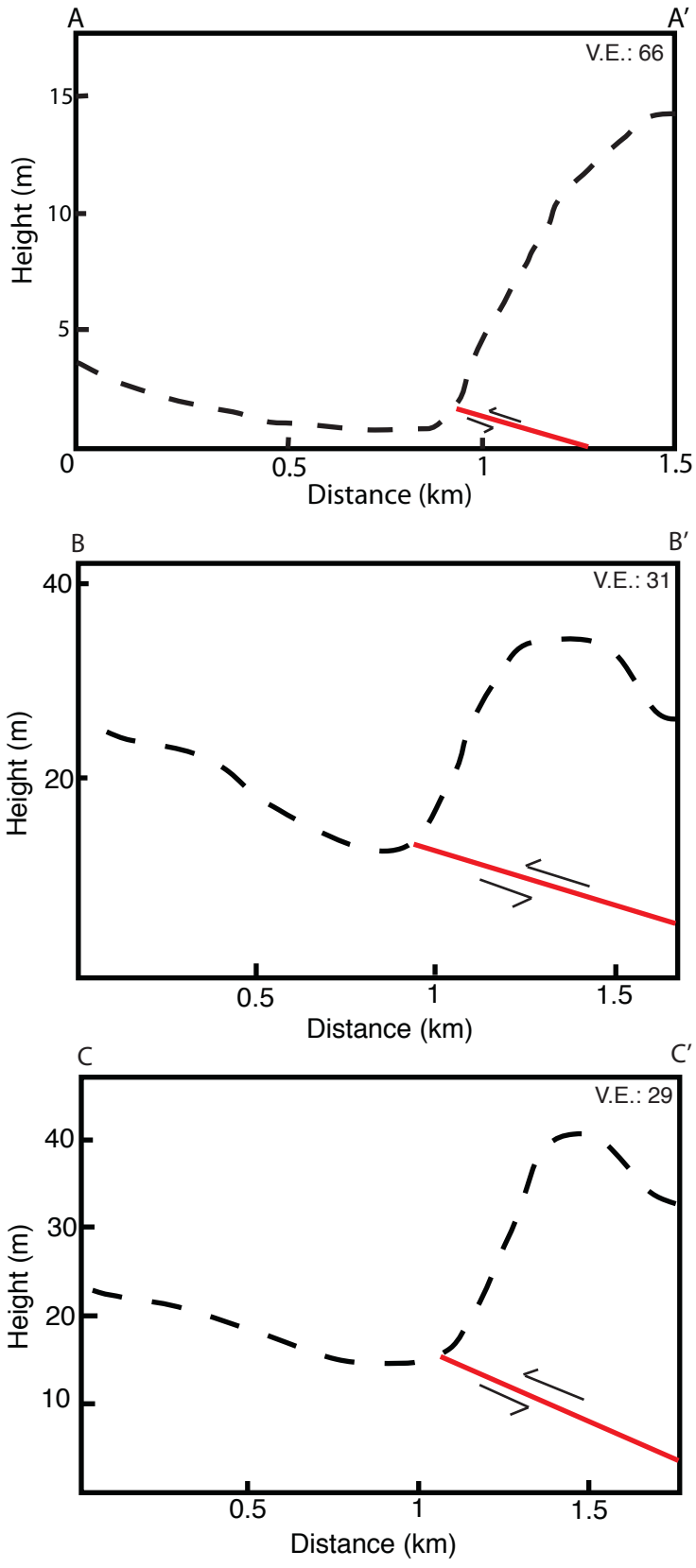

Figure 18: Cross-sections A-A' - C-C' for Barringer scarp complex.

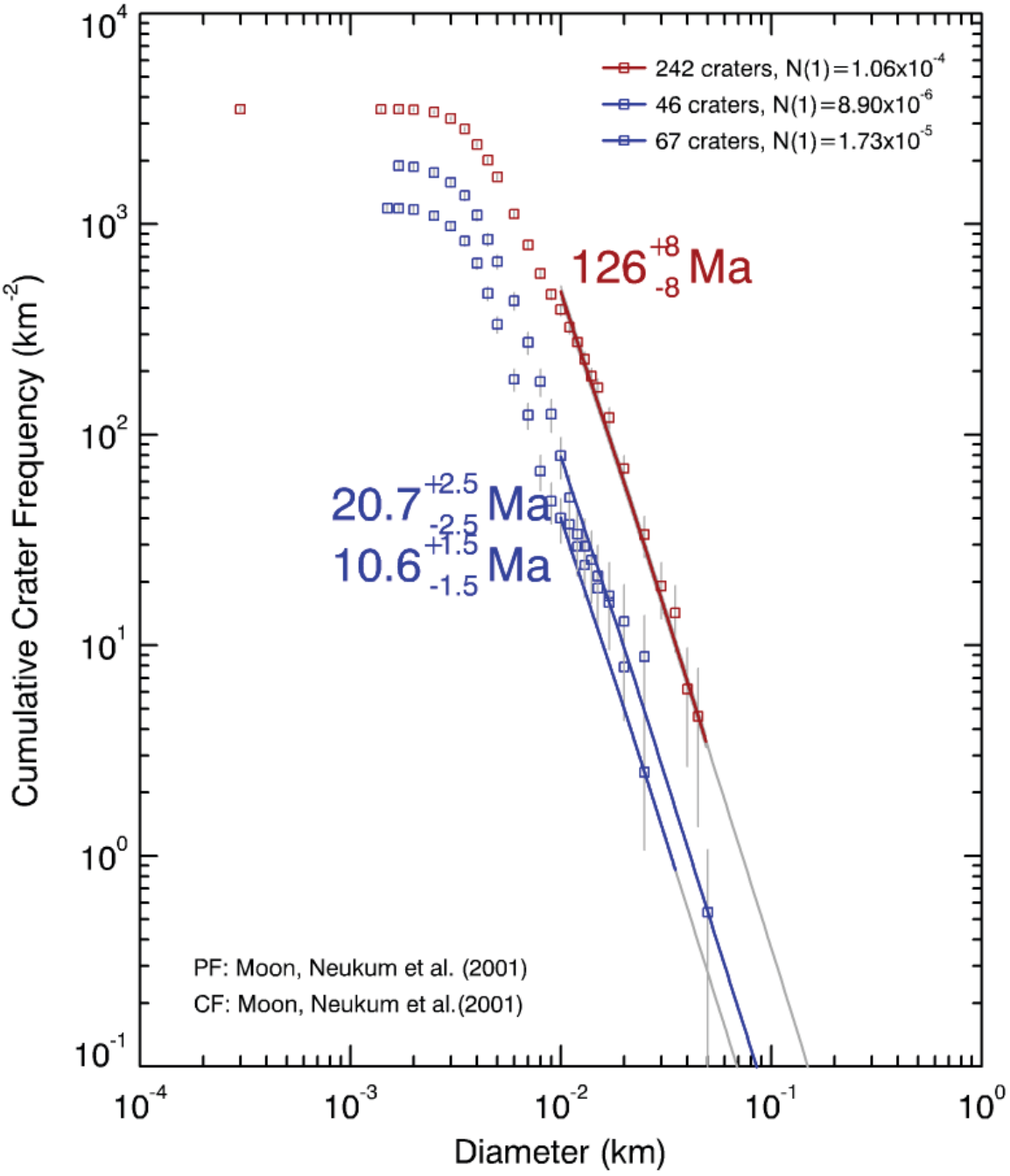

Figure 19: N_{cum} plot for Barringer scarp complex. The highlands cratered unit 1 (footwall) is 126 ± 8 Ma, the highlands cratered unit 2 (hanging wall) is 20.7 ± 2.5 Ma, and the highlands smooth unit (footwall and hanging wall) is 10.6 ± 1.5 Ma.

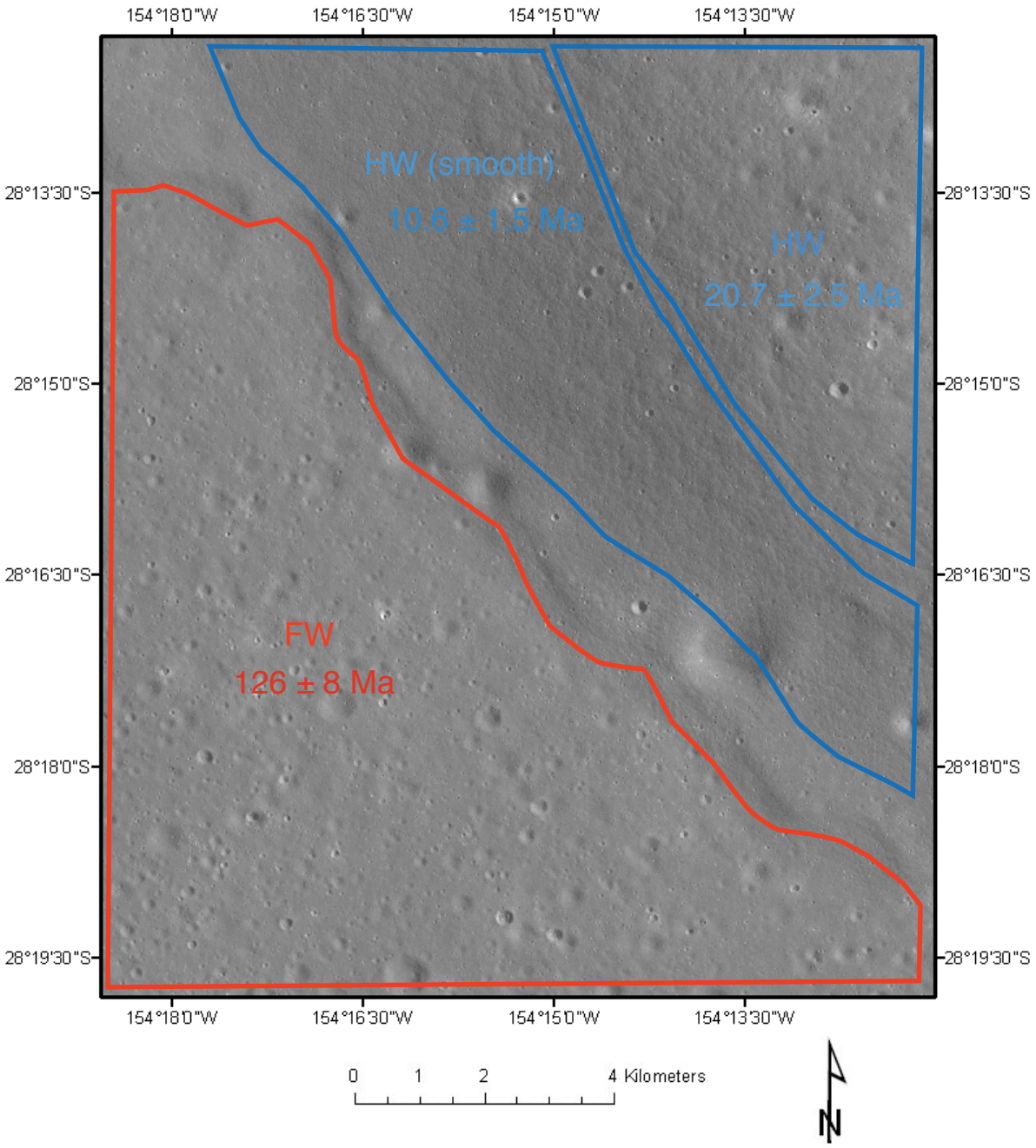

Figure 20: Map of Barringer scarp complex showing areas that were used for crater counting. Figure 19 has the N_{cum} plot.

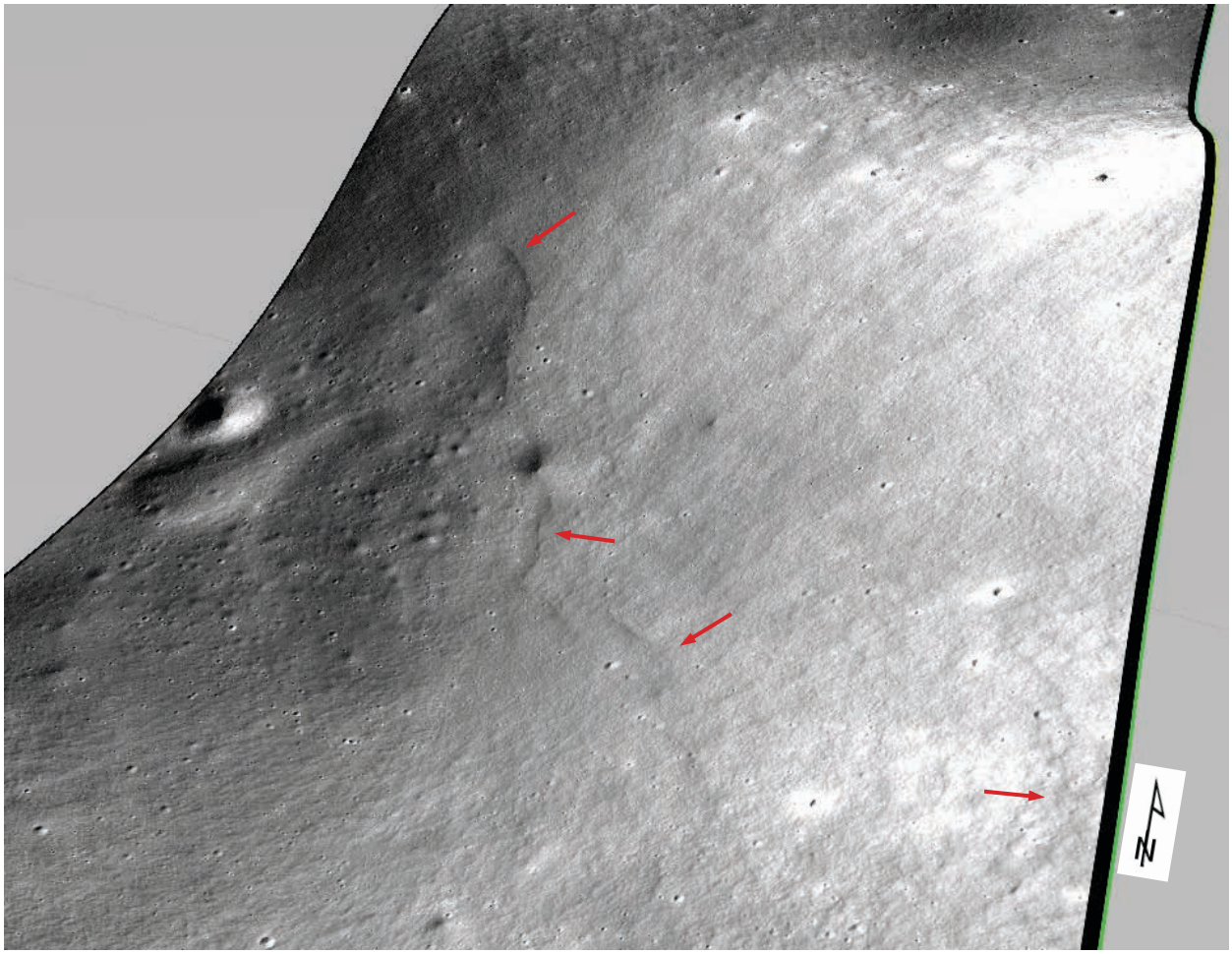

Figure 21: 3D visualization of Wilsing scarp complex created in Fledermaus. Red arrows point out lobate scarps. LROC NAC image M103174532RC draped onto LOLA DEM.

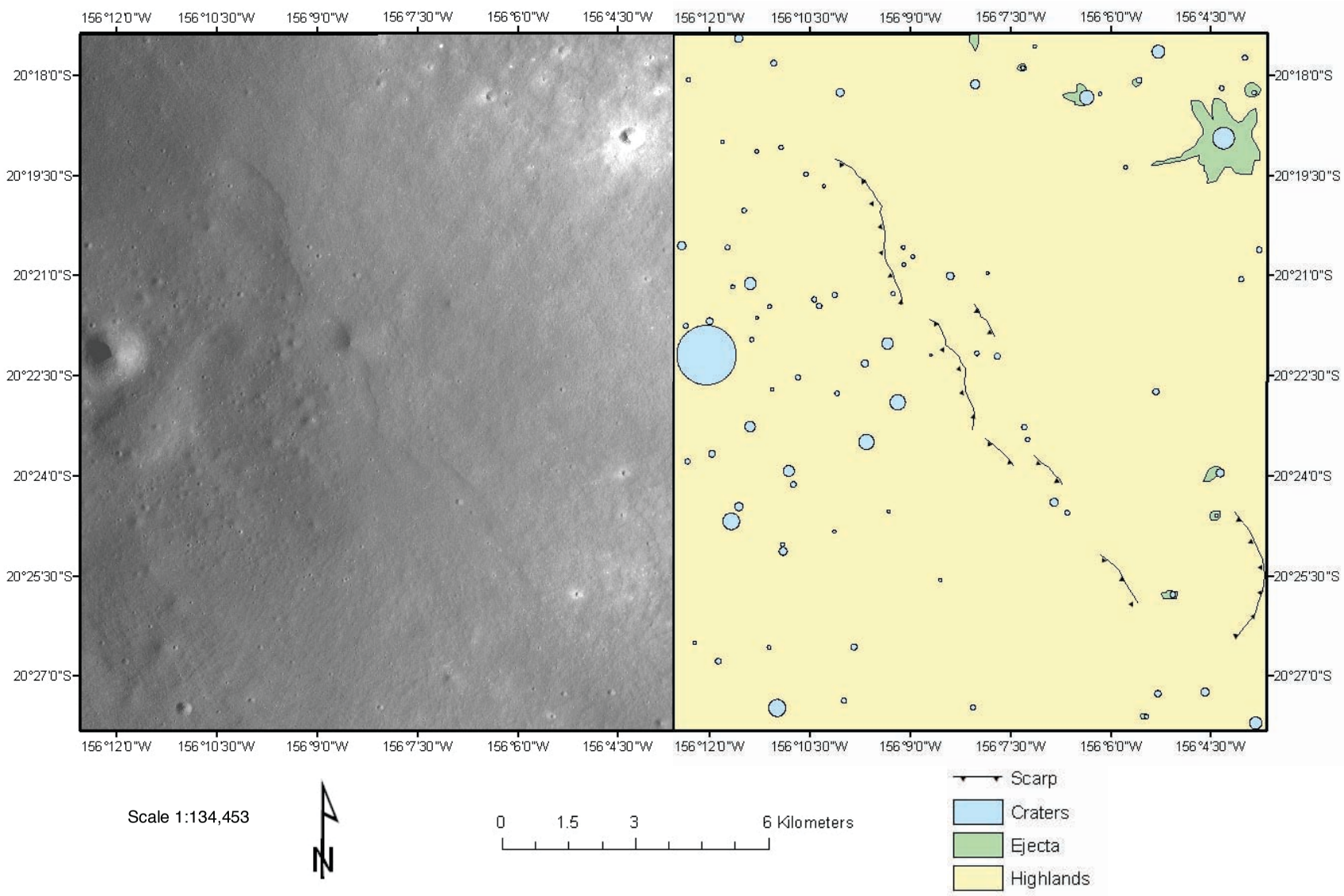

Figure 22. Wilsing scarp complex. On the left is LROC NAC image M1031744532RC and on the right is the photogeologic map.

Figure 23: Cross-sections A-A' - E-E' for Wilsing scarp complex.

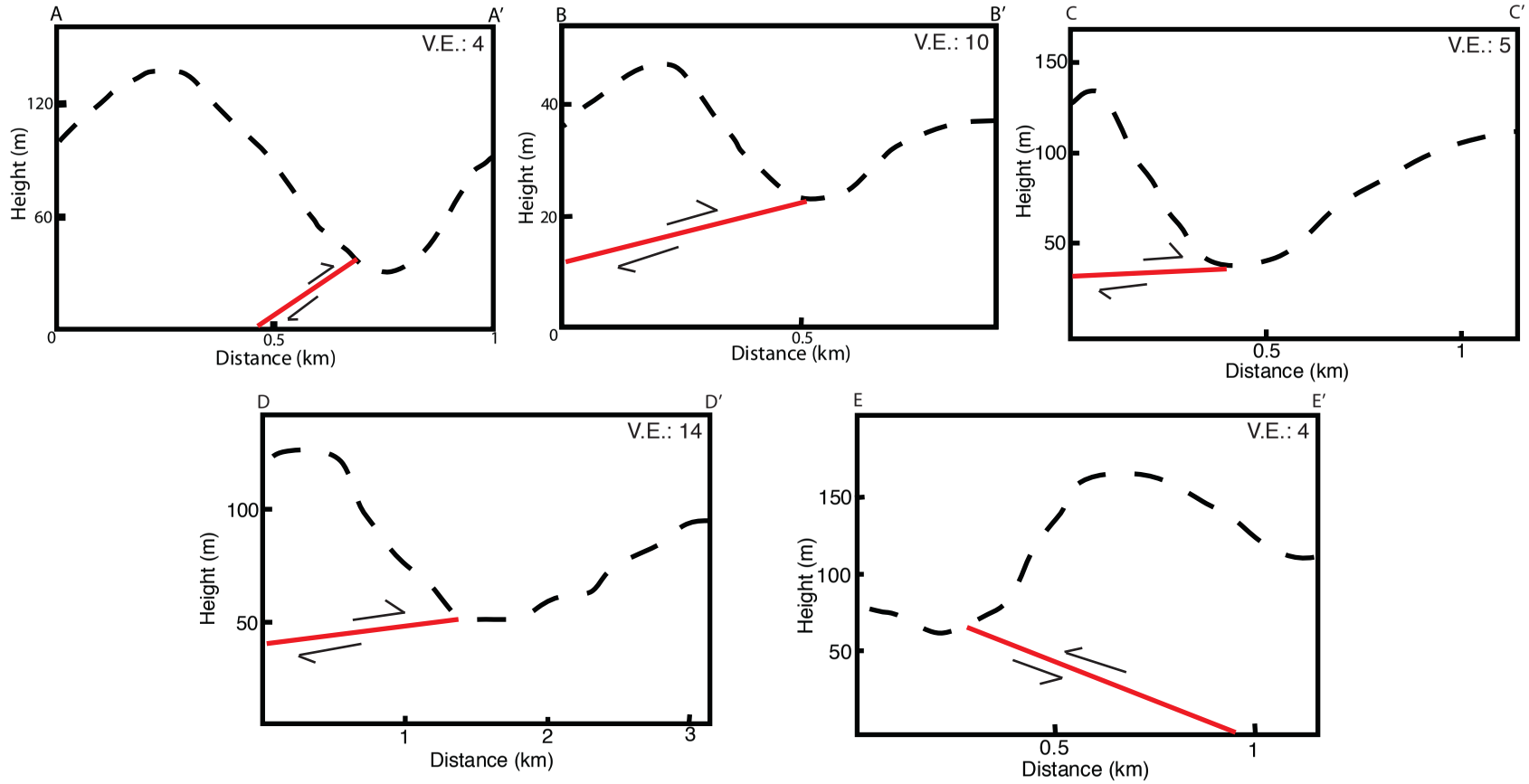

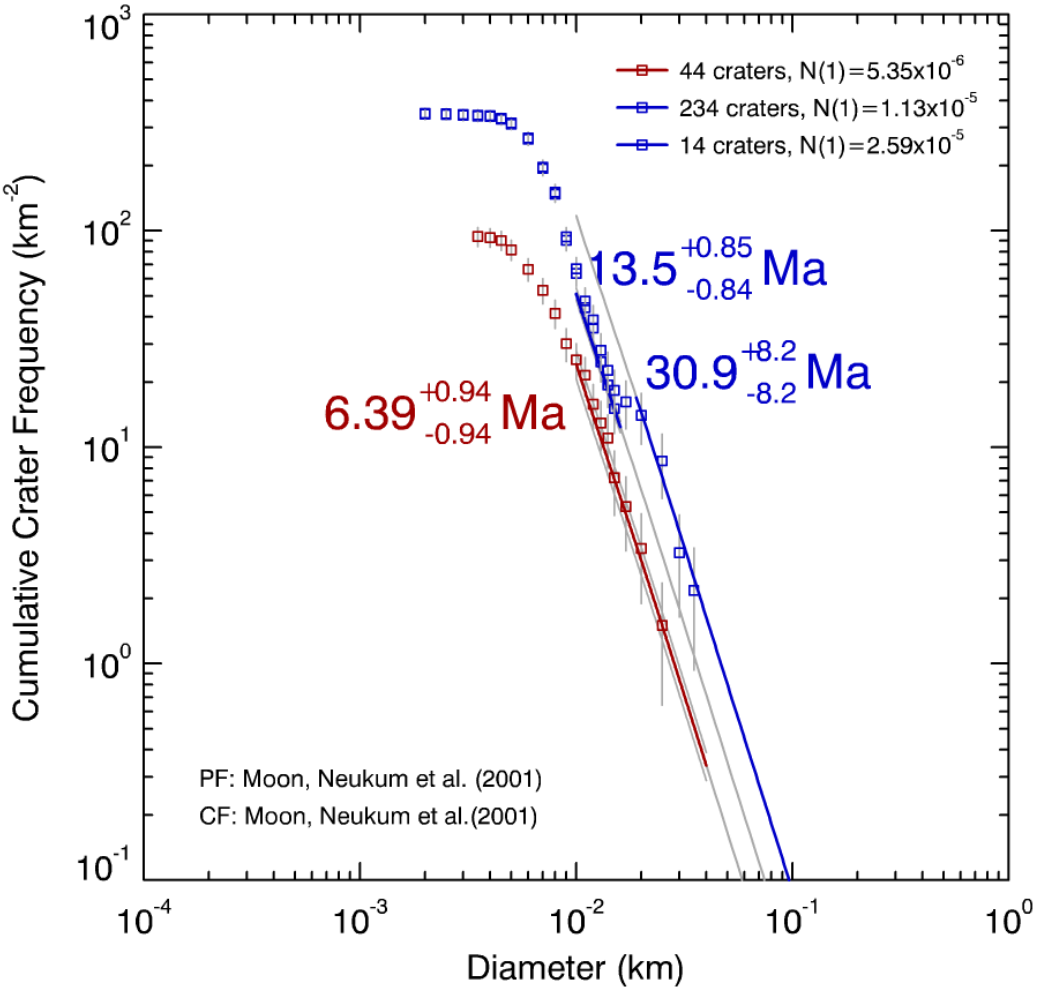

Figure 24: N_{cum} plot for Wilsing scarp complex. The highlands footwall is 6.39 ± 0.94 Ma. The highlands hanging wall has had two resurfacing events at 13.5 ± 0.85 Ma and 30.9 ± 8.2 Ma.

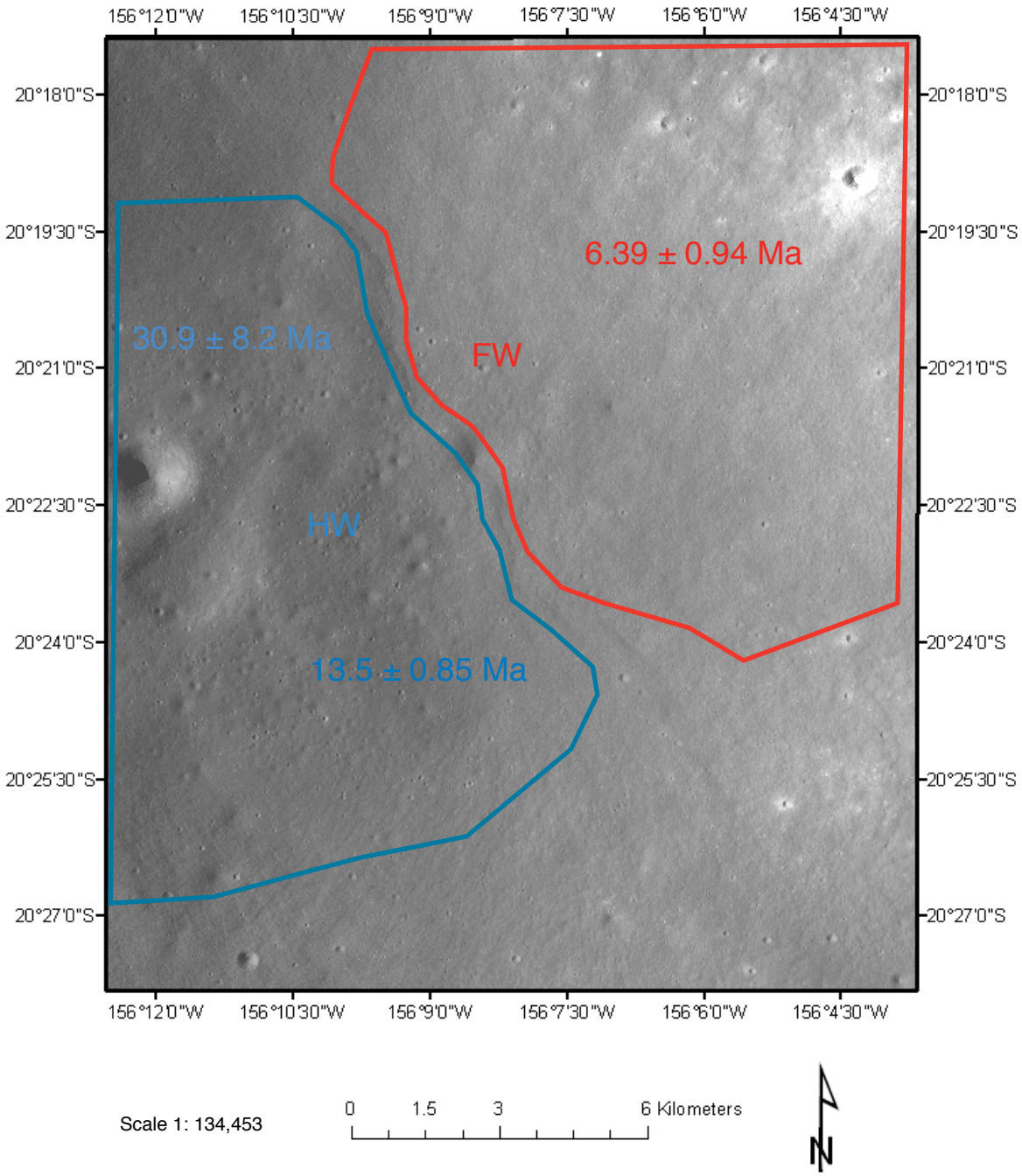

Figure 25: Map of Wilsing scarp complex showing areas that were used for crater counting. Figure 24 has the N_{cum} plot.

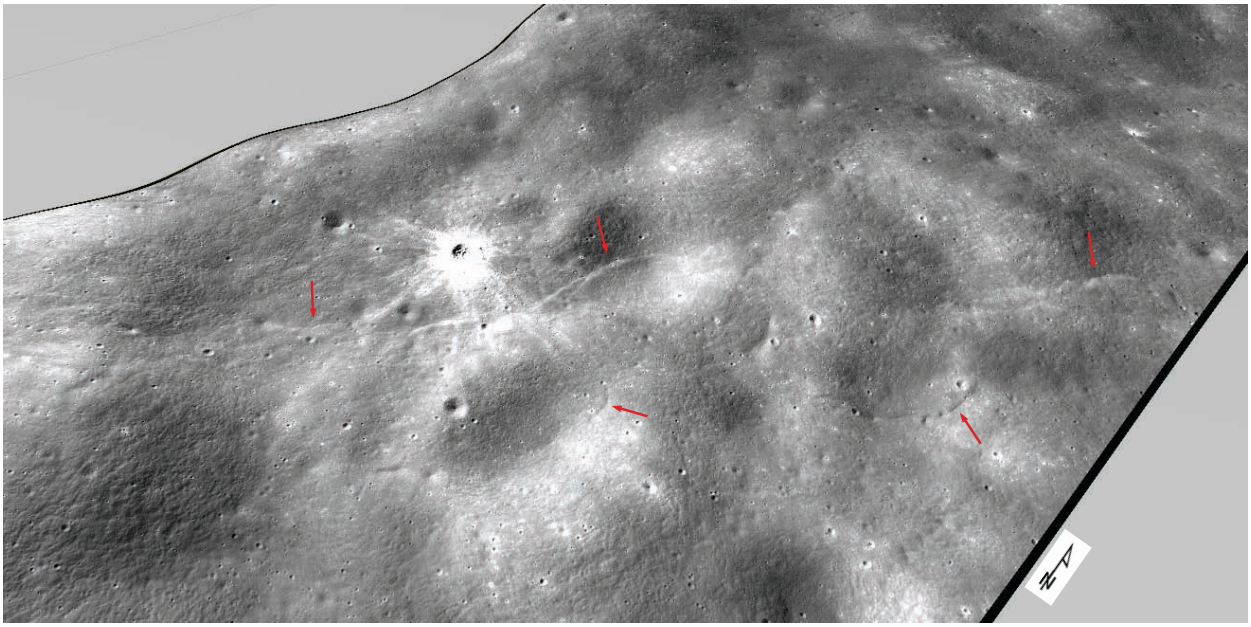

Figure 26: 3D visualization of Joy-1 scarp complex created in Fledermaus. Red arrows point out lobate scarps. LROC NAC image M104476195RC draped onto LOLA DEM.

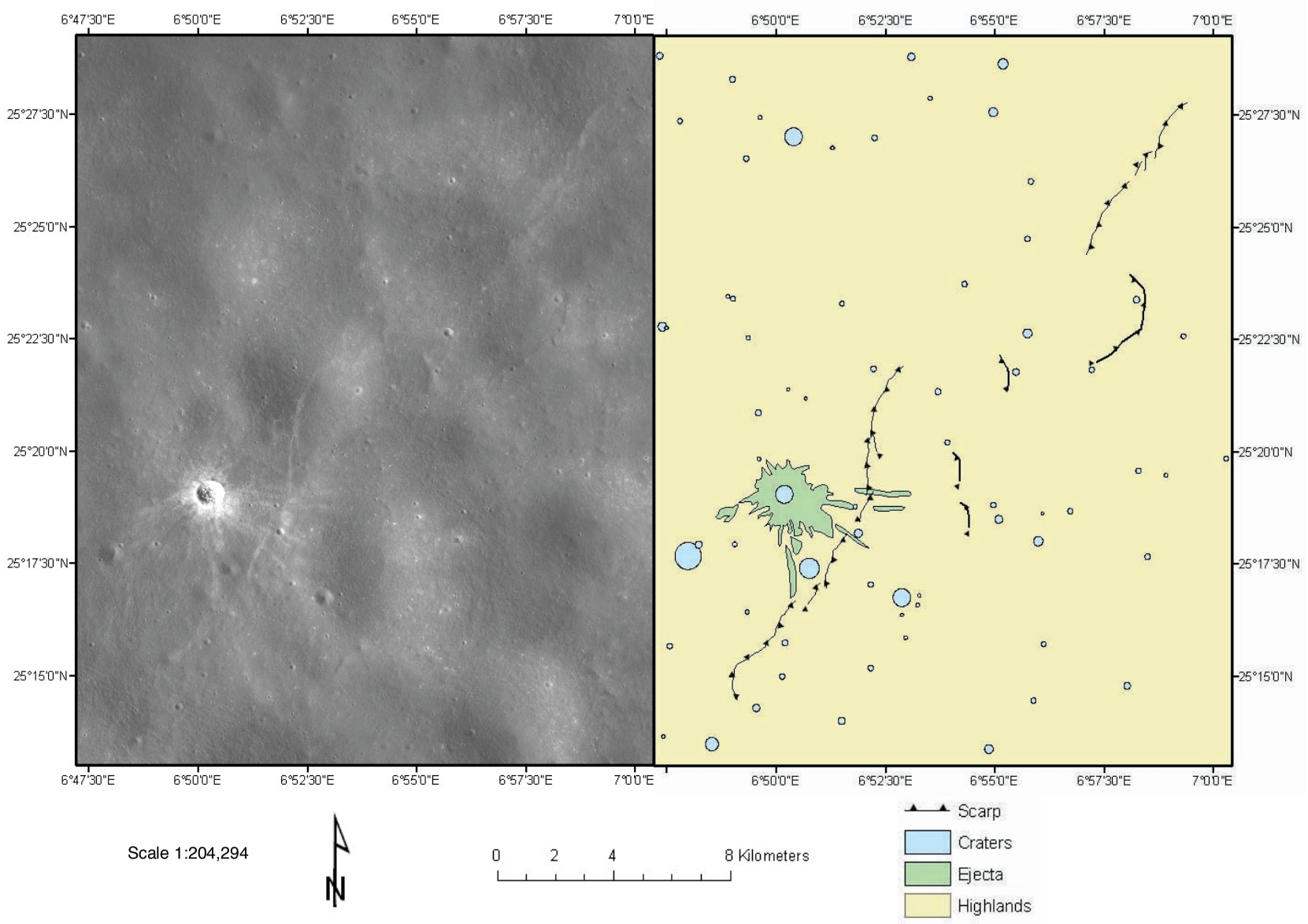

Figure 27. Joy-1 scarp complex. On the left is LROC NAC image M104476195RC and on the right is the photogeologic map.

Figure 28: Cross-sections A-A' - F-F' for Joy-1 scarp complex.

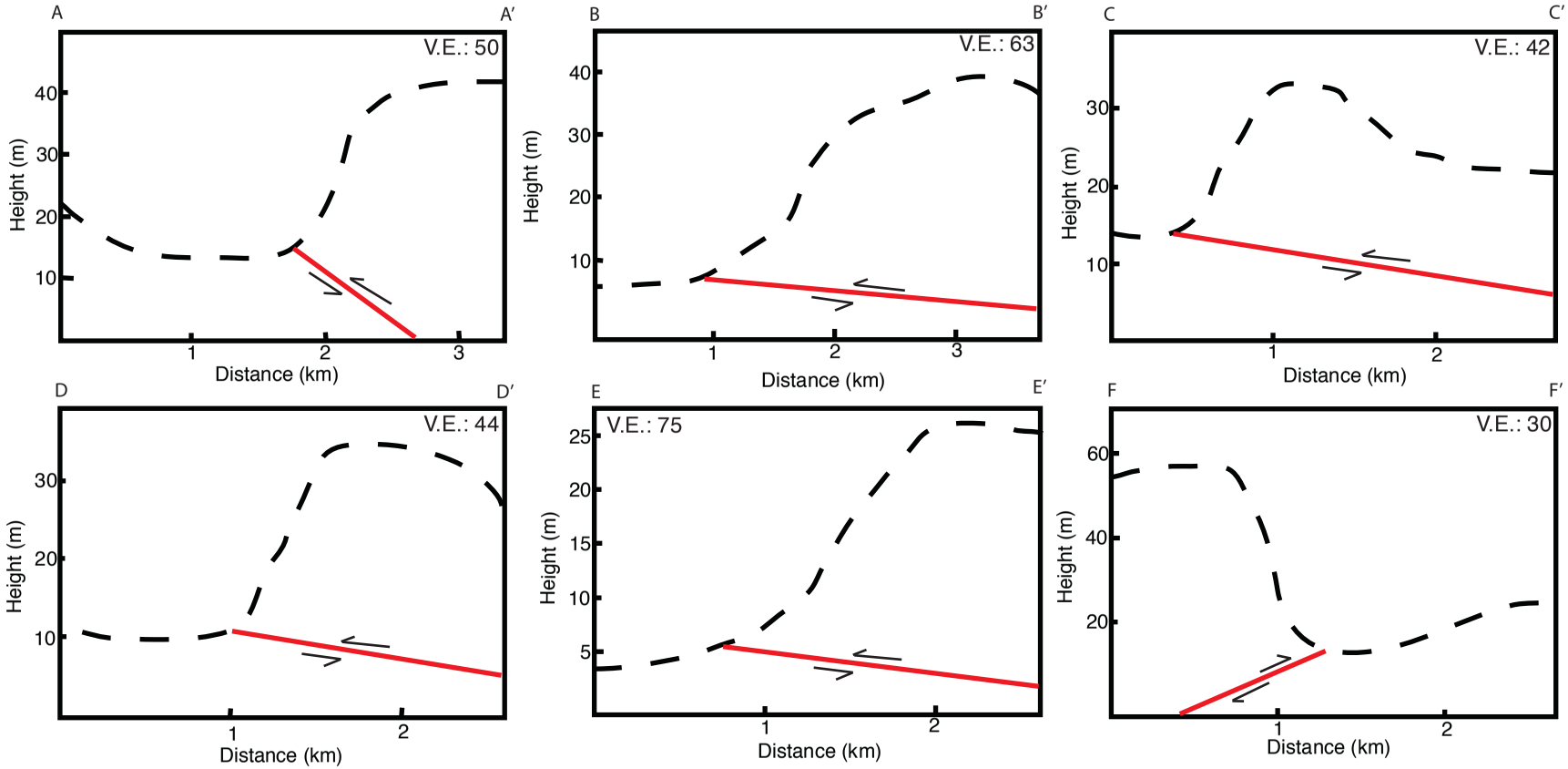

Figure 28 (continued): Cross-sections G-G' - K-K' for the Joy-1 scarp complex

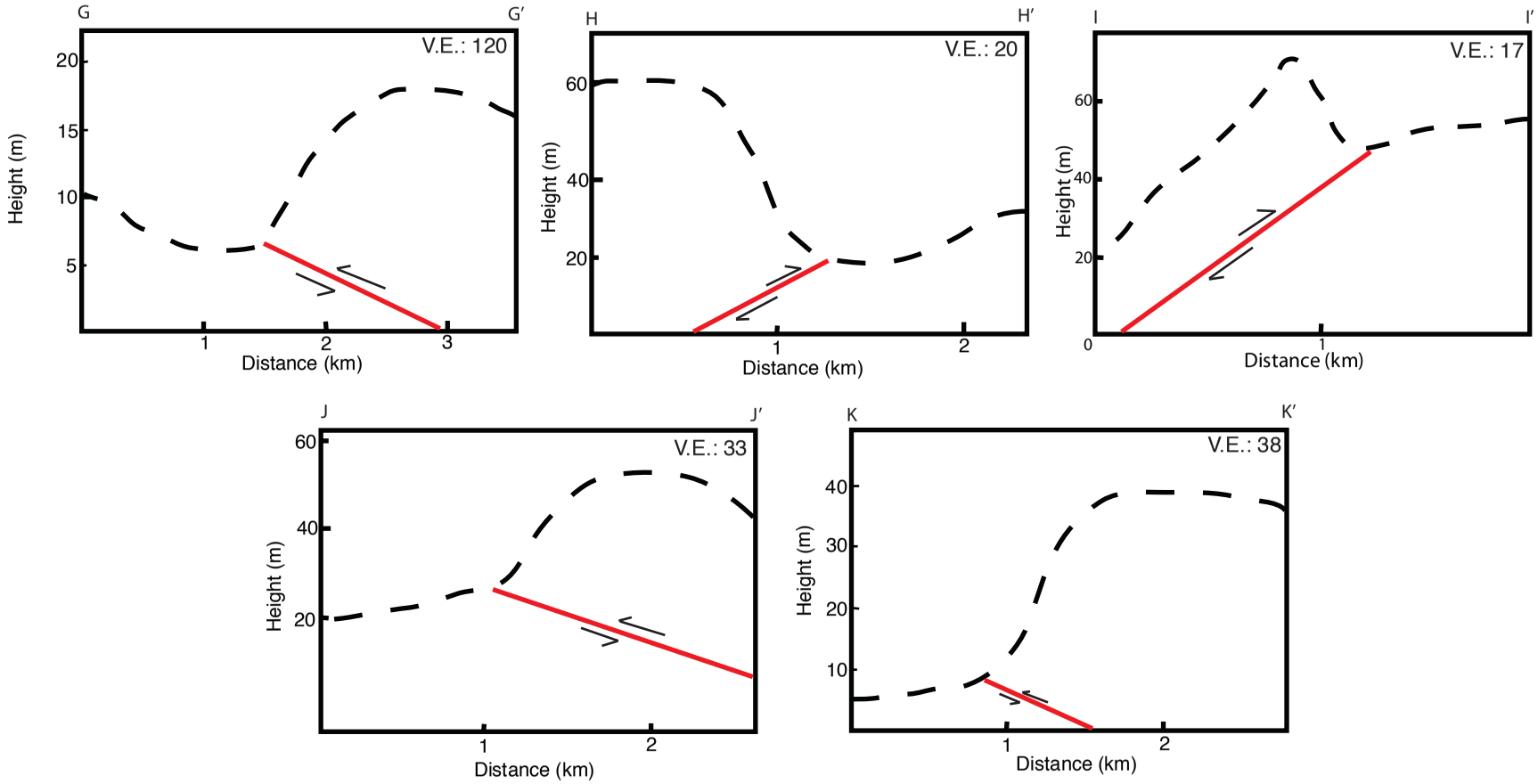

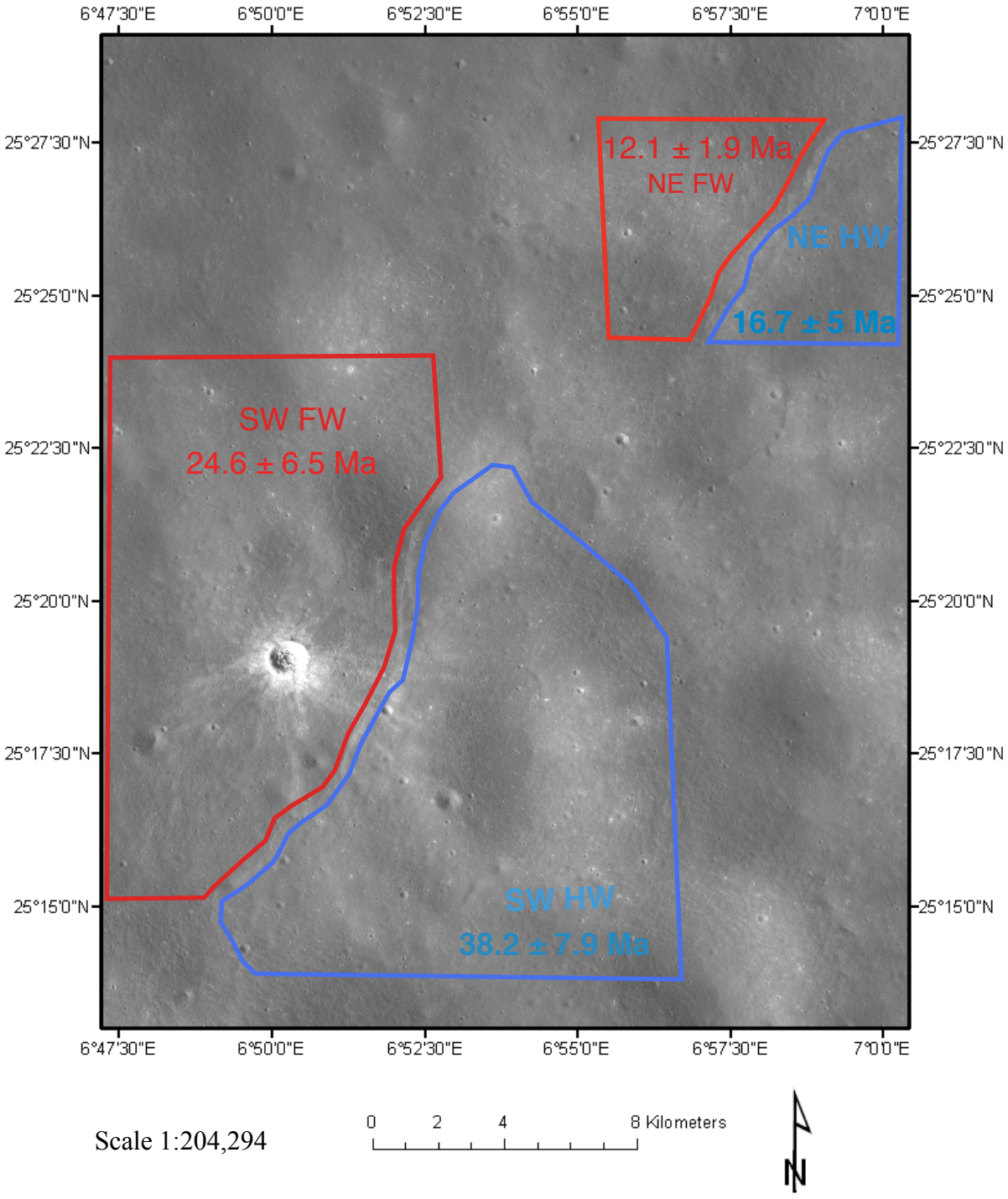

Figure 29: Map of Joy-1 scarp complex showing areas that were used for crater counting. One site was in the southwest section (Figure 30). The other in the northwest section (Figure 32).

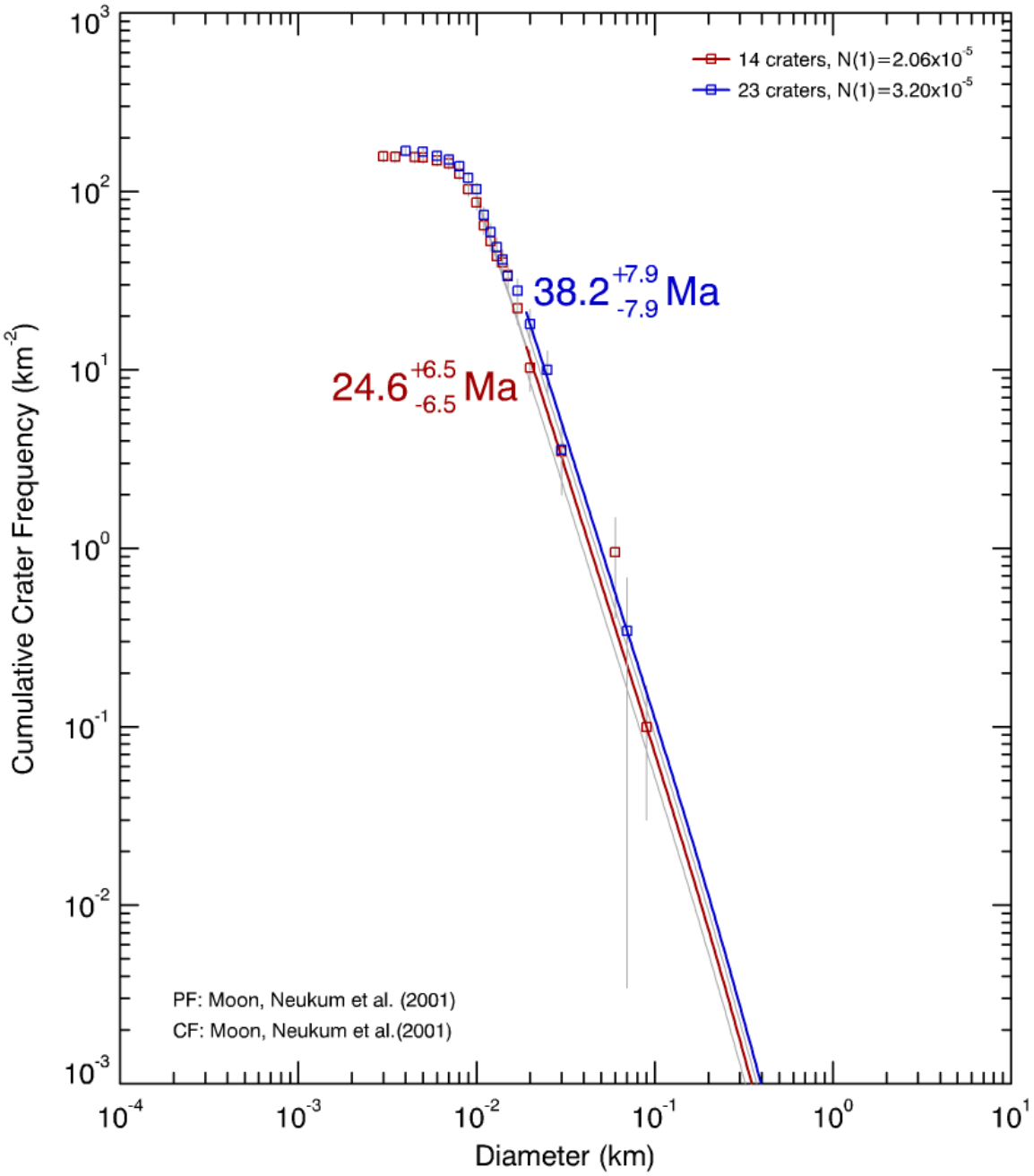

Figure 30: N_{cum} plot for southwest section of Joy-1 scarp complex. The highlands foot-wall is 24.6 ± 6.5Ma and the highlands hanging wall is 38.2 ± 7.9 Ma.

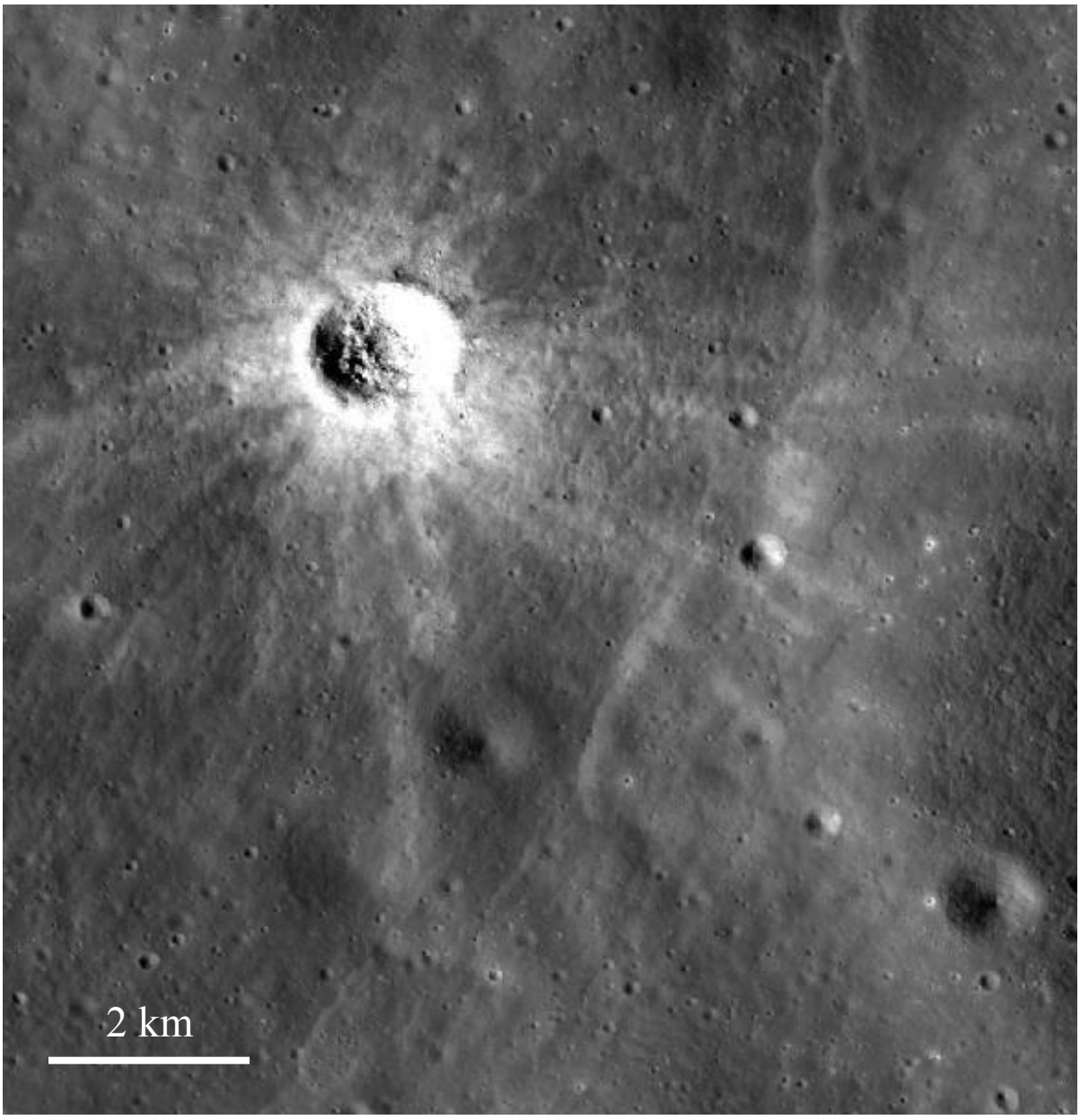

Figure 31: Zoomed in section of Joy-1 scarp complex. Fresh imapct crater with high albedo ejecta cross cut by the lobate scarp.

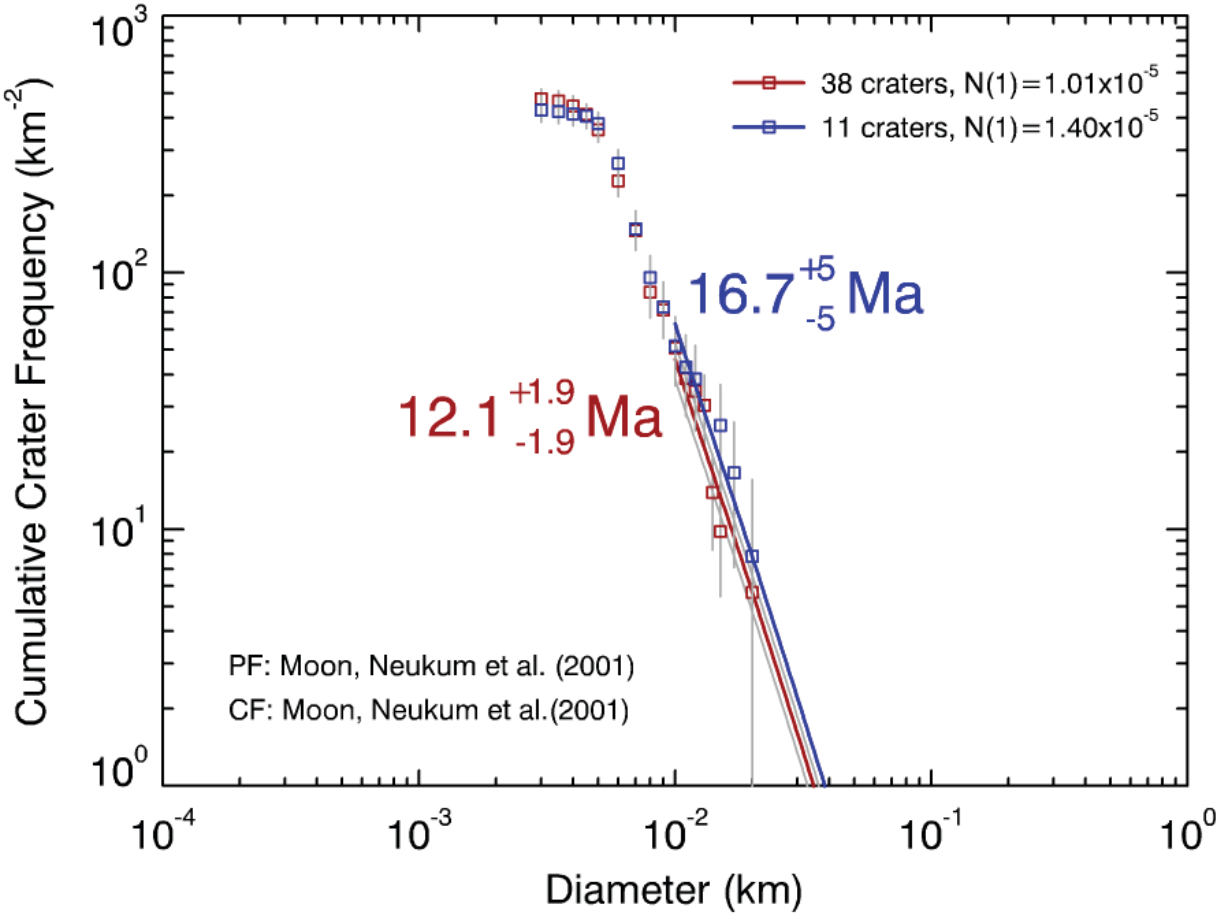

Figure 32: N_{cum} plot for northwest section of the Joy-1 scarp complex. The highlands footwall is 12.1 ± 1.9 Ma and the highlands hanging wall is 16.7 ± 5.

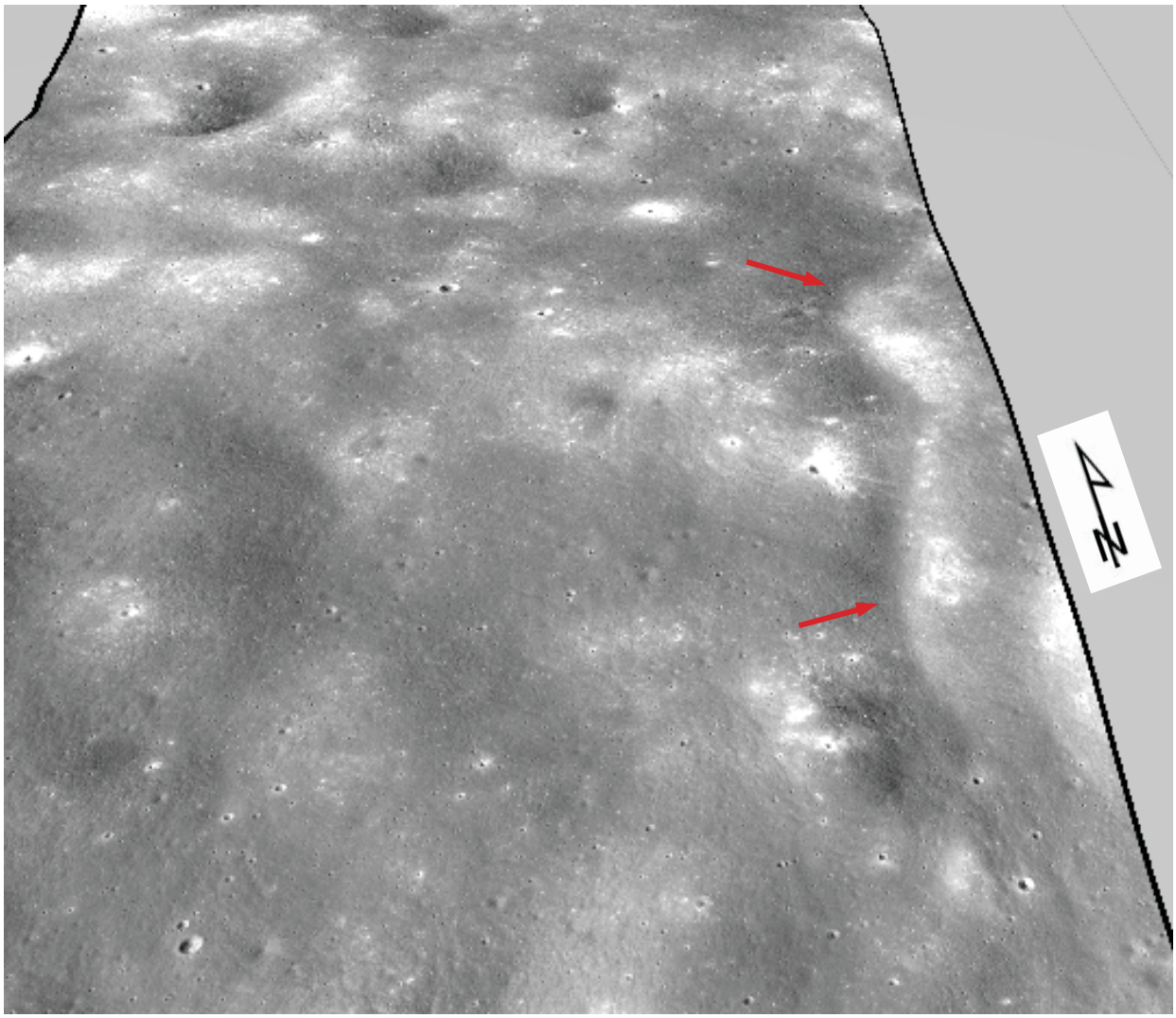

Figure 33: 3D visualization of Joy-2 scarp complex created in Fledermaus. Red arrows point out lobate scarps. LROC NAC image M104469044LC draped onto LOLA DEM.

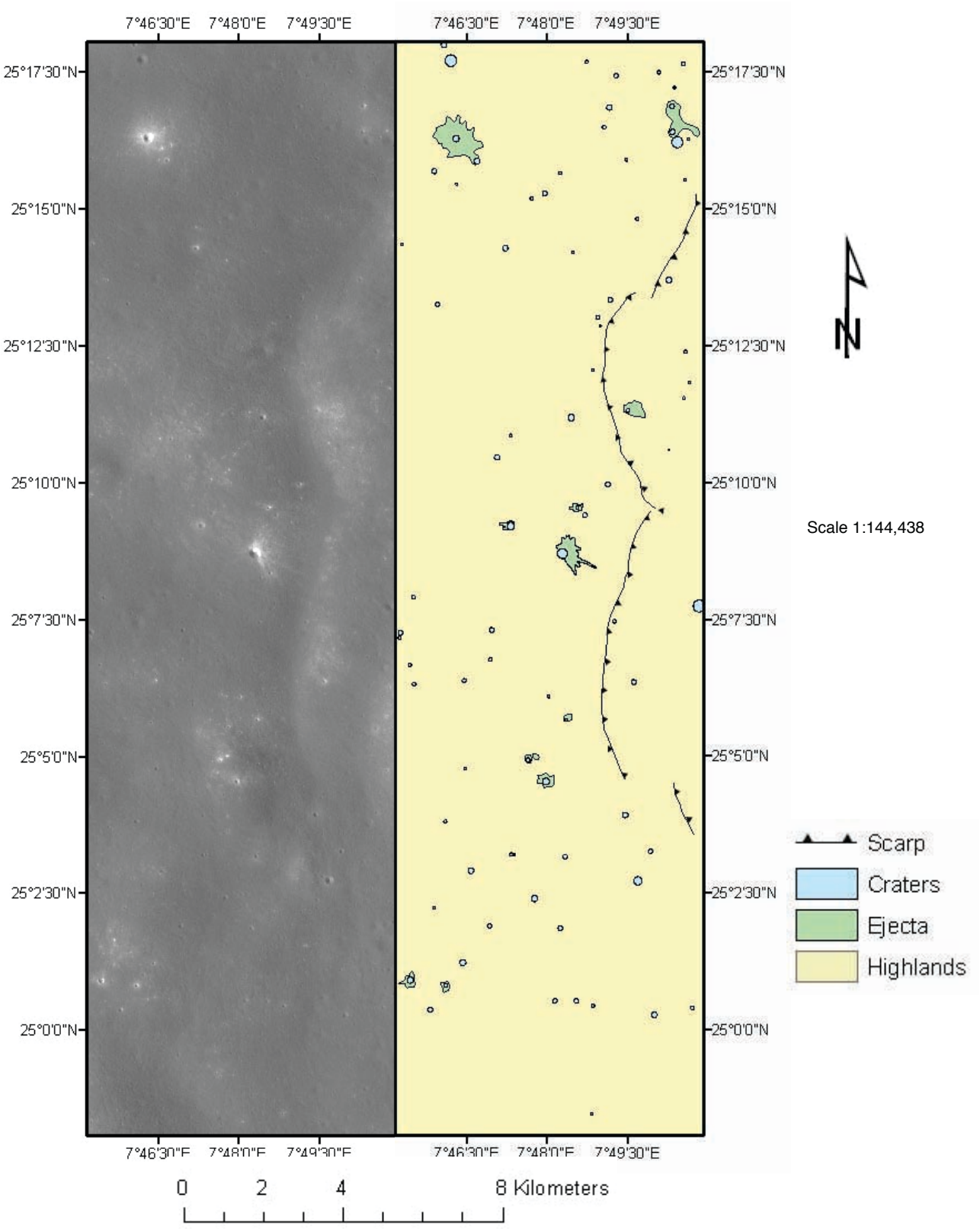

Figure 34. Joy-2 scarp complex. On the left is LROC NAC image M104469044LC and on the right is the photogeologic map.

Figure 35: Cross-sections A-A' - B-B' for Joy-2 scarp complex.

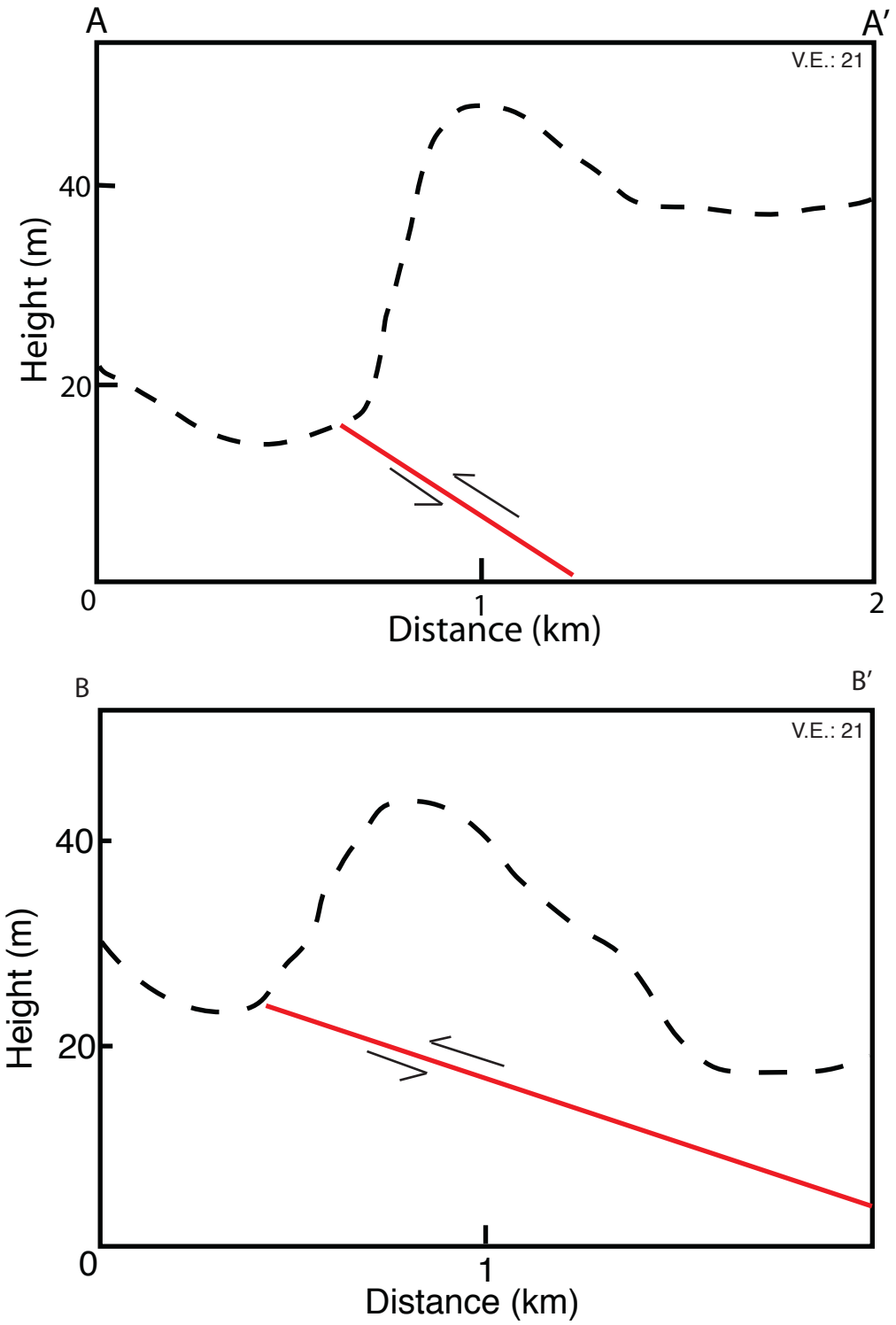

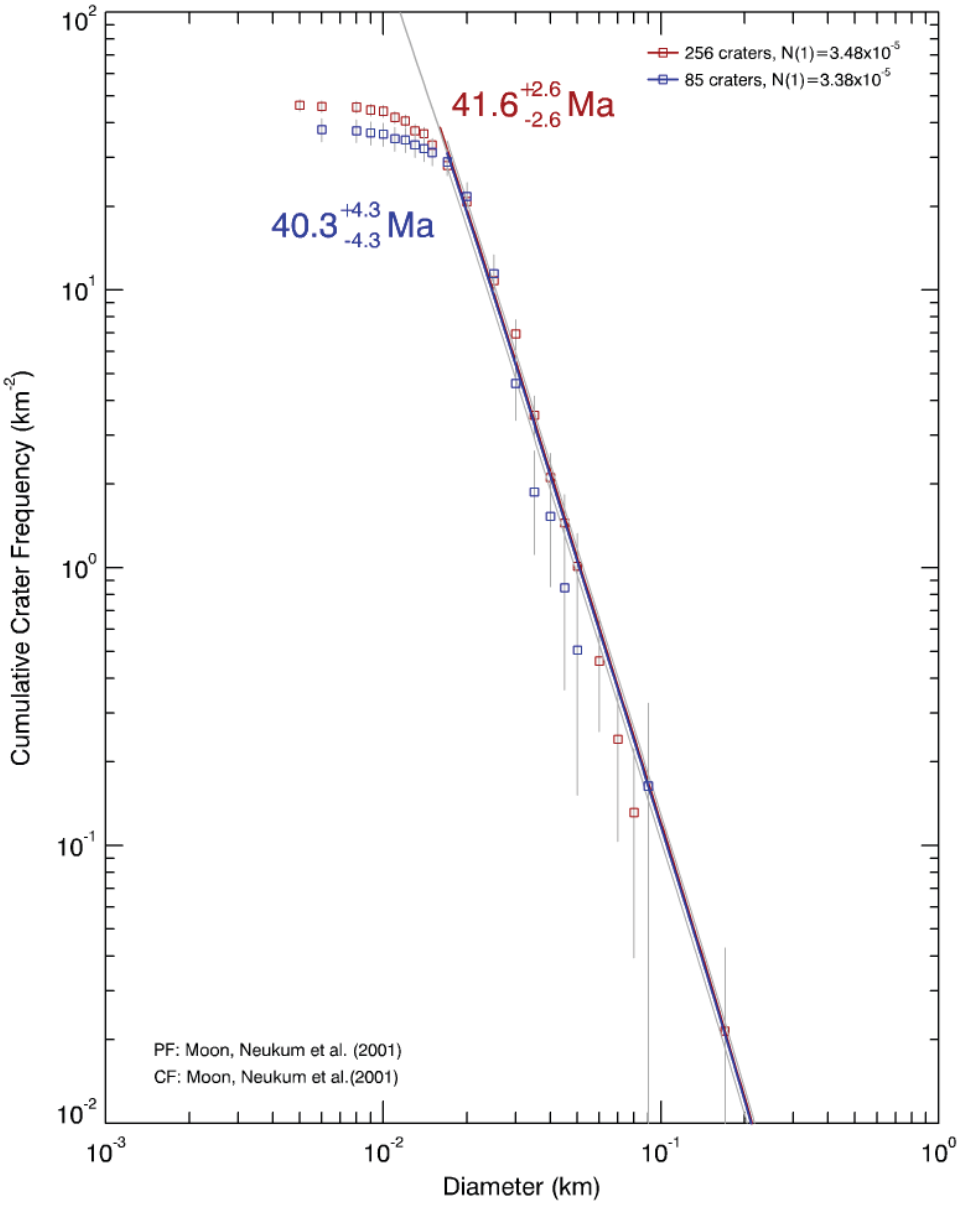

Figure 36: N_{cum} plot for Joy-2 scarp complex. The highlands footwall is 40.3 ± 4.3 Ma and the highlands hanging wall is 41.6 ± 2.6 Ma.

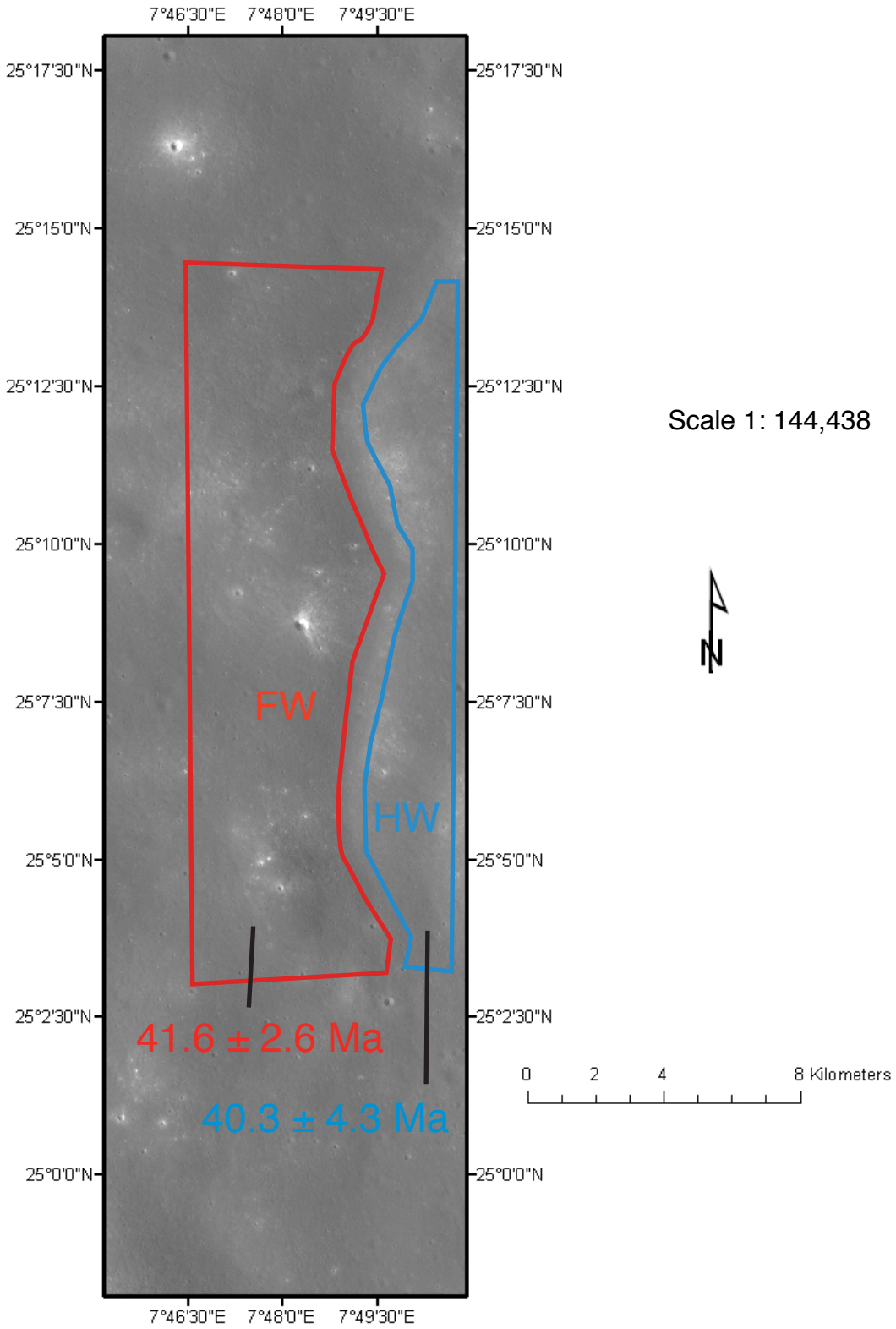

Figure 37: Map of Joy-2 scarp complex showing area that were used for crater counting. Figure 36 has the N_{cum} plot.

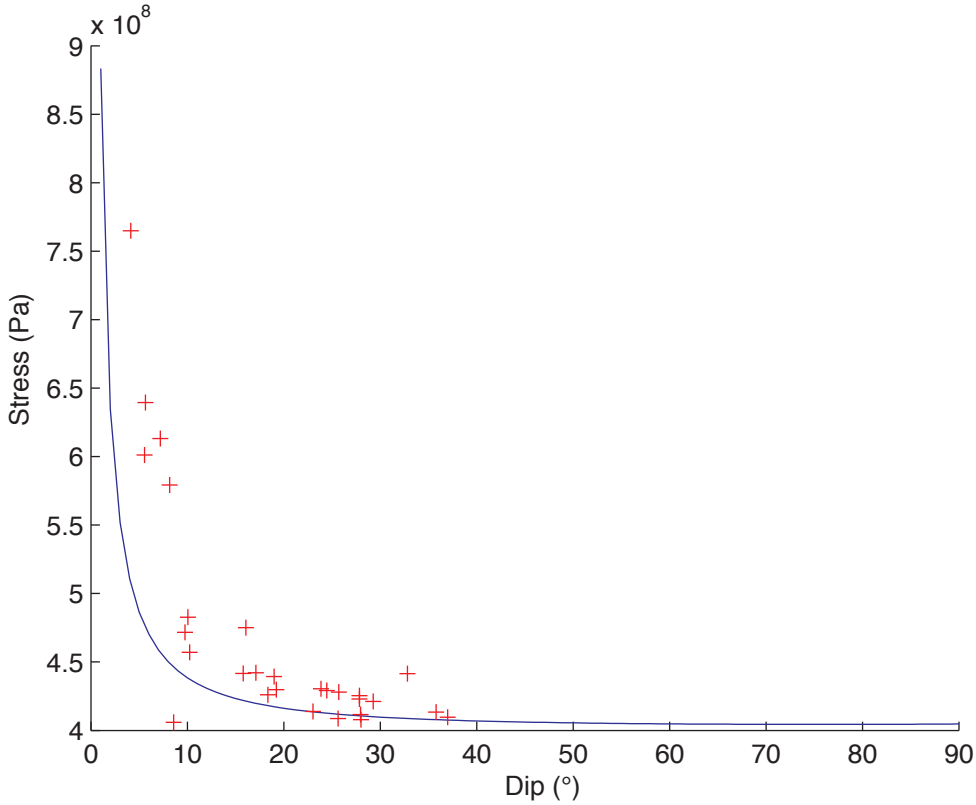

Figure 38. Stress as a function dip. Red crosses are calculated results for all lobate scarps investigated from both study areas. Blue line is the theoretical relationship calculated (Turcotte and Schubert, 2002).

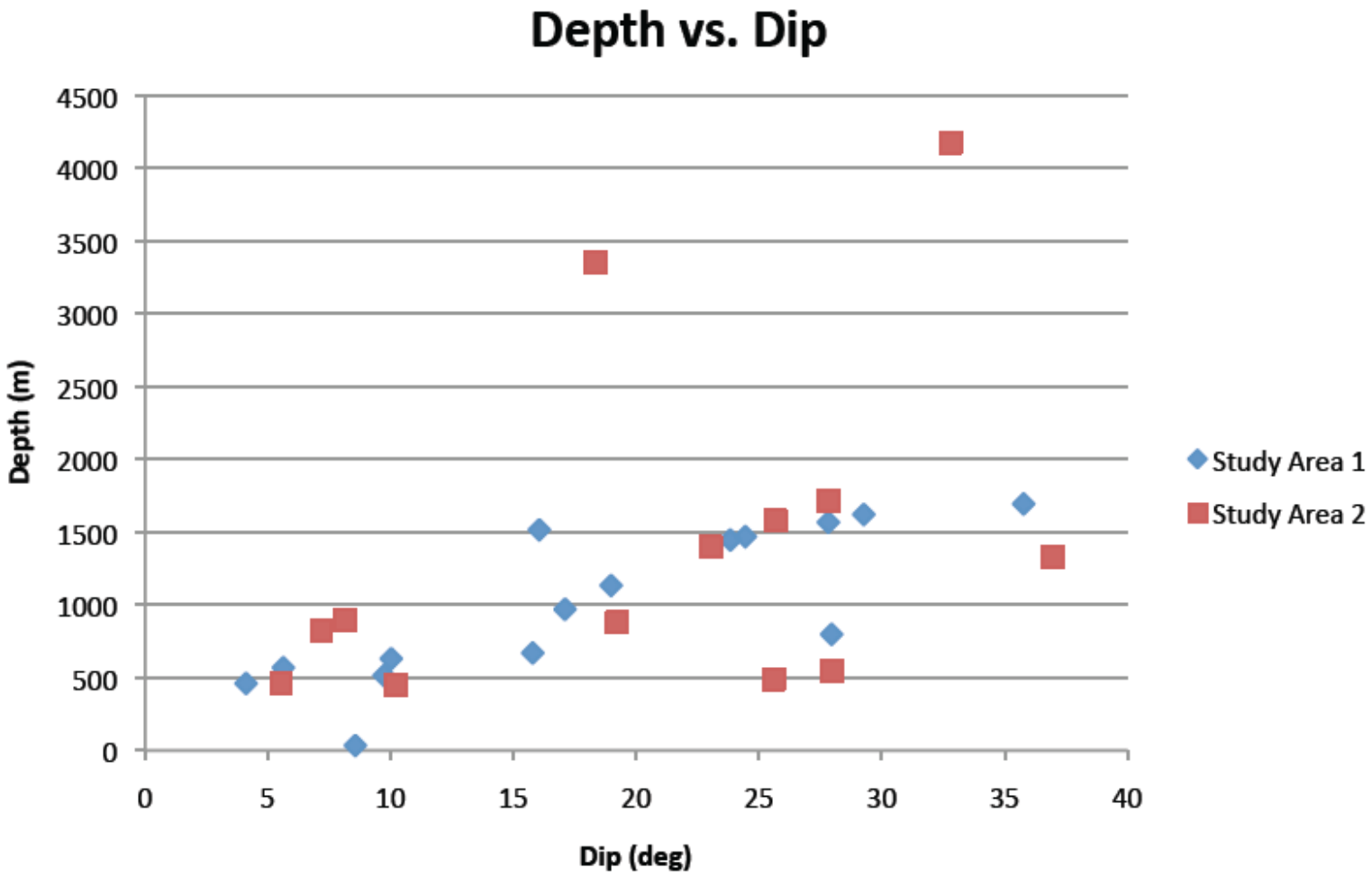

Figure 39: Results from both study areas: Depth as a function of dip of faulting

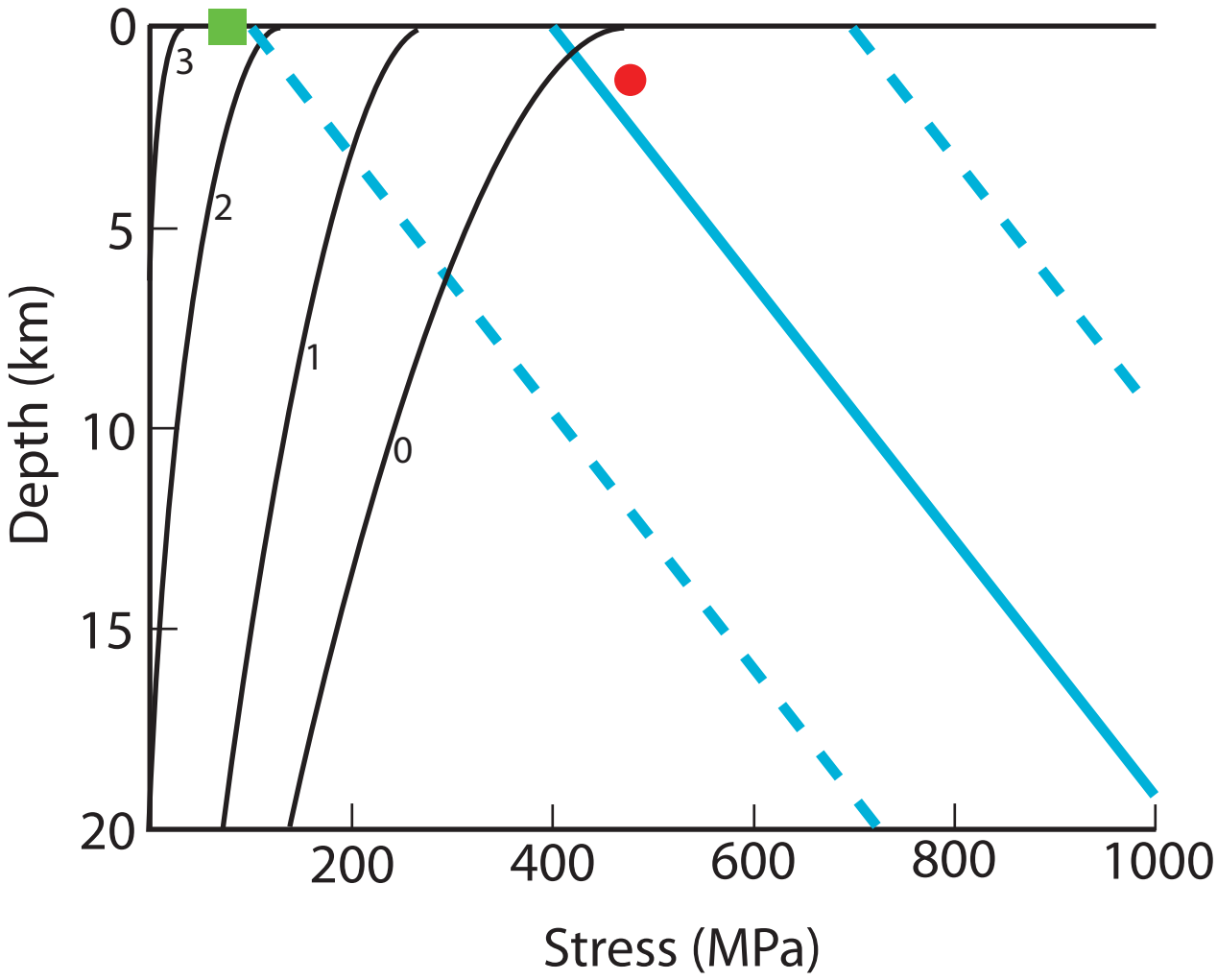

Figure 40. Stress as a function of depth showing predictions of the LMO and ITM models and the results of the Mohr-Coloumb calculations. Black, numbered curves give the stress as a function of depth for the ITM model at 3 Ga, 2 Ga, 1 Ga, and the present (Binder and Lange, 1980). The green square shows the maximum surface stress (73.3 MPa) allowed by the LMO model (Solomon and Head, 1979). The blue lines show the minimum and maximum (dashed) and average (solid) streses needed to initiate faulting according to the Mohr-Coulomb failure law (Equation (1) with $S = 400 \pm 300$ MPa) (Binder and Gunga, 1985). The red dot shows the average stress computed for the lobate scarps investigated in this study (473.2 MPa at an average depth of faulting of 1.21 km).

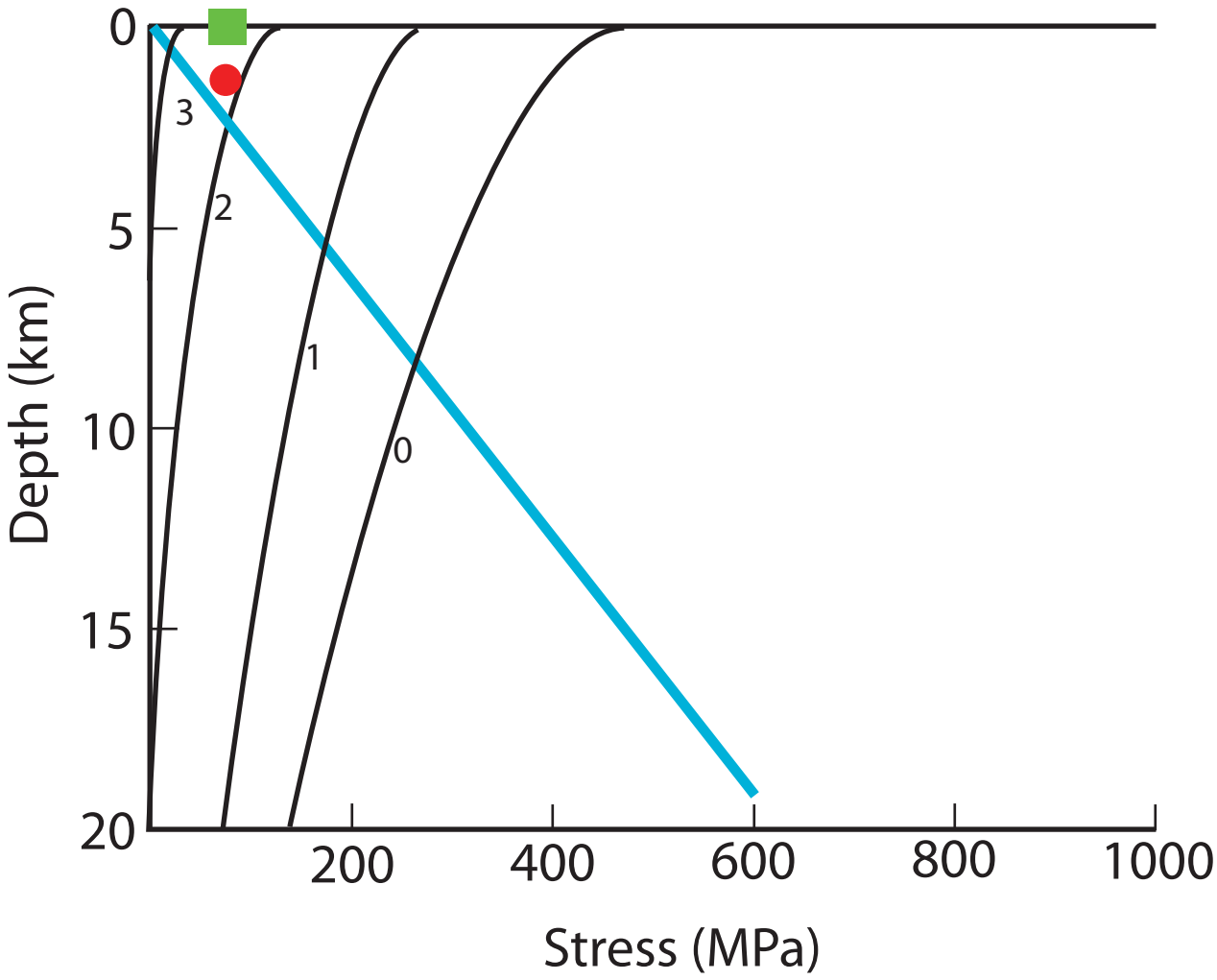

Figure 41. Stress as a function of depth showing predictions of the LMO and ITM models and the results of the Mohr-Coloumb calculations. Black, numbered curves give the stress as a function of depth for the ITM model at 3 Ga, 2 Ga, 1 Ga, and the present (Binder and Lange, 1980). The green square shows the maximum surface stress (73.3 MPa) allowed by the LMO model (Solomon and Head, 1979). The blue line shows the stress needed to initiate faulting according to the Mohr-Coulomb failure law (Equation (1) with $S = 0$ MPa). The red dot shows the average stress computed for the lobate scarps investigated in this study, adjusted for the choice of S = 0 MPa (73.2 MPa at an average depth of faulting of 1.21 km).

APPENDIX A: Mohr-Coulomb Fault Dynamics Code

```
%Thermoelastic equations

function [T,Z,theta,F,K] = AMC_equations_function (R, h)
%
%USAGE: [T,Z,theta, F,K] = AMC_equations_function (R, h)
%
% Inputs:   R = radius of the scarp
%           h = half angle of the scarp (in radians)
%           g = 1.623kg/sec^2 = lunar gravity
%           p = density = 3200kg/m^3 for Mare and 2500kg/m^3 for Highlands
%           s = 4kbar = crushing strength of rock

% Output:   T = tangential stress
%           H = half angle of scarp (in degrees)
%           Z = depth of faulting
%           theta = dip angle of faulting
%           F = coefficent of friction
%           K = function of the coefficient of friction


%need to be able to input variables in command window
%input Radius(R) in kilometers
%input Half angle(h) in radians
disp (' ')
disp (' ')
disp (' ')
disp (' ')
disp ('Input parameters ')

R = (input radius value in kilometers here)

h = (input half angle value in radians here)


%calculates the depth of faulting
%Depth of faulting will be in km
Z = R*tan(0.63*h);

%converts depth: Z(km) to z(m)
disp (' ')
disp (' ')
disp (' ')
disp (' ')
disp ('Depth z in meters')
z = Z*1000

%converts the crushing strength of rock: s(kbar) to S(pascal) to be used in
tangential stress eqn.
S = 4*100*1000000;

%calculates coefficent of friction
F = ( 1 / (tan(h/0.79)))
```

```
%calculates the function of the coefficent of friction
K = ((sqrt (1 + F^2) + F) / (sqrt (1 + F^2) - F))

%calculates tangential stress
%user will need to select the rock density(p)
%choose if highland or basalt
%Highland = 2500 kg/m^3
%Basalt = 3200 kg/m^3
disp (' ')
disp (' ')

decide = input ('Is this area in the: ( 1 = Highlands; 2 = Mare ) ' );
if decide == 1
    p = 2500;
    disp (' ')
    disp ('    You have choosen HIGHLANDS ' )
    disp (' ' )
elseif decide == 2
    p = 3200;
    disp (' ')
    disp ('    You have choosen MARE ' )
    disp (' ')
    return

end

%now code can execute tangential stress equation
%gravity of Moon: 1.623 m/sec^2
%depth of faulting is in m (coverted in an equation above)
t = K*p*1.623*z + S;

%converts stress: t(pascals) to T(mega pascals)
disp (' ')
disp (' ')
disp ('Compressional Stress in Megapascal')
T = t/1000000

%converts the half angle: h(radians) to H(degrees)
%half angle (h) must be in degrees(H) to be used in dip angle equation
H = h*(180/pi);

%calculates the dip angle of faulting
disp (' ')
disp (' ')
disp ('Dip Angle')
theta = ( 2/pi )* H

disp (' ')
disp ('Equation execution completed ')
disp (' ')
```

APPENDIX B: Integer to Floating Point DEM Conversion Code

```
%for opening a n x n unsigned integer 8 bit envi file
fid = fopen( 'dem_15N_30N_000_030' , 'r' , 'l' ) ;
m = 11264;
n = 10240;
myimage = fread( fid , [ n , m ] , 'uint16' ) ;
fclose( fid ) ;
myimage = myimage' ;



%solves permissions problem
%note that this also includes an alternative to specifying the rows and
%columns, but requires the image to be reshaped after opening...
%fid = fopen( 'myimage') ;
%myimage = fread( fid , inf , 'uint8' ) ;
%fclose( fid ) ;

%reshaping for BSQ image
%myimage2 = reshape( myimage , envi_columns , envi_rows .* envi_bands ) ;
%myimage2 = myimage2' ;
%myimage2_band1 = myimage2( 1 : envirows , : ) ;

%plot image
%figure( 1 )                % Makes a new figure window.
%hold off               % Allows the figure to be overwritten.
%magesc( myimage )      % Plots the image.
%colormap( pink )       % Sets the colormap.
%axis image             % Formats the axes.
%title( ' My Image  ' ) % Sets the title.
%xlabel( ' column ' )   % Labels the x axis
%ylabel( ' row ' )      % Labels the y axis
%hold on                    % Prevents the figure from being overwritten.

%myimagefloat = double( myimage ) ;
%myimagefloat = single( myimage ) ;

%figure( 2 )                % Makes a new figure window.
%hold off               % Allows the figure to be overwritten.
%imagesc( myimagefloat )        % Plots the image.
%colormap( pink )       % Sets the colormap.
%axis image             % Formats the axes.
%title( ' My Image  ' ) % Sets the title.
%xlabel( ' column ' )   % Labels the x axis
%ylabel( ' row ' )      % Labels the y axis
%hold on

%save image to envi compatible format
myimagefloat = myimagefloat' ;
fid = fopen( 'dem_15N_30N_000_030.img' , 'wb' ) ;
fwrite( fid , myimagefloat , 'single' ) ;
fclose( fid )
```

APPENDIX C: Photoclinometry Code

```
%crater.m
%
%Consolidated MATLAB code for analysis of crater morphology
%
%Includes:
% (1) "Carlotto" method of photoclinometry for extracting DEMs from imagery
% (2) Routines for visualizing DEM and extracting topographic profiles
% (3) Routines for interactively calculating alpha and beta values
%
% 041311-jmh
%

disp( 'START PROGRAM ' )
disp( ' ' )

makedem = input( ' Do you need to create a DEM first? ( 1 = yes ; 0 = no ; no is default ) ' ) ;
if makedem == 1
   [ dempixelsize , dem ] = carlotto_fun
else
   matname = input( ' What is the .MAT filename containing the DEM (as a variable called "dem") ? ' , 's' ) ;
   load( matname , 'dem' )
   dempixelsize = input( ' What is the pixel size of the DEM (in m/pixel)? ' ) ;

   figure( 2 )
   imagesc( dem )
   colormap( 'jet' )
   axis image
   saveas( gcf , 'demfigure2' , 'fig' )
end

%profile extraction routine

disp( 'PROFILE EXTRACTION ROUTINE (INCLUDING MORPHOLOGIC ANALYSIS) ' )
disp( ' ' )

i = 1 ;
keepgoing = 1 ;
while keepgoing == 1
   whichfig = input( ' On which figure would you like to define your topographic profile line? ( 1 or 2 only ; 2 is
default ): ' ) ;
   if whichfig == 1
   elseif whichfig == 2
   else
      whichfig = 2 ;
   end

   profilename = input( ' Enter a name for this profile: ' , 's' )

   figure( whichfig )
   hold on
   disp( ' Define the profile by selecting the start and end points ' )
   disp( ' Select the start point: ' )
   [ startx , starty ] = ginput( 1 ) ;
   disp( ' Select the end point: ' )
```

```
[ endx, endy ] = ginput( 1 ) ;

startx
starty
endx
endy

[ CX , CY , C , xi , yi ] = improfile( dem , [ startx , endx ] , [ starty , endy ] , 'nearest' ) ;

plot( CX , CY )

for j = 1 : ( length( C ) - 1 )
   profileresolution( j ) = sqrt( ( ( abs( CX( j ) - CX( j + 1 ) ) ).^2 ) + ( ( abs( CY( j ) - CY( j + 1 ) ) ).^2 ) ) ;
end
profileres = mean( profileresolution ) .* dempixelsize
clear profileresolution

profilevert = C ;
profilehoriz = profileres .* [ 1 : 1 : length( C ) ] ;

figure( 3 + i )
plot( profilehoriz , profilevert )
xlabel('Distance [meters]')
ylabel('Depth [meters]')
title('Topographic Profile')
saveas( gcf , profilename , 'fig' )

goahead = input( ' Would you like to now analyze this profile? ( 1 = yes ; 0 = no ; no is default ) ' ) ;
if goahead == 1
   [ Lrim , Rrim , D , diameter , alphavalue , betavalue ] = morphology_fun( i , profileres ) ;
else
   disp( 'SKIPPING MORPHOLOGIC ANALYSIS ROUTINE ' )
   disp( ' ' )
end

%save results to files
save %saves all variables to a file called matlab.mat
%save( profilename , 'profileres' , 'startx' , 'starty' , 'endx' , 'endy' , 'Lrim' , 'Rrim' , 'D' , 'diameter' , 'alphavalue' ,
'betavalue' , -ASCII -TABS )
%save profilename profileres startx starty endx endy Lrim Rrim D diameter alphavalue betavalue  -ASCII -TABS
outputmatrix = [ profileres startx starty endx endy Lrim Rrim D diameter alphavalue betavalue ] ;
csvwrite( profilename , outputmatrix )

dummy = input( ' ' ) ;
dummy = input( ' ' ) ;
dummy = input( ' ' ) ;
dummy = input( ' ' ) ;
dummy = input( ' ' ) ;
dummy = input( ' ' ) ;
dummy = input( ' ' ) ;
dummy = input( ' ' ) ;
dummy = input( ' Press return to continue... ' ) ;

decide = input( ' Would you like to do another profile? ( 1 = yes ; 0 = no ; no is default )' ) ;
if decide == 1
  keepgoing = 1 ;
```

```
      disp( 'DOING ANOTHER PROFILE ' )
      disp( ' ' )
      i = i + 1 ;
    else
      keepgoing = 0 ;
      disp( 'END PROFILE EXTRACTION ROUTINE (INCLUDING MORPHOLOGIC ANALYSIS) ' )
      disp( ' ' )
    end
end

disp( 'END PROGRAM ' )
disp( ' ' )
```

```
function [ pixelsize , dem ] = carlotto_fun

% carlotto_fun.m
%
% MATLAB implementation of the Carlotto (1996) and Evans (2006) photoclinometry
% methods.
%
% Code gives user option to use either the original Carlotto (1996) iterative
% method or the variant described by Evans (2006) that uses elevation gradients.
%
% Initially assumes a Lambetian surface which reflects light proportionally to
% the cosine of the angle between the sun and the zenith vector (solar zenith
% or incidence angle).  The Lambertian assumption requires that:
% (1) the image is acquired far from the limb;
% (2) the lighting is oblique with at most 25 degree solar altitude; and
% (3) the surface does not vary excessively in albdeo.
%
% Code also includes options for correcting for non-Lambertian reflectance and
% dark-subtraction to account for scattering path-radiance.  These are based on
% procedures described in Lena (2009).
%
% ####### NOT YET FULLY IMPLEMENTED #######
% Non-Lambertian correction requires photometric functions from McEwen (1991).
% ####### NOT YET FULLY IMPLEMENTED #######
%
% TO DO: IMPLEMENT OTHER METHODS OF READING IMAGES WITH OTHER FORMATS
% TO DO: COMPLETE THE NON-LAMBERTIAN CORRECTION
% TO DO: AUTOMATICALLY CREATE THE NECESSARY ENVI .HDR FILE
%
% jmh 041311

%clear
%clf
%clc

disp( 'CARLOTTO PHOTOGRAMMETRY PROGRAM (JMH 041311) ' )
disp( ' ' )

% load image

filenamein = input( 'What is the name of the file containing the image? ' , 's' ) ;
rows =  input( 'How many rows (lines) does the image have? ' ) ;
cols =  input( 'How many columns (samples) does the image have? ' ) ;

disp( ' Is this image a JPEG or an ENVI-compatible image? ' )
imagetype = input ( '  Enter 0 for "JPEG" or 1 for "ENVI": ') ;

if imagetype == 0
   imagein = imread( filenamein , 'JPG' ) ;
elseif imagetype == 1
   fid1 = fopen( filenamein ) ;
   imagein = fread( fid1 , 'int16' ) ;
   fclose( fid1 ) ;
   imagein = reshape( imagein , cols , rows ) ;
   imagein = imagein' ;
else
```

```
   % room here for other image types as necessary...
   disp( '  Pick 0 or 1 only!' )
   %break
   return
end

image = double( imagein ) ;
clear imagein

disp( ' ' )

% plot image
% image should be rotated so that illumination is from the left
% code interactively determines correct orientation and allows rotation

i = 0 ;
ii = 0 ;

while i == 0

   figure( 1 )
   imagesc( image )
   colormap( 'bone' )
   axis image
   hold off

   disp( 'Is the illumination in the image from the left (270 azimuth)? ' )
   j = input ( ' Enter 0 for "No" or 1 for "Yes": ') ;

   if j == 0
      disp( '  Rotating image counterclockwise by 90 degrees... ' )
      image = rot90( image ) ;
      i = 0 ;
      ii = ii + 1 ;
   elseif j == 1
      disp( '  Image illumination is in the correct orientation... ' )
      i = 1 ;
   else
      disp( '  Pick 0 or 1 only!' )
      %break
      return
   end

end

% check if you rotated it an odd number of times...
% if so, the rows and columns will need to be flipped!

if rem( ii , 2 ) == 1
   trows = rows ;
   tcols = cols ;
   rows = tcols ;
   cols = trows ;
   clear trows tcols
end
```

```
disp( ' ' )

% define parameters
% for LRO, all these parameters are given in the index spreadsheets...

zenith = input( 'What is the incidence (or solar zenith) angle for this image? (degrees) ' ) ;
% angle from vertical to sun e.g. 90 - solar altitude
% incidence angle > 90 is a night image
% incidence angle = 90 means sun at horizon
% incidence angle = 0 means sun directly overhead

if zenith <= ( 90 - 25 )
   disp( ' Small zenith angles (< 65 degrees) may give marginal results... ' )
end

emission = input( 'What is the emission angle? (degrees) ' ) ;
% angle from vertical to the observer

phase = input( 'What is the phase angle? (degrees) ' ) ;
% angle between the sun and the observer
% phase = 0 means sun, target, and observer collinear on same side of zenith
% phase = 180 means sun, target, and observer collinear on opposite sides of zentih

if phase <= 30
   disp( ' Small phase angles (< 30 degrees) may give marginal results... ' )
end

pixelsize = input( 'What is the ground resolution (pixel size) of this image (assuming square pixels)? (meters) ' ) ;

long =  input( 'What is the center longitude of the image? ' ) ;
lat =  input( 'What is the center latitude of the image? ' ) ;

disp( ' ' )

disp( 'Do you wish to do a dark subtraction correction? ' )
k = input ( ' Enter 0 for "No" or 1 for "Yes": ') ;

if k == 1

   % do dark subtraction correction ("shadow offset")
   % code interactively defines area to use for correction

   disp( '  Applying dark-subtraction correction... ' )

   figure ( 1 )
   clf
   imagesc( image )
   colormap( 'bone' )
   axis image
   hold on

   disp ( '   Select an area that should be in perfect shadow.  Pick the opposing corner points of a small, rectangular
region of interest in this shadow... ' )
   disp ( '    Click on the upper left corner... ' )
   [ x1 , y1 ] = ginput( 1 ) ;
   x1 = round( x1 ) ;
```

```
    y1 = round( y1 ) ;
    plot( x1 , y1 , 'r.' )
    disp ( '    Click on the lower right corner... ' )
    [ x2 , y2 ] = ginput( 1 ) ;
    x2 = round( x2 ) ;
    y2 = round( y2 ) ;
    plot( x2 , y2 , 'r.' )

    imagedssubset = image( y1 : y2 , x1 : x2 ) ;
    imagedssubsetarea = image ;
    imagedssubsetarea( y1 : y2 , x1 : x2 ) = max( max( imagesc ) ) + 1 ;

    disp ( '   Drawing rectangle... ' )

    imagesc( imagedssubsetarea )

    disp ( ' ' )

    offset = mean( mean( imagedssubset )  )

    minval = min( min( image ) )

    if ( offset > minval )
       disp( '  There appears to be a darker shadow somewhere... ' )
       disp( '  That minimum will be used for the shift instead... ' )
       disp( ' ' )
       image = image - minval ;
    elseif ( offset <= minval )
       image = image - offset ;

    end

elseif k == 0
    disp( '  Skipping dark-subtraction correction... ' )
else
    disp( ' Pick 0 or 1 only! ' )
    %break
    return
end

disp( ' ' )

% calculate topography

z = zeros( rows , cols ) ;

disp( 'Which method do you wish to employ: Carlotto (1996) iterative method or the Evans (2006) elevation
gradients variant? ' )
o = input ( ' Enter 1 for Carlotto or 2 for Evans: ') ;

if o == 1

    %% using Carlotto (1996) iterative equation
    %% note that rows and columns notation in MATLAB is opposite that for "images"

    disp( '  Using the Carlotto (1996) iterative method... ' )
```

```
    for m = 1 : rows
        a = mean( image( m , : ) ) ./ cosd( zenith ) ; % assuming a simple Lambertian model e.g. Evans (2006)
        for n = 1 : cols
            if n == 1
                z( m , n ) = 0 + ( ( image( m , n ) - ( a .* cosd( zenith ) ) ) ./ ( a .* sind( zenith ) ) ) ;
            else
                z( m , n ) = z(  m , ( n - 1 ) ) + ( ( image( m , n ) - ( a .* cosd( zenith ) ) ) ./ ( a .* sind( zenith ) ) ) ;
            end
        end
    end

elseif o == 2

    % using Evans (2006) "rolling sum of elevation gradients" method
    % note that rows and columns notation in MATLAB is opposite that for "images"

    disp( '  Using the Evans (2006) elevation gradients method... ' )

    for m = 1 : rows
        a = mean( image ( m , : ) ) ; % Note: this is *not* the same parameter as "a" used in the Carlotto method
(above), it is just the same variable name!
        for n = 1 : cols
            Dz( m , n ) = ( image( m , n ) - a ) ./ ( a .* tand( zenith ) ) ;
            if n == 1
                z( m , n ) = 0 + Dz( m , n ) ;
            else
                z( m , n ) = sum( Dz( m , 1 : n ) ) ;
            end
        end
    end

else
    disp( ' Pick 1 or 2 only! ' )
    %break
    return
end

dem = pixelsize .* z ;

disp( ' ' )

disp( 'Do you wish to correct for non-Lambertian photometry? ' )
l = input ( ' Enter 0 for "No" or 1 for "Yes": ') ;

if l == 1

    % correct for non-Lambertian surface e.g. Lena (2009)

    disp( '  Applying non-Lambertian correction... ' )

    delta = cosd( long ) .* cosd( lat ) ;

    % ####### ADD CODE #######

    L = 0.6 ; % from McEwen (1991)
```

```
    lambda = 0 ; % from Lena (2009)

    % ####### ADD CODE #######

    correctionfactor = ( 2 .* ( 1 ./ ( 1 + delta ) ) ) + lambda ;

    dem = dem .* correctionfactor ;

elseif l == 0
    disp( '  Skipping non-Lambertian correction... ' )
else
    disp( ' Pick 0 or 1 only! ' )
    %break
    return
end

disp( ' ' )

% replot image

figure ( 1 )
clf
imagesc( image )
colormap( 'bone' )
axis image
saveas( gcf , 'demfigure1' , 'fig' )

% plot dem

figure( 2 )
imagesc( dem )
colormap( 'jet' )
axis image
saveas( gcf , 'demfigure2' , 'fig' )

% plot 3-D perspective view

figure( 3 )
mesh( dem )
saveas( gcf , 'demfigure3' , 'fig' )

% save results

disp( 'Saving both an ENVI-compatible binary file and a MATLAB .mat binary file... ' )

% export DEM for use in ENVI

dem = dem' ;
filenameout = input( ' What do you want to name the file containing the DEM? ' , 's' ) ;
fid2 = fopen( filenameout , 'wb' ) ;
fwrite( fid2 , dem , 'float' ) ;
fclose( fid2 ) ;
disp( '  Remember to also prepare the appropriate .hdr file for use in ENVI! ' )
disp( '   The number of rows (lines) and columns (samples), respectively are: ' )
rows
```

```
cols

% save variables for this MATLAB run in a .MAT file

save( filenameout )

disp( 'END CARLOTTO PHOTOGRAMMETRY PROGRAM ' )
disp( ' ' )
```

CURRICULUM VITA

Jaclyn Clark was born in Wiesbaden, Germany to an Air Force family. For most of her life she grew up in Michigan and graduated from Grand Ledge High School in 2005. She studied at Central Michigan University where she completed her B.S. degree in Geology and a minor in Geographic Information Sciences in 2010, with a thesis focusing on metamorphic fluid control on slip systems and recrystallization of the EJB aureole in eastern California. Jaclyn continued her education at the University of Texas at El Paso pursuing a M.S. in geological sciences under Dr. José Hurtado. During his time at UTEP, Jaclyn served as Mission Science Team for NASA Desert Rats 2011, participated in the AAPG Imperial Barrel Award competition where her team took first place in the regional competition and were runners up in the international competition, and worked as a research assistant for Dr. José Hurtado funded by the UTEP Center of Space Exploration Technology Research.

Permanent Address: 11219 Stoney Brook Dr.

Grand Ledge, MI 48837

jdclark@miners.utep.edu

This thesis was typed by Jaclyn D. Clark.